

Scaling Up 4D Printing: Direct Pellet Extrusion of Shape Memory Polymer Composites

by

Marco Vinicio Paez Estrella

A thesis submitted in partial fulfillment of the requirements for the degree of

Master of Science

Department of Mechanical Engineering
University of Alberta

© Marco Vinicio Paez Estrella, 2024

ABSTRACT

Shape Memory Polymers (SMPs) exhibit responsiveness to stimuli, characterized by the Shape Memory Effect (SME) which enables them to temporarily store a shape and return to their permanent/original form upon the application of a stimulus. However, SMPs face challenges in being applied to large-scale applications due to their limited stress recovery response. A promising solution to this problem are Shape Memory Polymer Composites (SMPCs).

This study aims to explore the feasibility of producing SMPCs with Additive Manufacturing (AM), which is also known as 4D printing, for large-scale manufacturing. In the future, the aim is eventually to be able to 4D print drone wings that can change their shape to maneuver in the air. Therefore, the goal is to leverage the unique properties of SMPCs, enhancing their applicability in the engineering field. In this work, a large-scale Extrusion Based 3D printing platform is modified and adapted with a pellet extruder. A polymer blend made of SMP polyurethane based MM4520 and PLA with 15% weight content of carbon fibers (CF) were used to create SMPC samples. Compositions of 0, 10, and 20 weight % CF15 PLA on SMP were manufactured and studied for shape recovery, shape recovery fixity ratio and shape recovery flexural stress. Results demonstrated that higher contents of CF15 PLA led to higher shape recovery flexural stresses that increased more than 400% compared to the raw printed material. However, a counter effect occurred to the shape recovery ratio and shape fixity. The shape recovery ratio decreases a maximum of 7% in comparison to the raw material. The shape fixity decreased from 22% from the raw material. This study is the first step to achieve scalability of 4D printing.

ACKNOWLEDGEMENTS

The completion of this thesis has only been possible thanks to the support I have received from all the people around me.

I'd like to acknowledge my supervisors, Dr. Cagri Ayranci and Dr. Irina Garces, for their patience and effort during my master's program. They always support my career and personal growth.

I would like to thank my lab mates Laura, Ismail, Rishabh, Jose, Gizem and Yu Chen for providing advice and assistance when I needed it.

I would like to thank all the people I have had the pleasure of meeting in Canada. They provided me with valuable support in this journey and I am eternally grateful with them. I would especially like to mention Anita, Gopu, Ruth, Toño, Paolo, Doug, Paulina, Antonio, Amy, Susy, Jyoti, Irene and Esteban. They all have a very special place in my chest.

I believe that gratitude has no end, I owe this thesis to many people I especially acknowledgment my family. Ana Patricia Estrella Moreno, my beloved mother and Marco Vinicio Paez Arias, my beloved father. The person I have become is thanks to my parents and this achievement is simply theirs. Thank you very much for all the support to my dear sisters Belen and Michu, my spoiled nephews Pame and Thiago. Heartfelt thanks to my grandmother Eva.

I want to thank God for always blessing my path. Anything is possible when you have people who love and support you.

Table of contents

| | |
|---|----|
| 1. INTRODUCTION | 1 |
| 1.1. Introduction..... | 1 |
| 1.1.1. Additive manufacturing and development of the 3D printer market..... | 1 |
| 1.1.2. Scaling up 3D printers | 1 |
| 1.1.3. 4D printing..... | 2 |
| 1.1.4. 4D printing and scalability..... | 3 |
| 1.2. Motivation..... | 5 |
| 1.3. Thesis objectives..... | 6 |
| 1.4. Thesis outline | 6 |
| 2. BACKGROUND | 8 |
| 2.1. Concepts brief review | 8 |
| 2.1.1. Additive manufacturing advantages-Fused deposition modeling..... | 8 |
| 2.1.2. Large scale 3D printing and its challenges. | 11 |
| 2.1.3. Fused Granular Fabrication..... | 15 |
| 2.1.4. 4D printing, smart materials, and shape memory polymers | 17 |
| 2.1.5. Shape recovery characterization: | 19 |
| 2.1.6. Reinforced polymers..... | 21 |
| 2.2. Conclusions..... | 24 |

| | | |
|--------|---|----|
| 3. | COMMISSIONING OF THE MACHINE | 25 |
| 3.1. | Large scale equipment | 25 |
| 3.2. | Integration of pellets extruder system..... | 26 |
| 3.3. | Installation of pellet extruder head in large scale 3D printer. | 28 |
| 3.4. | Auxiliary systems and electrical wiring of Pulsar Pellet Extruder | 33 |
| 3.4.1. | Auxiliary systems..... | 33 |
| 3.4.2. | Electrical wiring and firmware update..... | 35 |
| 3.5. | 3D-Printing Calibration | 37 |
| 4. | MATERIALS AND EXPERIMENTAL TECHNIQUES | 42 |
| 4.1. | Raw materials..... | 42 |
| 4.2. | Thermal Analysis | 42 |
| 4.2.1. | Thermogravimetric Analysis (TGA)..... | 43 |
| 4.2.2. | Differential scanning calorimetry (DSC)..... | 44 |
| 4.3. | Experimental approach | 46 |
| 4.3.1. | Laminate composite..... | 46 |
| 4.3.2. | Pellet extrusion..... | 47 |
| 4.4. | Obtaining test specimens | 48 |
| 4.4.1. | Material preparation..... | 48 |
| 4.4.2. | Sample fabrication..... | 50 |

| | | |
|--------|--|----|
| 4.4.3. | Annealing of samples..... | 52 |
| 4.5. | Sample testing..... | 54 |
| 4.5.1. | Shape Recovery Flexure Stress (SRFS)..... | 55 |
| 4.5.2. | Shape Recovery Ratio (SRR) and Shape Recovery Fixity (SRF) | 60 |
| 4.5.3. | Data obtained for analysis..... | 62 |
| 5. | RESULTS AND DISCUSSION..... | 63 |
| 5.1. | Annealing and its effects..... | 63 |
| 5.2. | Shape Recovery Flexural Stress (SRFS)..... | 67 |
| 5.3. | Shape Recovery Displacement and Ratio | 71 |
| 6. | CONCLUSIONS..... | 77 |
| 6.1. | Conclusions..... | 77 |
| 6.2. | Future work..... | 80 |

LIST OF FIGURES

| | |
|--|----|
| Figure 2.1. a) Shape memory samples designed on SolidWorks b) samples sliced on Simplify 3D. | 10 |
| Figure 2.2. Big format 3D printer model 300Workbench from 3D Platform printing a cylinder. .11 | |
| Figure 2.3. Real size 3D printed chair using big format 3D printer 300Series WorkbenchPro [47]. | 14 |
| Figure 2.4. Scheme of FGF system..... | 15 |
| Figure 2.5. Schematic of shape recovery ratio and shape recovery fixity tests. | 20 |
| Figure 3.1. Big format 3D printer model 300 Series Workbench Pro with high flow extruders (HFE 300). | 26 |
| Figure 3.2. a) Pulsar Pellet Extruder by DYZE [82] b) Internal heating elements of Pulsar Pellet Extruder modified from [82]..... | 28 |
| Figure 3.3. Dismounting nozzles from 3D printer. a) Single nozzle mounted b) Initial plate to hold nozzles..... | 29 |
| Figure 3.4. Plates design. a)3D printed plates iteration b) Example of interferences in designs c) Testing of plates. | 30 |
| Figure 3.5. a) SolidWorks design for plates b) Plates done in machine shop..... | 31 |
| Figure 3.6. a) Plates bolted to the frame. b) Pulsar Pellet Extruder Mounted. | 31 |
| Figure 3.7. a) Cross beam that will support the weight of the toolheads. b) Simplification of loading scenario. | 32 |
| Figure 3.8. Liquid Cooling System. a) Heat exchanger and pump. b) Power supplies | 34 |
| Figure 3.9. a) Pellet Feeding System b) Liquid cooling system. | 35 |
| Figure 3.10.Duet 2 Ethernet board [83]...... | 36 |

| | |
|--|----|
| Figure 3.11. Different flow rates 3D prints. a) Extrusion multiplayer of 30, 25, 20 b) Extrusion multiplayer of 12, 14, 16..... | 38 |
| Figure 3.12. 3D printed part using Pulsar Pellet Extruder(pellets) and HF300 (filament) toolhead. | 39 |
| Figure 3.13. 3D printed parts with shifting between layers..... | 39 |
| Figure 3.14. Results after tuning time for stepper motor pulse. | 40 |
| Figure 3.15. Object 3D printed after tuning 3D printer. | 41 |
| Figure 4.1. TGA of PLA with 15% content of carbon fibers and TGA of shape memory polymer MM4520 (SMP)..... | 43 |
| Figure 4.2. Modulated DSC of PLA plus 15% carbon fiber (CF PLA) and Shape memory polyurethane MM4520 (SMP)..... | 45 |
| Figure 4.3. Extrusion temperature profile..... | 47 |
| Figure 4.4. Delamination between layers in specimen, layers completely separated showing a clean surface (left), as printed sample (right)..... | 47 |
| Figure 4.5. Different percentages of carbon fiber and SMP..... | 48 |
| Figure 4.6. Comparison of material with moisture trapped and dried material. (a)Presence of bubbles in extruded material. (b) Material after a drying stage in vacuum oven | 49 |
| Figure 4.7. Phase separation between SMP and CF PLA. The proportion was 50% of each one. Picture taken with a USB digital microscope. | 49 |
| Figure 4.8. 3D specimen designed on SolidWorks. | 50 |
| Figure 4.9. 100% Shape memory polymer 3D printed sample..... | 51 |
| Figure 4.10. Pre-tests performed on SMP samples..... | 52 |
| Figure 4.11. Recovery over 100% for SMP samples..... | 52 |

| | |
|--|----|
| Figure 4.12. Weight placed on the top of samples before annealing. | 53 |
| Figure 4.13. Recovery for annealed samples. | 54 |
| Figure 4.14. Sample preparation procedure. | 54 |
| Figure 4.15. Real displacement and temperature running in shape recovery flexural tests. | 57 |
| Figure 4.16. Force exerted by sample during shape recovery flexural stress tests. (a) Force vs displacement. (b) Force vs temperature | 58 |
| Figure 4.17. Repeatability of the experiments for SMP, SMP with 10% weight content of CF PLA (C10) and SMP with 20% weight content of CF PLA (C20). | 59 |
| Figure 4.18. Preparation of SMP sample for SRR and SRF tests. | 60 |
| Figure 4.19. Trajectory tracked for shape recovery ratio analysis. | 61 |
| Figure 5.1. Height dimension comparison among composites with standard deviation. (a) Height of samples. (b) Width of samples. (c) Area of samples | 65 |
| Figure 5.2. Discarded sample comparison. | 67 |
| Figure 5.3. SMP constrained shape recovery test. (a) Shape Recovery Force. (b) Shape Recovery Flexural Stress. | 68 |
| Figure 5.4. SMP and 10 wt. % CF PLA (C10) constrained shape recovery. (a) Shape Recovery Force. (b) Shape Recovery Flexural Stress. | 69 |
| Figure 5.5. SMP and 20 wt. % CF PLA (C20) constrained shape recovery. (a) Shape Recovery Force. (b) Shape Recovery Flexural Stress. | 69 |
| Figure 5.6. Shape recovery flexural stress for 100 wt. %SMP, 90 wt. %SMP and 10 wt. %CF15 PLA, 80 wt. %SMP and 20 wt. %CF15 PLA. (a) Shape Recovery Force vs time. (b) Maximum median SRFS with standard deviation. | 70 |

Figure 5.7. Shape recovery displacement. (a) Displacement for SMP samples. (b) Displacement for C10 samples. (c) Displacement for C20 samples..... 72

Figure 5.8. Shape recovery ratio. (a) SRR for SMP samples. (b) SRR for C10 samples. (c) SRR for C20 samples 73

Figure 5.9. Median shape recovery displacement and ratio. (a) Median displacement. (b) Median SRR..... 74

Figure 5.10. Shape Fixity Ratio for SMP, C10 and C20 with standard deviation. 75

LIST OF TABLES

| | |
|--|----|
| Table 2.1. Large scale 3D printers available in 2023 [45]. | 13 |
| Table 3.1. Specifications 300 Series Workbench [81]. | 25 |
| Table 3.2. Pulsar Pellet Extruder System [82]. | 27 |
| Table 4.1. Printing parameters selected in Simplify3D. | 51 |
| Table 4.2. Shape recovery flexural stress test process | 56 |
| Table 5.1. Sample's cross-sectional area before testing for shape memory polyurethane (SMP), SMP with 10 wt. % of CF PLA (C10), and SMP with 20 wt. % of CF PLA (C20). | 64 |
| Table 5.2. Shape fixity ratio for SMP, C10, C20 | 74 |

LIST OF ABBREVIATIONS

| Abbreviation | Definition |
|--------------|--|
| AM | Additive Manufacturing |
| LSAM | Large scale additive manufacturing |
| FDM | Fused Deposition Modelling |
| FGF | Fused Granular Fabrication |
| FPM | Fused Pellet Modelling |
| SMP | Shape memory polymer- Shape memory polyurethane MM4520 |
| CF PLA | PLA with 15% content of carbon fibers |
| C10 | Shape memory polyurethane MM4520 with 10% of PLA with 15% content of carbon fibers |
| C20 | Shape memory polyurethane MM4520 with 20% of PLA with 15% content of carbon fibers |
| DSC | Differential Scanning Calorimetry |
| TGA | Thermogravimetric Analysis |
| Tg | Glass transition temperature |
| SRR | Shape recovery ratio |
| SRF | Shape recovery fixity |
| SRFS | Shape recovery flexural stress |

1. INTRODUCTION

1.1. Introduction

1.1.1. Additive manufacturing and development of the 3D printer market

A novel technology that promises great advantages in manufacturing and design is Additive Manufacturing (AM). AM encompasses seven different types of processes: material extrusion, material jetting, binder jetting, vat photopolymerization, sheet lamination, direct deposition energy, and powder bed fusion [1,2]. The focus of this research is on extrusion-based material printing, also known as 3D printing. This AM technology is no longer limited to the academic research. Nowadays communities of designers, engineers, hobbyists, and the industrial sector are diving in the use of this technology.

The main benefits of 3D printing that attract the interest of new sectors and keep the investment are minimum waste, easy access, easy customisation, design freedom and flexibility, adaptability, and cost-effective technology [3]. The astonishing growth that 3D printing market has faced is optimistic. According to Wohlers Report 2018, Industry grew by 25.9% in 2015, by 17.4% in 2016 to reach \$6.063 billion, and all goods and services offered by AM companies expanded by 21% to reach \$7.336 billion in 2017 [4]. Hence, this development demands research about how to overcome 3D printing limitations and expand its boundaries even more.

1.1.2. Scaling up 3D printers

The 3D printing market expansion is evident; there is a necessity of scaling up this technology to accomplish a jump from a desktop-scale to a big manufacturing environment. Opting for large-scale additive manufacturing (LSAM) allows printing of larger and more complex parts without

the need for assembly, which diversifies and enhances possible applications of this technology. For example, during COVID-19, a face shield was printed in 2h using a traditional 3D printer. However, Bishop et al., using a big format 3D printer reduced the printing time of the face shield in less than 5min, the improvement is important due to less printing time is directly related to cost and energy consumption reduction [5]. As another example, Billah et al., showed that LSAM has the potential to save the dying tooling industries in many countries, by reducing 10 to 100 times the cost of fabricated moulds with a reduced production time [6].

To enhance LSAM the approach taken in this thesis is integrating a pellet extruder mounted in a large-scale 3D printer to open the pathway to direct 3D printing using pellets, hence eliminating the use of filaments required for extrusion-based AM technique. Polymer pellets are 5 to 10 times cheaper than FDM filament, and when used in 3D printing, higher deposition rates can be achieved [7–9]. Furthermore, available materials in the market in pellet form are greater than filaments (all industrial polymers can be found as pellets) [10,11].

1.1.3. 4D printing

4D printing is the process of additive manufacturing (3D print) objects that show a visible response to a stimulus. This feature could be used to print objects that self-assemble after printing to their final/permanent shape, or thermoresponsive circuits without the need of complex wiring [12,13]. These 4D printed objects could skip stages of the manufacturing process, saving time and reducing money, making manufacturing line simpler.

Talking about 4D printing, it is inherent to talk about smart materials. Smart materials are materials that change any visible or tangible property when they are exposed to an external stimulus such as temperature, light, electric field, magnetic field, pH, moisture, ions, etc. [14].

Among smart materials, the ones that can change their shape are of interest in this thesis. Shape memory materials can be divided into three main groups. Shape memory alloys (SMA), shape memory ceramics (SMCr) and shape memory polymers (SMP). When SMA, SMCr and SMP are compared, the drawbacks seen on SMP are low strength, low moduli, and low operating temperatures. In contrast, the numerous advantages are large deformation, tuneable glass transition temperature (T_g), lightweight, high strain recovery, low density, biocompatibility, biodegradability, and typically simpler to produce on large scale [15,16]. Due to all the benefits described and looking for a kind of material that is able to be processed using 3D printing technology, this research will focus on 4D printing using SMPs. Specifically, a shape memory thermoplastic polyurethane MM4520 is used due to its ease of processing and relatively low glass transition temperature (45°C) [17].

Nevertheless, in the process of scaling up 4D printing there is still a lack of understanding in certain areas that need to be investigated in depth; such as, the influence of large temperature gradients in LSAM on thermal behavior of the smart material, internal thermal stresses of big parts (residual stresses), annealing of smart materials, enhancement of polymer properties with reinforced composites for industrial applications. Each contribution in these topics would allow to improve this technology and lead to early expansion of 4D printing market.

1.1.4. 4D printing and scalability

The compatibility between smart materials and big format 3D printers makes interesting to research about additive manufacturing of large-scale components using shape memory materials. In the beginning, this jump from a desktop size component to a relatively large size shape changing component could be described as 4D printing scaled up. However, it is not as easy as saying that

using bigger 3D printers is scaling up 4D printing. There are challenges related to LSAM as well as the smart materials used to tackle first and they are listed below.

The high deposition rate in LSAM makes it difficult to avoid agglomerations of undesirable material on sharp corners and small radii of curvature. These errors accumulate layer by layer leading to geometrical defects [18,19]. To address this drawback, a correct understanding and control of smart material rheological properties is essential to calibrate an ideal flow rate.

Another major obstacle that constrained the development of LSAM is the chamber volume of the printer, not only in terms of structural components but also in terms of temperature control [20].

The bigger the chamber, the greater the thermal gradients. Big 3D printing volumes means a big and power heated bed, with chambers acting as an oven to control temperatures and avoid unexpected air flows. However, it is very difficult to keep the temperature stable in such large areas and temperature gradients are inevitable, which causes problems of big relevance like warping, delamination and cracks due to thermal stresses [21,22]. These temperature gradients could influence negatively in 4D printing too, where materials are being affected in large extend by thermal stimulus.

Finally, one intrinsic disadvantage of SMPs is their low shape recovery stress. On a larger scale, this low reaction stress might cause components to be unable to recover their permanent/original shape under their own weight. [23],[24].

During the research done for this thesis, a big lack of literature related to large scale 4D printing was evident. There are studies about PLA and TPU polymers, and large-scale 3D printing but the emphasis was on mechanical properties instead of shape memory properties. This makes this thesis a valuable contribution to the field, bringing solutions to large scale 4D printing drawbacks.

SMPs have intrinsic low mechanical strength and shape recovery stress, which have largely restricted the applications of SMPs. On the other hand, shape memory polymer composites (SMPCs) have proved to be able to tailor properties and improve mechanical strength. Certain amount of reinforcing fillers are able to improve the mechanical performance and shape recovery stress of SMPs [12,25–27].

For a thermoplastic polyurethane (TPU) the addition of multi walled carbon nanotubes has shown an increment in Young's modulus [26]. And, for epoxy-based SMP, unidirectional carbon fiber improved the shape recovery stress [28]. Moreover, carbon fiber blends can be easily purchased in the market. With the previous insights, the study of carbon fibers and the possible enhancement of the properties of shape memory polymers incentives the realization of this thesis.

1.2. Motivation

4D printing has the potential to break the paradigm of how products have been made to date. Allowing to come up with novel solutions to the biomedical, electronics and soft robotic applications. To continue with the widespread and adoption of this technology, it is necessary to move from small models and scaled prototypes, to be able to create larger parts, which can have a direct end use or application.

This thesis is motivated to study the feasibility of 4D print a thermoplastic polyurethane MM4520 (SMP) reinforced with carbon fibers (CF PLA) using a large format 3D printer. It is expected that the use of fillers will improve the properties of the shape memory polymer and thereby broaden its potential applications. Previous studies suggest that the addition of fillers could enhance not only shape memory effects of the polymer but also reduce the risk of warping or cracking of the

part during printing being able to operate without the necessity of a big heating chamber [22,26,28,29]. This study provides valuable knowledge for 4D printing scalability.

1.3. Thesis objectives

Objective 1:

- Commissioning of a 3D printer capable of direct pellet printing towards the ultimate goal of large scale 4D printing.

Objective 2:

- Optimization of production of carbon fiber reinforced shape memory composites.

Objective 3

- Characterize and analyze the effect of the constituents of the 3D printed composites on the shape memory properties.

1.4. Thesis outline

The first chapter is a description of the reasons that motivated the realization of this thesis and the objectives that are expected to fulfill. The second chapter is a brief review of concepts related with this thesis. This review will help for a better understanding of the following sections. Chapter three, named machine commissioning, is related to the first objective of the thesis and details how a large size 3D printer was modified to work with a high flow pellet extruder, with the purpose of 3D print a composite shape memory polymer. The chapter four talks about the raw materials used, preparation of samples and testing of shape memory effect. Then, chapter five shows the data obtained in the previous chapters and compares the different cases of study. Finally, the last chapter

presents the outcomes of the development of this thesis. After this, the section called appendices provides extra information regarding previous chapters.

2. BACKGROUND

2.1. Concepts brief review

2.1.1. Additive manufacturing advantages-Fused deposition modeling.

Additive Manufacturing (AM) is a technology that has had a huge development during the past decade. Depending on the material and the type of AM technology used, it can be classified into seven categories: material extrusion, material jetting, binder jetting, vat photopolymerization, sheet lamination, direct deposition energy, and powder bed fusion [1,2]. Each category has its pros and cons in terms of resolution, cost, time, materials availability, and mechanical properties. However, among the different AM process technologies, extrusion-based AM, also known as fused deposition modeling (FDM), is the most well-known and developed technique.

The key factors for FDM's success are the availability of materials, process autonomy, on-demand manufacturing for remote locations, generation of little waste, the possibility of using recyclable materials, and innovation [7,30,31]. Although 3D printing was first intended for rapid prototyping, its uses have grown over time. The number of AM applications is enormous, ranging from the medical field with 3D printed tissues that interact with the human body to aerospace due to its advantage in a zero-gravity environment, where powder or liquids cannot be used [32]. Nowadays, AM is gaining more importance and influence as it brings solutions and tools to face significant problems. A good example can be seen during COVID-19 when face shields and respirators were 3D printed and donated to medics around the world [33],[34].

In general terms, the 3D printing process can be divided into stages. The first stage begins with obtaining a digital model. This model can be created using a modeling software known as computer assisted design (CAD). The CAD software is used to capture an idea and convert it into a digital

file, usually a file with .STL extension (see Figure 2.1). Digital models are not only available to people with expertise in AM, but also for common users at home. An alternative to avoid the design stage are online repositories where a huge variety of 3D models can be downloaded.

In the next stage, the model is sliced into several layers by a software that in general terms is called slicer, e.g. Ultimaker Cura, Prusa Slicer, Symplifi3D. The slicer provides all the instructions needed by the 3D printer to generate each layer (see Figure 2.1). It has been proven that parameters selected during the slicing stage play an important role in the final properties of the 3D printed part and its selection is always a trade off [35,36]. Printing parameters for conventional desktop-size FDM machines have been studied by many researchers [37–39]. These parameters are highly dependent on the chosen material, but some general criteria can be used as a guide. If a tedious post processing wants to be avoided and a nice surface finish is desired, a low layer height must be used (0.1mm to 0.15mm). However, the lower the layer height the longer the printing time. For mechanical strength, printing orientation plays the most important role. Depending on the loading conditions the orientation of the part must be chosen because the weakest zone in a 3D printed part is the contact surface between layers (layer bonding). So, the printing orientation should be aligned with the load. Moreover, the percentage of infill has a big influence on the strength, printing time, and amount of material required (infill increments will increase the mentioned features too). Although enclosed desktop 3D printers are more expensive, they help to have a low temperature variation of temperature during 3D printing. This is important when materials with high thermal retraction are used. After all parameters are tuned depending on the specific application, these instructions are saved in G-code format.

It is evident that 3D printing parameters like infill, printing orientation, layer height, printing temperature and their influence on end-specimen properties are well studied in the literature for

desktop 3D printers. Nevertheless, to expand the boundaries of 3D printing, scalability is a must. Large scale 3D printing increases the number of applications where this manufacturing method can be used.

The stages described up to now related design and slicing of parts are followed independently of the size of the 3D printer (desktop or large-scale 3D printer). In Figure 2.1 a 3D printed part designed and sliced. It was desired to have a rectangular specimen to be tested under bending conditions, hence SolidWorks (student license) was used to draw it and the file was saved as .STL extension. Then, Simplify3D was used to set up all the parameters related to the 3D process. The parameters used in this thesis are detailed in Table 4.1. In Figure 2.1b can be seen the preview that the slicer offers of the sample before 3D printing. The numbers of layers and type on infill can be distinguish by colors.

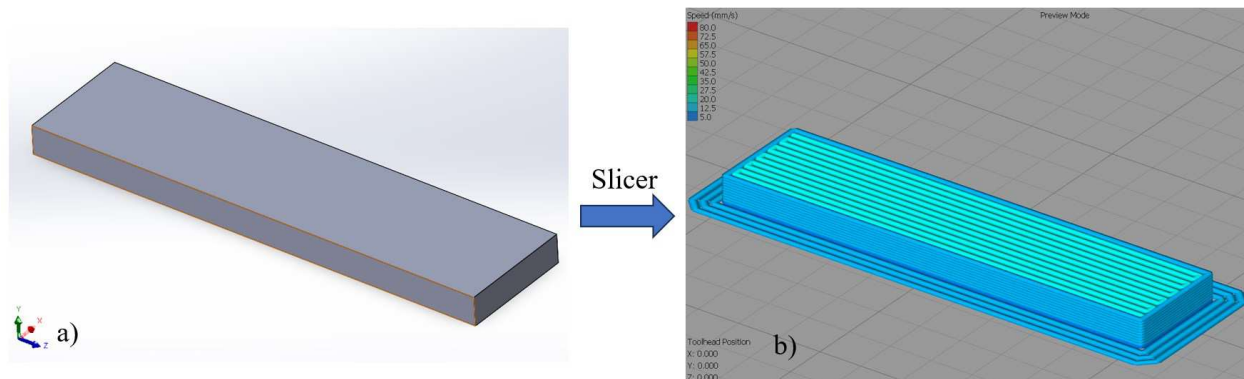


Figure 2.1. a) Shape memory samples designed on SolidWorks b) samples sliced on Simplify 3D.

Once all parameters are selected in the slicer and the G-code was generated, the final stage corresponds to the functioning of the 3D printer. In this stage, the polymer is heated up to the melting point and deposited layer by layer in a according to the parameters in the G-code. Also, it is a common practice to have a heated bed to promote good adhesion of the 3D printed part and avoid warping due to thermal stress gradients. The general elements described before can be seen

in large-scale or desktop 3D printers. In Figure 2.2 is observed a cylinder being 3D printed in a large-scale 3D printer



Figure 2.2. Big format 3D printer model 300Workbench from 3D Platform printing a cylinder.

As 3D printing is being more widely adopted, it is expected in the future to have places working with multiple 3D printers where the users could avoid previous stages. Instead, users will be limited only to buy digital models, send it to be 3D printed and just pick up the product in person or have it delivered [40].

2.1.2. Large scale 3D printing and its challenges.

Industries are always looking for manufacturing methods that could produce parts and products in a cost-effective manner. Large scale additive manufacturing (LSAM) brings the principles of a desktop 3D printer and offers a reliable, flexible, and relatively easy to use technology with a variety of optional materials. However, it is not as easy as just building a big 3D printer. The upsizing involves many challenges. The main challenges found in literature are: 1) Enormous

heating chambers to avoid warping and cracking due to unexpected air flows. 2) Generation of internal stresses due to high temperature gradients along the extruder, 3D printed part and heated bed. 3) The availability of bulk material for large 3D prints could be a big issue (imagine buying a spool for 3D print a 35kg weight part). 4) Selection of a correct flow rate 5) Poor resolution in large parts that leads to tedious post-processing [41].

The first challenge arises when desktop 3D printers designs were extrapolated to large scale. Desktop 3D printers are classified as open frame and enclosed frame. An enclosed frame, where the part is 3D printed inside an enclosure (walls usually made of MDF, glass or acrylic), provides protection against air flows and stable thermal environment. Although scaling an enclosed frame could help to improve the temperature control and at the same time protect internal components from dust, could be costly and extra mass would be added due to the frame. That extra mass of the components added plus the weight of large 3D printed parts could cause vibrations on the moving components of the printer and negatively affect the print quality[42]. Furthermore, a big heating chamber will transfer a considerable amount of heat to the environment that could cause ergonomic concerns for people working around and the electronics performance could be compromised [41].

The generation of internal stresses is another challenge in LSAM. Large size 3D printed parts need high amounts of material deposited at high temperatures. The temperature difference between the top layers and bottom layers is large which causes that material to shrink and expand at the same time. These temperature gradients lead to thermal stress in the material (internal stresses) [21,22]. New materials with low thermal coefficients will help to mitigate the influence of thermal gradients.

The available material to be used during printing is another issue. Filaments are only commercially available from 5kg to 10 kg, which restricts the size of the printed parts. A feasible solution used by researchers and companies is to work with pellets instead of filament [13,43,44].

Another aspect to consider is the amount of material that is effectively melted and deposited when 3D printed. To produce big parts using LSAM, large rates of material deposition are used. The hot end temperature and printing speed must be perfectly tuned to ensure correct heat conduction between the nozzle and the polymer being melted. This ensures good layer adhesion and dimensional accuracy [41]. Finally, with more material being extruded, a topic always in discussion is the trade-off between print quality (related to layer height) and overall print time. In LSAM the use of large layer height and its influence on surface smoothness and interfacial bonding of layers is more notorious. And post-processing steps like sanding and polishing can be time-consuming. However, none of these drawbacks have stopped the development of this technology. LSAM is already being commercialized around the world. Table 2.1 shows a summary of big format 3D printers with prices and specifications. Additionally, an important equipment that must be mentioned is the one developed by The Oak Ridge National Laboratory (ORNL) and Cincinnati Inc. which has a surprisingly high print volume of 6096×2286×1828 mm [22].

Table 2.1. Large scale 3D printers available in 2023 [45].

| Brand | Product | Build size[mm ³] | Country | Price |
|----------------------|---------------------|------------------------------|---------------|-----------|
| Modix | BIG-Meter V4 | 1010×1010×1010 | Israel | \$13,500 |
| CreatBot | F1000 | 1000×1000×1000 | China | \$29,999 |
| 3D Platform | 400Series Workbench | 1000×1500×700 | United States | \$49,999 |
| Tractus3D | T3500 | ∅ 1000x2100 | Netherlands | \$59,000 |
| Filament Innovations | POSEIDON | 1060×1080×1050 | United States | \$125,000 |
| The Industry | MAGNUM | 1500×1200×1200 | Sweden | \$179,000 |

| | | | | |
|-------|--------------|----------------|---------------|---|
| Modix | MAMA | 2000×5000×1000 | Israel | - |
| ORNL | BAAM printer | 6096×2286×1828 | United States | - |

All 3D printers shown in Table 2.1 use a filament and the last three printers are hybrid (are able to work with filament and pellets). To mention a few applications of polymer based LSAM, Local Motors 3D printed a functioning vehicle except the powertrain using ABS and carbon fiber in 2014 [43]. More than a thousand parts were produced by Airbus using 3D printing for its new A350 XWB aircraft [46]. And during COVID, Bishop et al., printed a face shield in under 5 min (which normally would take 1-2 hours) [5].

In specific, this thesis was developed using the 3D printer 300 Series Workbench (a previous version from 400 Series Workbench listed on Table 2.1). Previous thesis has been done on this equipment and proved that is able to 3D print parts on a large scale [47]. A 3D printed real size chair of 770mm x440mm x450mm using PLA was produced as a case study (see Figure 2.3) [47].



Figure 2.3. Real size 3D printed chair using big format 3D printer 300Series WorkbenchPro [47].

As mentioned, one of the limiting factors of this machine is its dependency on filaments that are available on the market. A direct 3D printing using pellets is more desirable due to the wider availability of materials as pellets in the market.

2.1.3. Fused Granular Fabrication

Fused Granular Fabrication (FGF), also known as Fused Pellet Modelling (FPM). FGF uses pellets as the raw manufacturing material. Even though LSAM is a flexible technology and can work with FDM or FGF systems, the last one offers numerous benefits when large scale parts are manufactured. In Figure 2.4 can be seen a schematic of an FGF system that in brief consist of a screw that conveys pellets into a heating element where they are melted and then extruded through a nozzle [48,49].

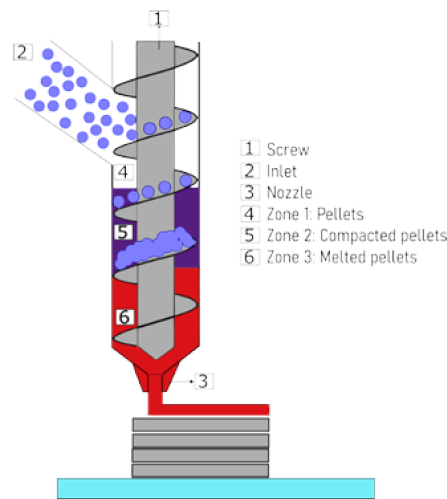


Figure 2.4. Scheme of FGF system.

FGF tackles some disadvantages related to LSAM and FDM. Common filament spools for LSAM available in the market are 5kg or 10kg, which restricts the size of 3D printed parts that can be done without pausing the print. Furthermore, big filament spools demand high torque motors to feed the extruder. In this sense pellets are an easier system where they are sucked into the extruder

screw. In addition, pellets can be purchased in bulk and due to it less processing are cheaper. Pellets price is at least four times cheaper than filament and the difference can be even higher for special materials (e.g. fiber reinforced fillers) [7–9].

Using pellets avoids subjecting the material to as many heating cycles as when the filament is used. Numerous heating cycles negatively affect molecule structure and consequently material mechanical properties [50–54]. Pillin et al., reported PLA's viscosity strongly decreased from 3960 to 713 [Pa s] after only one injection cycle [53]. And Cruz Sanches et al., have shown that PLA for 3D printing decreases its mechanical properties (elastic modulus, tensile strength, tensile strength) by more than 70% after 5 recycling cycles [54].

Furthermore, the use of pellets avoids the necessity of strict filament dimensions control (inconsistency in filament can cause over extrusion or under extrusion, clogging, or even blocking 3D printer's feed mechanism, resulting in failed 3D prints [55,56]). Moreover, the availability of materials in the market in pellet form is greater than filament (all industrial polymers can be found as pellets) [10,11].

Related to waste management and environmental care, a life cycle analysis about polymer recycling done by Kreiger et al., has shown that the use of FDM to recycle plastic at home (plastic waste is processed and used for 3D printed again), uses less embodied energy than centralized recycling in a consolidation center (recycled plastic is consolidated and transported to a specialised recycling centre) [57]. Although, the study is related to FDM technology, the results are promising for FGF because it is a simpler technology in terms of recycling. FGF can use shredded plastics and skip the filament production necessary for FDM. FGF offers a simpler, cheaper, and faster recycling process in comparison with FDM. The excellent performance of large-scale 3D printed

parts using recycled plastic has already proven environmental and financial viability in the study [58].

Furthermore, using pellets avoids subjecting the material to as many heating cycles as when the filament is used. Numerous heating cycles negatively affect molecule structure and consequently material mechanical properties [50–54]. Pillin et al., reported PLA's viscosity strongly decreased from 3960 to 713 [Pa s] after only one injection cycle [53]. And Cruz Sanches et al., have shown that PLA for 3D printing decreases its mechanical properties (elastic modulus, tensile strength, tensile strength) by more than 70% after 5 recycling cycles [54].

2.1.4. 4D printing, smart materials, and shape memory polymers

Working with pellets allows to study various engineering polymers and among them there are so-called smart materials that are materials that react to external stimuli. These materials change their properties (such as shape) when they are exposed to stimuli such as physical, chemical, or biological [59].

In the case of smart materials that can show a change in shape we refer to them as shape memory materials. These materials can be ceramics (SMCs), alloys (SMAs) and polymers (SMPs). Polymeric smart materials can be classified into hydrogels, liquid crystal elastomers (LCE), and SMPs. Shape memory polymers (SMP) are a special class of shape memory materials that offer great advantages such as low cost, lightweight, and tailorable properties over other shape memory materials [60].

Moreover, when 3D printing is used with shape memory materials, it is called 4D printing where the 4th dimension is considered as time. One of the first mentions of 4D printing was at the 2012 TED conference when Tibbits defined the concept of 4D printing as an object that can be additively

manufactured and could change its shape over time [61]. Manufacturing complex objects using 4D printing that responds to external stimuli has many potential applications. A few conceptual ideas can be listed as clothing that could react to body temperature allowing ventilation or thermal insulation, any wearable device that changes colors in response to environmental conditions like light, moisture, or temperature is useful for camouflage, and components that can self-fold like a kayak that could be transported easily without the necessity of a big space [62,63]. In particular, SMPs are already being used in several engineering applications like customized airflow 3D-printed cardiovascular stents, splints and staples for open wounds in biomedical applications, thermo-responsive actuators in electronic circuits, robotic fingers, actuators for soft grippers for robotics [64–68].

SMP can be classified as thermoplastics or thermosets depending on the nature of their bonds [13,69]. SMP thermoplastics consist of hard-crystallized and soft-amorphous segments with different transition temperatures (the temperature at which polymeric chains acquire mobility) that leads to a shape memory effect (SME) [70]. SME is a consequence of internal stress generated during the programming process [71]. This stored energy is released in the recovery stage and can respond to several stimuli like heat, magnetic fields, moisture, electrical current, light exposure, PH value, and water immersion [23,71].

This research focuses on thermally induced shape memory polymers, more specifically in shape memory polyurethane and from this point onwards we refer to it in general as SMP. SME of SMP can be observed when the material reaches the activation temperature, i.e. the glass transition temperature (T_g), to transition between a temporary deformed shape and a permanent shape. When the polymer is heated above T_g , it softens, making it easy to deform. Then, the distorted shape can be fixed by cooling it down below T_g while a constraint is applied to the material. This process is

called programming [13]. Then, when the sample is re-heated above T_g , it recuperates its original form due to the SME [72].

2.1.5. Shape recovery characterization:

The shape memory effect (SME) for a SMP mentioned above can be characterize based on shape recovery ratio (SRR), shape recovery fixity (SRF), and shape recovery stress (SRS), and shape recovery flexural stress (SRFS).

Shape recovery ratio (SRR) describes the amount that SMP can recover after being deformed and corresponds to the relationship between the initial position of any point of the sample analyzed and the final position of the same point when a recovery stimulus is applied after the programming. Cersoli et al., used a flat, rectangular specimen that is bent into a "U" form around a rod. The reference angle for the flat specimen is $\theta_{max}=180^\circ$ and the angle that is obtained after heating above T_g is noted as θ_r . SRR is determined by dividing θ_r by θ_{max} [13]. Even though this setup for the experiment seems simple, it has too many uncontrollable variables as the deformation rate, deformation force, and accuracy to measure deformation angles. On the other hand, Fengfeng et al., used the setup for three-point bending tests. The specimen was simply supported inside a heating chamber, deformed under bending, and it is activated to recover [28]. This approach allows to have high repeatability among various experiments due to it follows the standard ASTM D790 for bending, and it is the approach taken for this thesis. A deeper explanation of the methodology can be found in Chapter 4.

SRF describes the difference between the location of a point of the sample when is deformed, constrained, and cooled with the location when the constraint is removed. In the schematic of Figure 2.5, in a) can be seen the initial stage with the sample and its initial/permanent shape, follow

by b) where the sample is deformed at $T_g+15^\circ\text{C}$ and cooled while it is constrained, then in c) the constraint is removed and the sample heated until it reaches the final shape in d).

Finally, shape recovery flexural stress (SRFS) describes the relation between the force generated for the sample when it is heated and the cross-sectional area while it tries to recover the initial shape.

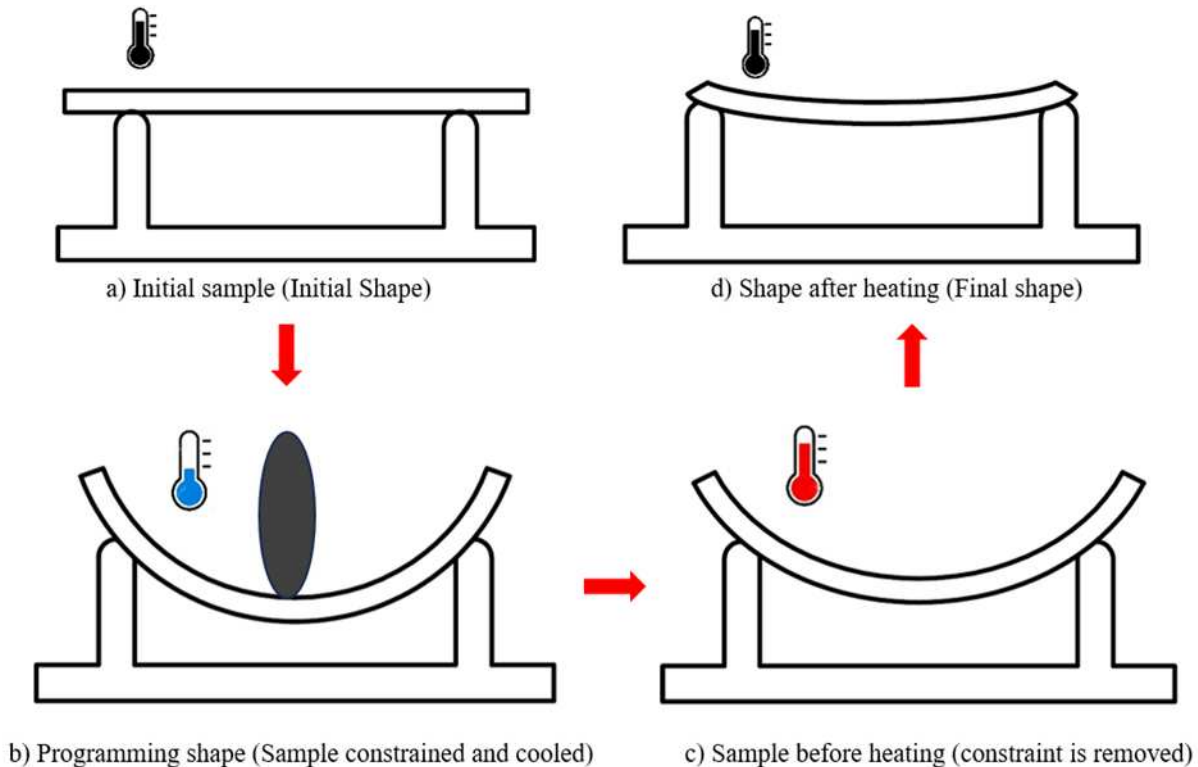


Figure 2.5. Schematic of shape recovery ratio and shape recovery fixity tests.

A thermoplastic shape memory polymer is studied below due to its characteristic of being 3D printed. Furthermore, studies on SMPs and their compatibility with FDM printability have been already done at the University of Alberta. Villacres et al., studied the effects of print orientation and infill percentage in the mechanical properties of SMP [35]. As well as most 3D printed parts, SMP showed that high infill percentages increase the elastic modulus and UTS of SMP.

Additionally, a print orientation aligned with the load applied increases the UTS and elastic modulus as well [35,73]. Raasch et al., analyzed the influence of annealing in 3D printed SMP properties. Different annealing temperatures were tested, concluding that the best combination of dimensional stability and shape recovery properties is obtained when samples are annealed at 85°C for 2 hours [72]. Zonoobi et al., propose an algorithm based on classical laminate plate theory (CLPT) to estimate the elastic modulus of the EBAM parts. For the longitudinal elastic modulus for any stack sequence, information on the elastic modulus of 0° and 90° raster angle needs to be known as input in the model [74]. And Garces et al., studied the effects of moisture on SMP, observing a negative effect of moisture on print quality, mechanical and shape recovery properties of the material [70].

A common outcome in the studies presented before is the low actuation stress of SMPs. This drawback becomes important when large scale parts are manufactured. In a large part after being deformed (programming stage), a low shape recovery stress could make it impossible for the part to recover under their self-weight during the recovery stage [24]. To overcome this drawback the literature suggests the addition of fillers to improve the properties of [23,75].

2.1.6. Reinforced polymers

Composite materials are a feasible way to enhance the properties of SMPs. Researchers have proved that the addition of certain fillers makes possible to tailor desired properties such as young and enhance the SME of SMPs. Related to polymeric blends and SME, Zhang et al., reported that PLA modified with PEEK content of 15% can have a shape recovery ratio and a shape recovery fixity of more than 99% with a fast response of 2s [76]. Moreover, the shape-memory characteristics of PLA are increased by the addition of modified graphene oxide because it decreases the relaxation time of molecule motion and improves the entanglement density

according to [77]. For TPU, Wang et al., showed the feasibility of 3D printing a PLC/TPU composite with a fixity ratio of 100% and a SRR of 81.1% [78]. Horastani et al., reported that for a PLA/TPU blend is possible to lower the glass transition temperature (T_g) when 5% of nanoclay content and 10% of PEG content are added to the composite [79].

Cho et al., with the aim to electroactive actuators, studied Polyurethane composites with multi-walled carbon nanotubes (MWCNTs) using voltage as a stimulus (not heat) [27]. The surface of MWCNTs was chemically modified looking for improvement of interfacial bonding. Results showed that surface modified composites improved mechanical properties. However, the electrical conductivity decreased in comparison to non-surface modified composites[27]. To balance mechanical properties with electroactive shape recovery properties, a 5 wt. % modified MWCNT is recommended [27].

Similar studies done using additive manufacturing are done by Tzounis et al., and Nguyen et al., 3D printed TPU/MWCNTs were done by [26], observing a material that reacts to the thermal and electrical stimulus with enhanced mechanical properties. While Nguyen et al., compared a composite SWCNT/SMP 3D printed with SMP combined with silver paste using PolyJet to create the internal silver paste lines. Although the heat energy supplied was the same for both samples, the MP/silver paste samples reached a higher temperature than SMP/SWCNT composite. Hence the recovery time on SMP/SWCNT was longer than SMP/silver paste. However, regarding mechanical properties, a higher Young's modulus is observed on SMP/SWCNT[25]. An interesting finding that must be mentioned is that when different ratios of SWCNTs are tested, can be seen that the higher the ratio, the less likely it is to recover [25].

Another study made by Ly et al. about polyurethane-based thermoplastic (SMP) with 3%wt of CNT observed that high temperatures, high infill rate, and low fee rate increase the conductivity

of the 3D printed sample [59]. Moreover, the researcher faced some issues with nozzle clogging [59].

Finally, the research made by Li et al., studied SMP epoxy base samples reinforced with different mass fractions (16%,23%, 30%,37%) of carbon fibers are tested under bending conditions. When the samples are compared, the results show an increase in maximum recovery stress with ratios of 47.7% (23 wt%), 140.3% (30 wt%), and 197.5% (37 wt%) making it possible to say that higher the contents of carbon fibers lead to a higher recovery stress on base epoxy SMP [28].

From the literature reviewed about developing SMPCs, it is always important to keep in mind that filler material decreases polymer mobility, which might impact the raw material's SME properties [80].

This thesis is motivated to find ways to improve the properties of SMP so they can be used in large scale applications. As was stated above, the use of fillers seems to be a feasible solution. Hence, PLA reinforced with carbon fibers a chosen to create a composite with SMP due to its wide availability in the market, affordability, and especially due to previous literature that has shown the enhancement of SMP using carbon fibers or carbon nanotubes (single and multiwalled). The novelty that this work presents is the study of the influence of carbon fibers in a thermoplastic shape memory polyurethane composite that is obtained using a large-scale 3D printer. Furthermore, the method used to obtain the samples tested is much simpler and does not require a sophisticated equipment in comparison with the methods described above.

2.2. Conclusions

Shape memory materials have proved to have the potential to have countless applications in the industry, especially when they are adapted to be manufactured using additive manufacturing techniques. The term used to refer to the process to obtain 3D printed materials that response to external stimulus is 4D printing. Although 4D printing is a promising manufacturing method, its widespread has been limited to small scale size applications.

To scale up this technology and facilitate an early adoption in the market it is necessary address its drawbacks such as the low recovery stress of shape memory polymers and the negative influence of thermal gradients in large scale 3D printed parts. It is evident that there is still missing in the literature an approach that connects 4D printing with large-scale applications and solves the issues described before. A promising candidate are reinforced composites.

For this reason, shape memory polyurethane MM4520 reinforced with PLA-Carbon fibers is studied and parameters such as SRR, SRF, and SRFS are obtained to evaluate the performance of the composite in a standard framework.

3. COMMISSIONING OF THE MACHINE

3.1. Large scale equipment

A big format 3D printer from 3D Platform, model 300 Series Workbench Pro was used in this thesis. The technical specifications are detailed in Table 3.1

The printer has installed two Fused Filament Fabrication (FFF) nozzle systems also known as high flow extruders (HFE 300) that allow printing a single part with two different filament spools. In Figure 3.1 can be seen the big area 3D printer with a 3D printed part using black and white PLA (both filaments were used to print different sections of the same part).

However, one of the limitations of fabricating large scale SMP composites is the filament availability. A solution is to 3D print using direct pellet extrusion. Hence the commissioning of the 3D printer with a pellet extruder system was necessary.

Table 3.1. Specifications 300 Series Workbench [81].

| 300 Series Workbench Pro | |
|--------------------------|---|
| Maximum Volume | 1000mm x1000mm x700mm (0.7 m ³) |
| Extruder type | HFE 300 |
| Nozzle diameter | 1mm |
| Max Flow rate | 70mm ³ /s |
| Filament diameter | 2.85 mm |

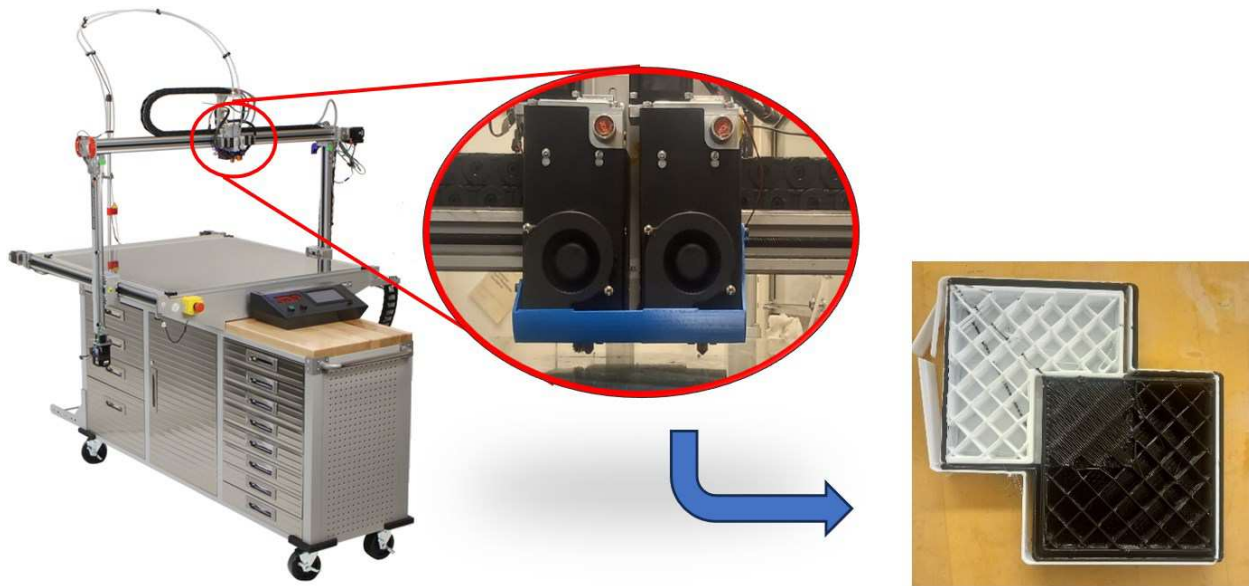


Figure 3.1. Big format 3D printer model 300 Series Workbench Pro with high flow extruders (HFE 300).

3.2. Integration of pellets extruder system

As it is stated in previous sections, it is desirable to work with pellets to avoid additional heating and melting cycles of the raw material. After evaluating several options in the market, a system able to print (extrude) with pellets and be adapted to the 300 Series Workbench Pro 3D printer was bought from Dyze Design [82]. The items listed by the manufacturer for the system called Pulsar Pellet are shown in Table 3.2. For ease of explanation, the installation of the system will be divided into three sections: pellet extruder head, electrical connections and firmware, and auxiliary systems.

Table 3.2. Pulsar Pellet Extruder System [82].

| Item | Quantity |
|--|----------|
| Pulsar™ Pellets Extrusion System (Liquid cooling system and pellet feeding system) | 1 |
| Pulsar™ Heatcore | 1 |
| Pulsar™ Extrusion Screw | 1 |
| NEMA23 Stepper Motor | 1 |
| 10A Solid State Relay (SSR) | 3 |
| Digital Stepper Motor Driver | 1 |

The core of the pellets extrude system is the new toolhead called Pulsar Pellet Extruder bought from Dyze Design. This toolhead is capable to extrude pellets at a high flow rate of 500 mm³/s (2.5kg/h) with a high resolution due to the customized screw design for 3D printing and high torque motor NEMA23 (Figure 3.2a). The Pulsar Pellet extruder has three heating zones that ensure a constant temperature in the polymer. With 1100 watts of heating power, each heating zone can reach a maximum temperature of 500°C in the nozzle and keep a stable high flow. The reliable and precise temperature readings are ensured using PT 100 temperature sensors placed 0.50 mm away from the molten polymer (Figure 3.2b). About printing resolution, nozzle diameters available are from 1mm up to 5mm.

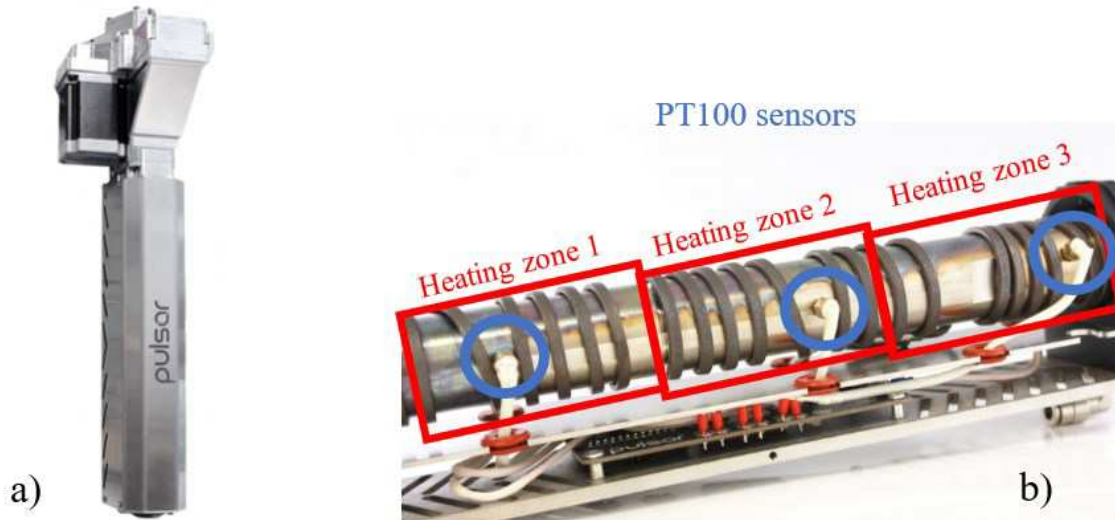


Figure 3.2. a) Pulsar Pellet Extruder by DYZE [82] b) Internal heating elements of Pulsar Pellet Extruder modified from [82]

3.3. Installation of pellet extruder head in large scale 3D printer.

To have a machine that can handle pellets and filament as printing materials, the installation process began with the dismantling of an extruder (HFE 300) to make room for the Pulsar pellet extruder (see Figure 3.3a). The existing aluminum plate, where the HFE 300 was mounted doesn't have holes for the new toolhead and there is not enough room for modifications. Hence, new mounting plates to mount Pulsar Pellet Extruder and HFE 300 were designed. Therefore, the two nozzles were disassembled from the printer and distances between the holes for the new aluminum plate were measured to avoid any interference (Figure 3.3b). A proper alignment between the toolheads and the frame is necessary to ensure a consistent layer height along the 3D printed part which means good quality conditions.

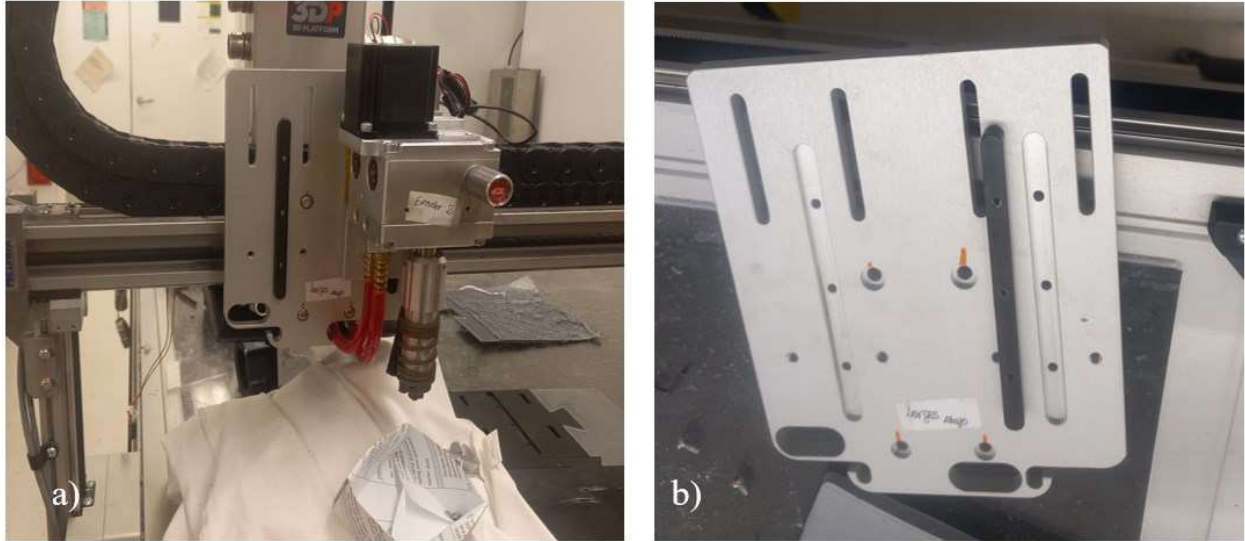


Figure 3.3. Dismounting nozzles from 3D printer. a) Single nozzle mounted b) Initial plate to hold nozzles

To prototype and test the mounting mechanism, several plates were 3D printed and tested. In Figure 3.4a from right to left can be seen the first design of the plates and the final design respectively. Designs were improved with the premise of reduce the amount of material in the plates as much as possible, so the extra weight added does not affect the 3D printer functioning. Moreover, interference between elements, as the one that is seen in Figure 3.4b between extruder cables and the mounting plate, was checked and corrected. Finally, the distance between holes of the plates and the frame is adjusted until a successful mounting is achieved (Figure 3.4c). Furthermore, requirements like adjustable toolhead height with respect to the bed, modifications to accomplish a lightweight design as well as machinability were considered.

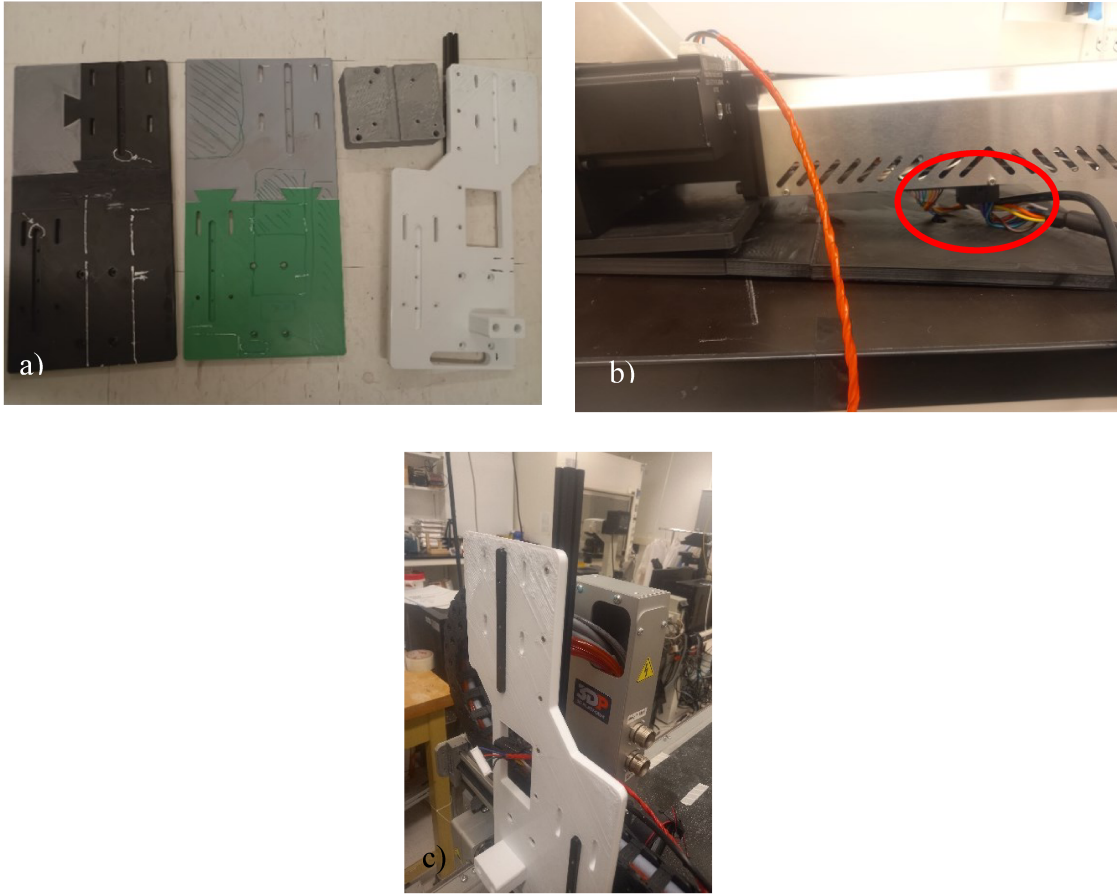


Figure 3.4. Plates design. a)3D printed plates iteration b) Example of interferences in designs c)

Testing of plates.

With the final design generated in SolidWorks (Figure 3.5a), the plates were sent get manufactured to the mechanical engineering machine shop of the University of Alberta, one plate was machined and the other two were done with laser cut (Figure 3.5b). 6061 aluminum was used for the plates due to its relative low cost ease of obtaining. Furthermore, the final setup of the plates with the frame and the Pulsar Pellet Extruder can be seen in Figure 3.6. Detailed drawings of each plate can be found in Appendix 1.

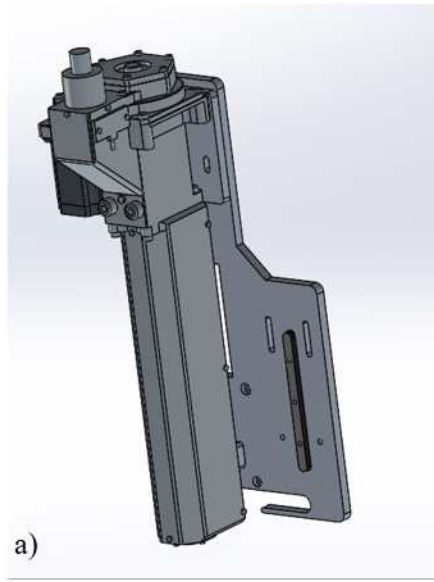


Figure 3.5. a) SolidWorks design for plates b) Plates done in machine shop

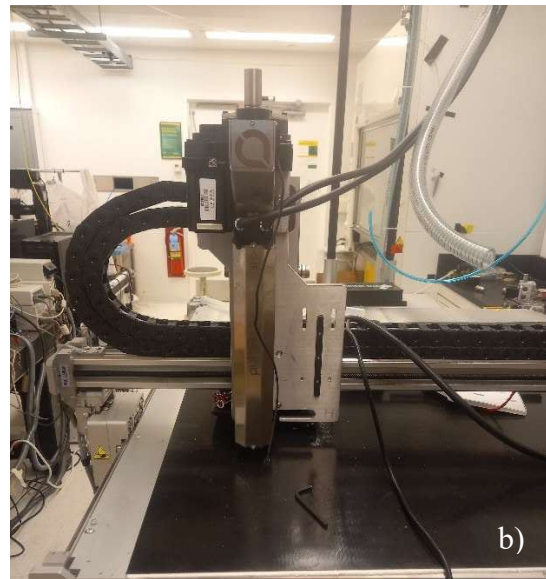


Figure 3.6. a) Plates bolted to the frame. b) Pulsar Pellet Extruder Mounted.

Due to the extra weight added, the deflection of the beam that support the toolheads is calculated to check any deformation that can influence negatively in the functioning of the equipment. On

Figure 3.7a is presented the front view of the beam supporting the filament extruder and in Figure 3.7b can be seen the simplification of the loading scenario. For the following calculations the cross beam that support the toolheads is considered as a simple-supported beam with a load in the midspan (in order to calculate the maximum deflection).

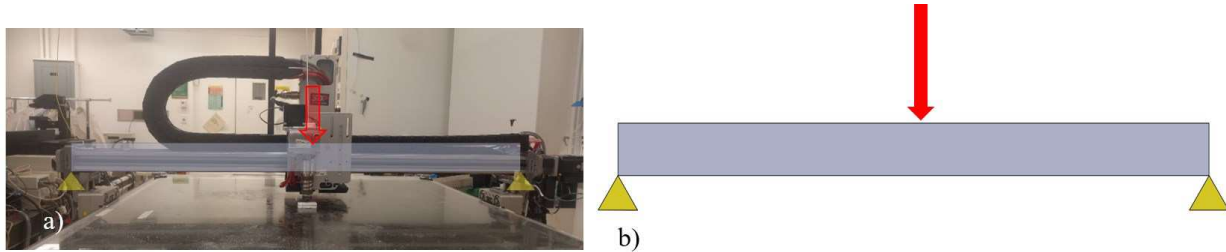


Figure 3.7. a) Cross beam that will support the weight of the toolheads. b) Simplification of loading scenario.

The equation that describes the deflection of the beam is:

$$Deflection = \frac{-PL^3}{48EI} \quad \text{Equation 3.1}$$

Where:

supports. It was considered the pellet extruder (7kg), filament extruder (3.03kg), aluminum plates (2.12kg), bolts (2kg).

L= Length of the span=1000[mm]

E= Young's modulus for aluminum 6061 = 69×10^3 [N/mm²]

I= Moment of inertia. This value was calculated according to geometry of the cross-sectional area of the beam=336380.7 [mm⁴]

Substituting the values on Equation 3.1, the beam deflection corresponds to 0.124 [mm]. In large scale 3D printed parts, the influence of that maximum beam deflection could be neglected due to commonly used layer heights. Moreover, that deflection could be easily corrected with proper bed leveling of the 3D printer.

3.4. Auxiliary systems and electrical wiring of Pulsar Pellet Extruder

3.4.1. Auxiliary systems

The two auxiliary systems were installed for the pulsar pellet extruder were the liquid cooling system and the pellet feeding system. The liquid cooling system consists of a heat exchanger that pumps distilled water (recommended by the manufacturer) to cool down the pulsar pellet extruder, then the hot water returns to the heat exchanger where it is cooled by air force convection to be pumped again and the process starts again. Holes were drilled in the frame of the printer to attach the heat exchanger on one side and black hoses were connected between the pulsar pellet extruder and the cooling liquid system (Figure 3.8a and Figure 3.9). Finally, this system uses a power supply of 12 volts that was placed on the rear part of the 3D printer, besides the power supply for the pellet feeding system and the printer (Figure 3.8b)

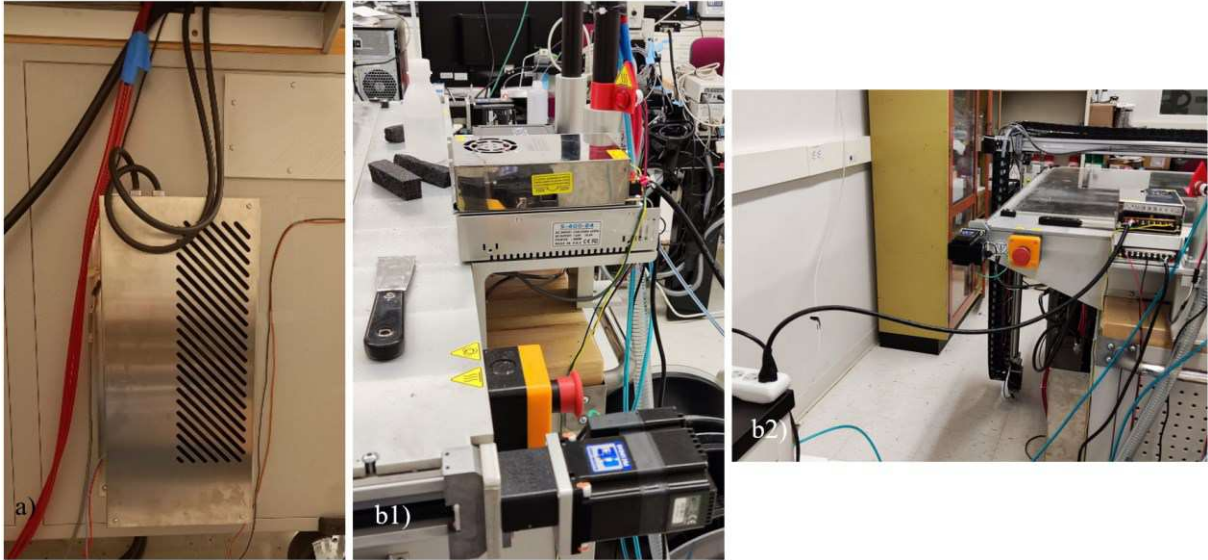


Figure 3.8. Liquid Cooling System. a) Heat exchanger and pump. b) Power supplies

The pellet feeding system consists of a controller that uses a sensor to check the presence of pellets in the hopper of the pulsar pellet extruder. In case of detecting a low pellets level, the controller making use of compressed air, sucks the pellets and conveys them to the hopper. The fume hood in the lab was chosen as source of compress air and the controller was placed at the rear part of the 3D printer (Figure 3.9a). The liquid cooling and the pellet feeding system connected and to the toolhead can be seen in Figure 3.9 b.

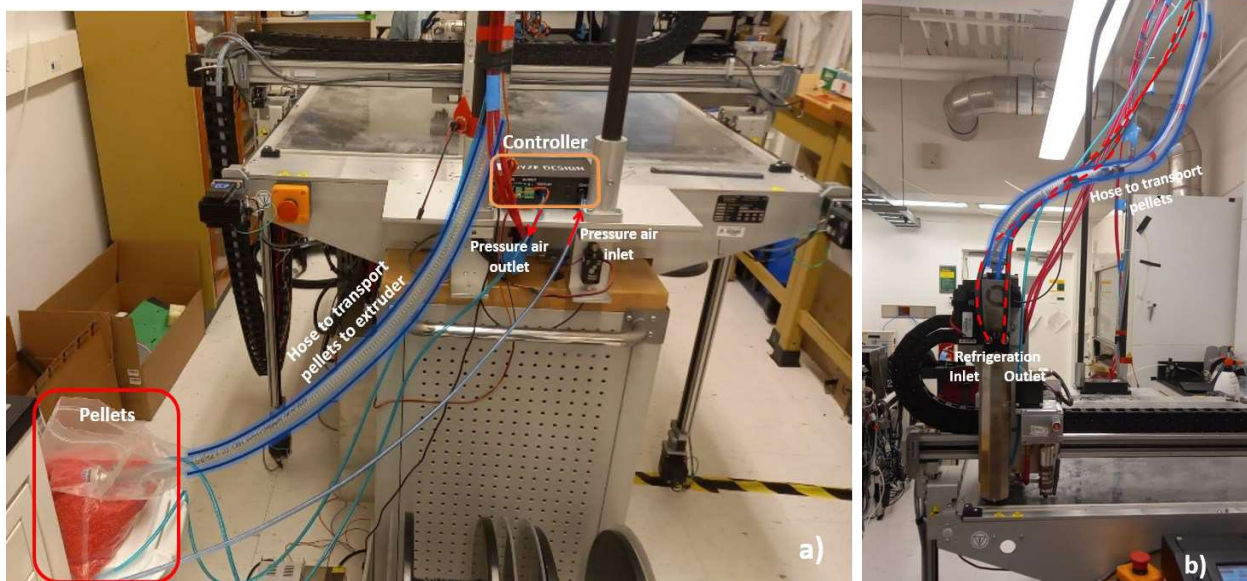


Figure 3.9. a) Pellet Feeding System b) Liquid cooling system.

3.4.2. Electrical wiring and firmware update

The new setup works with two toolheads. The first toolhead is the Pulsar Pellet Extruder that works with pellets. This toolhead has three heating zones and three temperature sensors. The second toolhead works with filament and has one heating zone and one temperature sensor. In total the new setup has 5 heating elements and 5 temperature sensors (one extra for the heated bed). Unfortunately, the controller called Duet 2 Ethernet installed on the 3D printer 300 Series Workbench Pro has not enough pins for the extra connections (see Figure 3.10). It was necessary to purchase an expansion board for the extra heating elements and a two PT100 daughterboards for the extra temperature sensors.

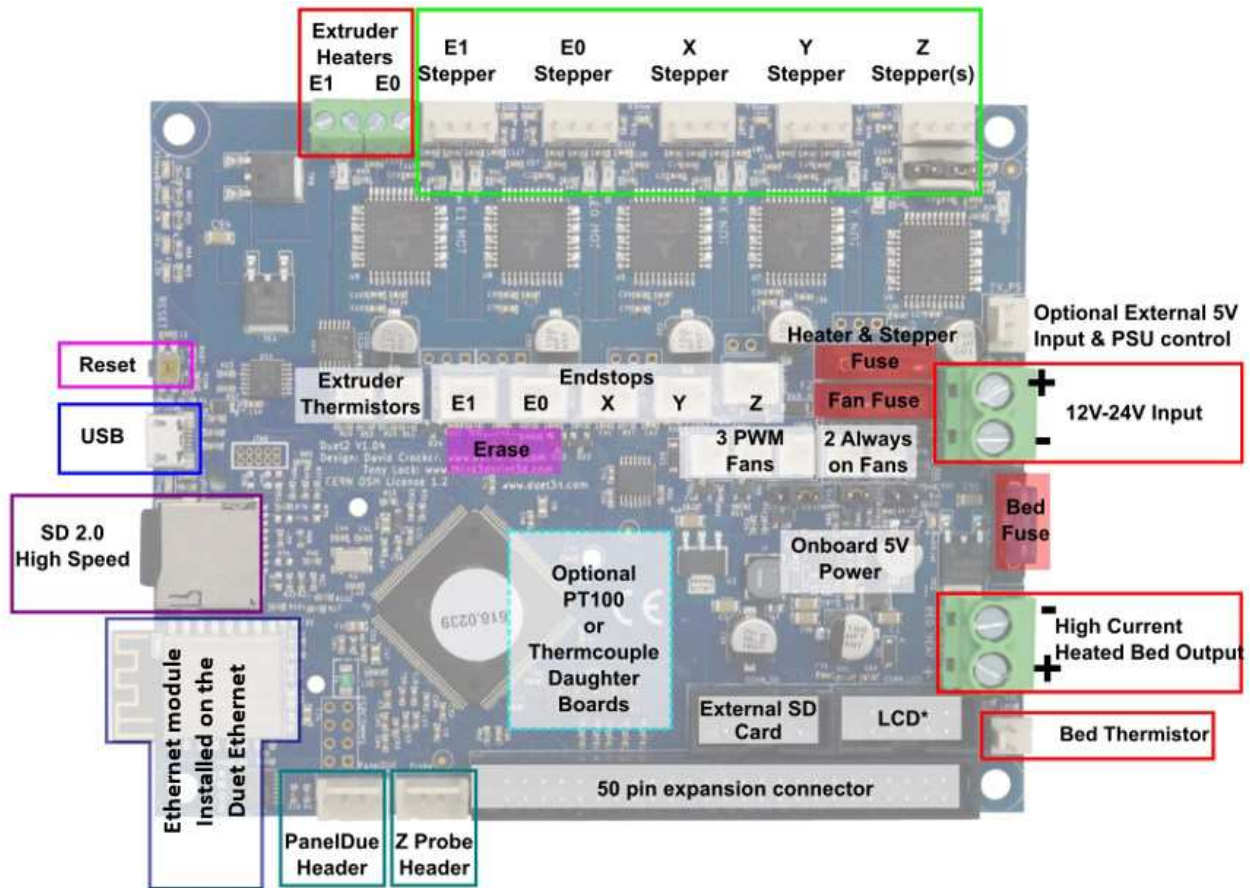


Figure 3.10.Duet 2 Ethernet board [83].

Moreover, for the new heaters, three solid state relays (SSR) were installed. And for motor that moves the screw that conveys the pellets through all the barrel of the pulsar pellet extruder, and external driver is installed too.

Finally, it is necessary to configure all the new components installed in the 3D printer. This process is done in the firmware and some general instructions are provided by DYZE [82]. The first attempt to configure the components was unsuccessful. The problem was that the version of the firmware used in the control board was an old version and new commands were no compatible. So, the firmware was updated to RRF3.3 and all the components worked correctly. The G code used to configurate the firmware can be found in Appendix 2.

3.5. 3D-Printing Calibration

The pulsar pellet extruder was calibrated on a trial-and-error basis with several tests. The calibration was done using PLA due to its ease of printability and well-known extrude temperatures. Although the parameters attached in the Appendix 3 works good with PLA and the materials used in this thesis, it is recommendable further tuning on flow rate, printing speed, bed leveling and toolhead offsets every time that a new material is 3D printed. To obtain the calibration parameters, the glass bed was levelled using a dial gauge and. Additionally, a BLTouch sensor (auto levelling sensor) was used to ensure a uniform and flat surface. Besides the use of a heated bed, a layer of water and sugar is sprayed to increase bed adhesion and protect the glass when 3D-printed parts are pulled out. During the calibration process, the main issues found in the equipment were the incorrect flow rate, toolhead offsets and layer shifting.

The first problem addressed was the calibration of the material flow rate in the extruder. Depending if the material is over-extruded or under-extruded, this can cause layers with excessive material on the surface or surfaces with voids respectively. To correct this problem, different flow rates (parameter known as extrusion multiplier in the slicer) were tested at the same time (Figure 3.11) using Simplify 3D as slicer software and a starving feeding philosophy of the hopper. The procedure was followed as:

- When inspected visually, if the 3D printed part has visible excessive material on the layers (over extrusion), the extrusion multiplier must be reduced.
- When inspected visually, if the 3D printed part has voids or empty spaces between layers (under extrusion), the extrusion multiplier must be increased.

The process was iterative until a good quality print could be achieved, this means an 3D printed object with high dimensional accuracy and great surface finish when it is inspected visually (without voids or excessive roughness). The value that works well is an extrusion multiplayer of 15. Other factors as layer height, printing velocity, nozzle temperature and cooling play an important role on printing quality but were not taken into account in the scope of this research.

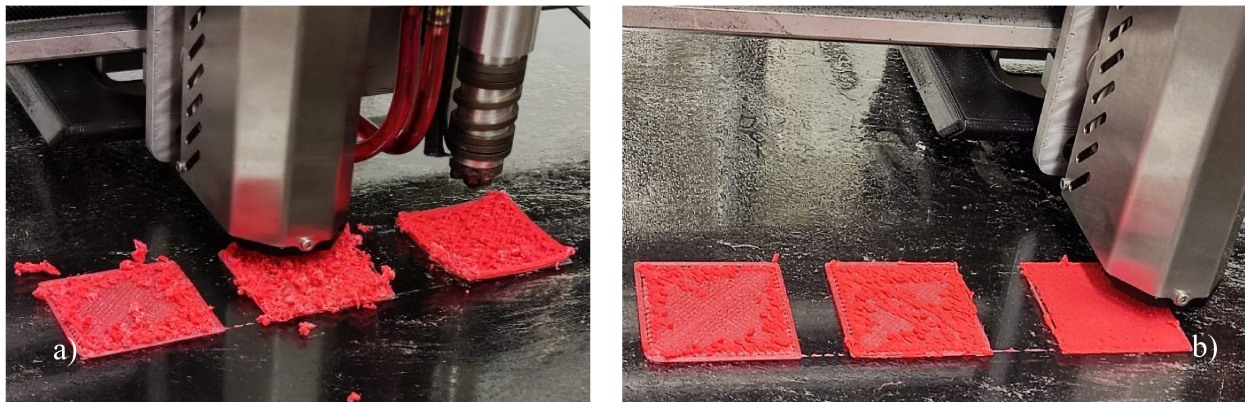


Figure 3.11. Different flow rates 3D prints. a) Extrusion multiplayer of 30, 25, 20 b) Extrusion multiplayer of 12, 14, 16.

The offset between the pulsar pellet extruder (work with pellets) and the HFE 300 (work with filament) is measured with a caliper and tested with 3D prints until no visible overlap is gotten when both toolheads print in conjunction. The offset (relative position) between toolheads is parameter that is configured in the firmware (Simplify 3D). The result after tuning that distance can be seen in Figure 3.12 where a single object is 3D printed using pellets (red part) and filament (black part). The boundaries between the red and black section are well defined and contours are not overlapping.

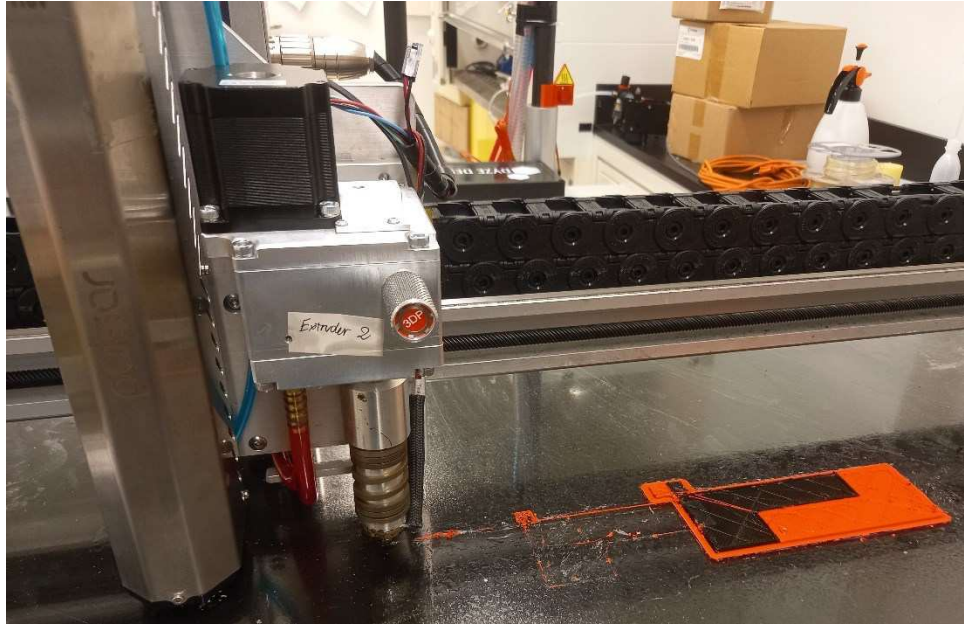


Figure 3.12. 3D printed part using Pulsar Pellet Extruder(pellets) and HF300 (filament) toolhead.

Finally, the last issue faced was the unexpected shifting between layers. Several geometries were printed to see the influence of the shape and corners on the shifting between layers, nevertheless, the result was the same and can be seen in Figure 3.13. The shifting between layers was independent of the position of the part in the heated bed too and could be confirmed by 3D printing parts in different places of the bed, having all the layers shifting.

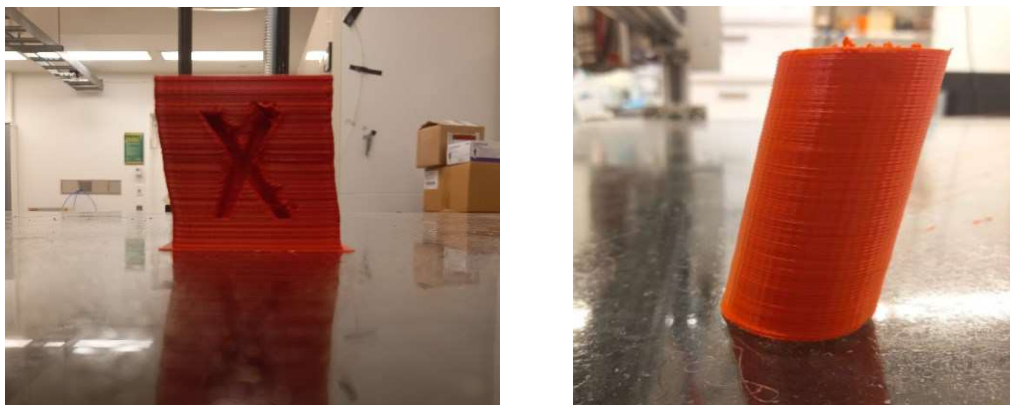


Figure 3.13. 3D printed parts with shifting between layers.

After several trials, the problem was identified to be related with the servomotors and their signal parameters programmed in the firmware of the control board (controls all sensors and actuators). The firmware was updated to install the pellet extruder, but in newest versions of RRF3.x firmware it is required to specify parameters of the signal to be sent to the servomotors also. Servomotors are controlled via Pulse Width Module (PWM) signals. This signal must be sent a specific width pulse within a certain frequency. These values are dependent of the external stepper driver used and usually are provided in the technical datasheet of the drivers. And in our case, the drivers corresponding to servomotors that carry the toolheads in the space (X, Y, Z coordinates) are different from the driver of the stepper motor that move the screw of the pulsar pellet extruder. A value of 2ms for the minimum driver step pulse width and interval worked perfectly to calibrate the servo motor. For the stepper motor of the pellet extruder, a value of 3ms was chosen for the calibration. Results after tuning pulse time are shown in Figure 3.14.

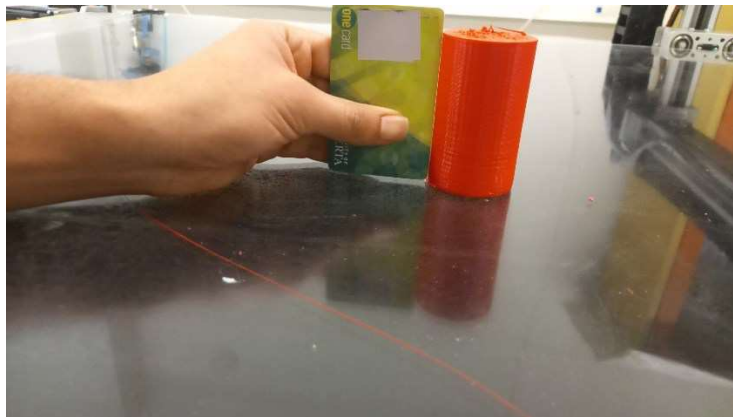


Figure 3.14. Results after tuning time for stepper motor pulse.

Finally, in Figure 3.15, it is possible to see a 3D printed object with a good quality (smooth surface finish), no overlap between contours and proper alignment between layers (no shifting).

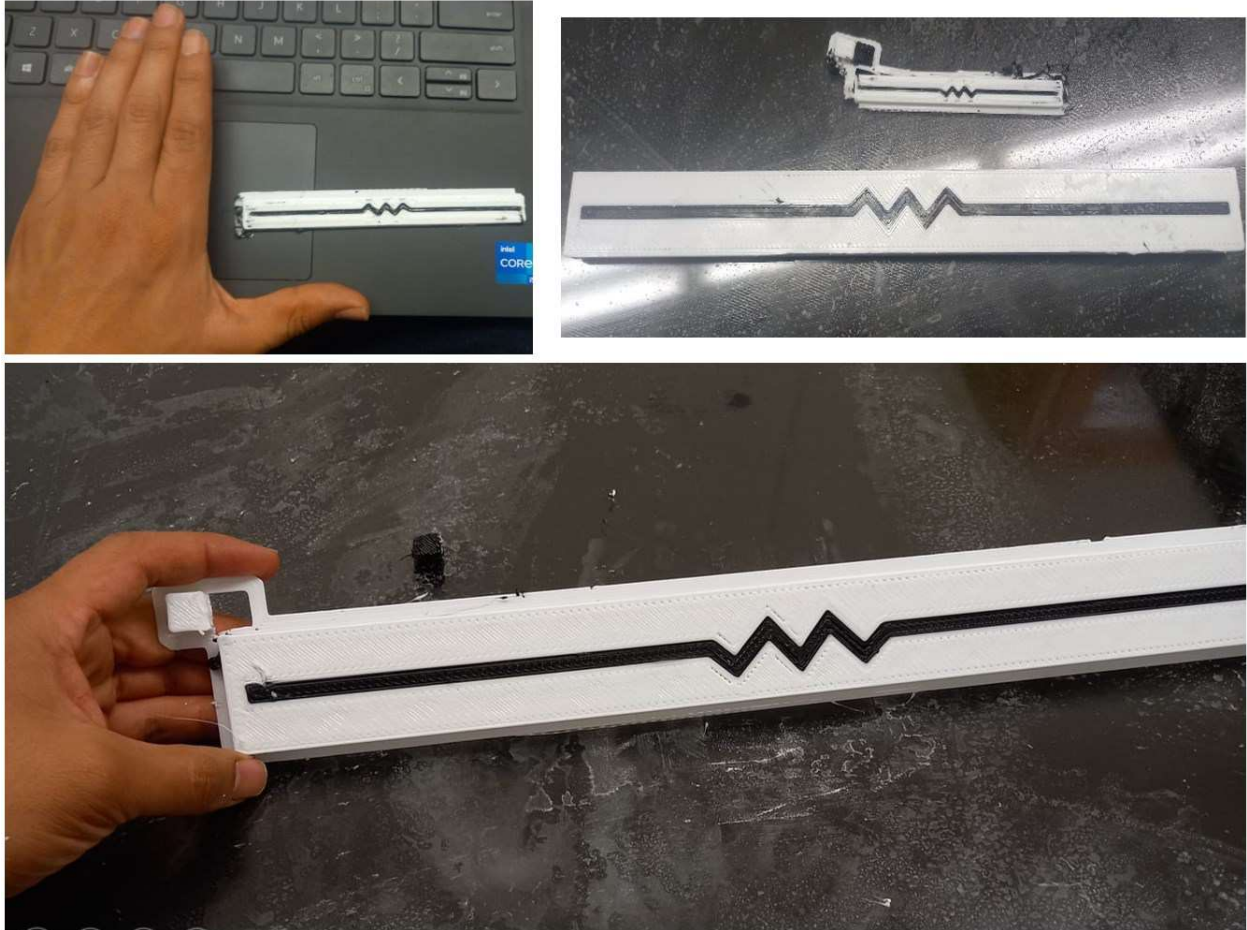


Figure 3.15. Object 3D printed after tuning 3D printer.

After the 3D printer has been setup, the following chapter talks about the preparation of the material to be used in this research.

4. MATERIALS AND EXPERIMENTAL TECHNIQUES

4.1. Raw materials

To study the properties of shape memory polymers reinforced with polymeric blend (PLA plus carbon fibers), shape memory polymer pellets type MM4520 were bought from SMP technologies. The material came in cylindrical form (2.85mm chopped). According to the datasheet provided by the manufacturer, this material has a glass transition temperature (T_g) of 45°C and a melting point around 170°C [69]. In the section below these values are confirmed using a differential scanning calorimetry (thermal technique for polymers). This MM4520 SMP is a thermoplastic elastomer, which means that it becomes soft after heating and hardens upon cooling. This feature allows us to thermal processing again the material to obtain a desire specimen using additive manufacturing techniques. Related to 3D printing, its melting point is compatible with the melting point of the other material used. Furthermore, its relative low recovery temperature (45°C) allows to perform the experimental part without need of extra sophisticated equipment. Shape memory polyurethane MM4520 is hereinafter referred to as SMP unless otherwise stated.

For reinforcement, PLA pellets with a content of 15% carbon fibers (CF PLA) were bought from 3DXTECH [84]. This material is also thermoplastic, and the manufacturer's recommended extrusion temperature range is $160\text{-}190^\circ\text{C}$.

4.2. Thermal Analysis

The thermal techniques used in this thesis to characterize the polymers used are thermogravimetric analysis (TGA) and differential scanning calorimetry (DSC).

4.2.1. Thermogravimetric Analysis (TGA)

TGA monitors the change in weight of a sample with respect to temperature or time. The sample is placed in a controlled environment (usually with a flow of an inert gas) and subjected to a controlled heating.

For CF PLA, a sample size of 12.037 mg was tested under a heating rate of 10°C/min ramp from room temperature up to 700°C. The inert gas used inside the chamber was nitrogen. TGA's results can be seen in Figure 4.1.a This plot confirms content of carbon fibers in PLA with the data provided by the seller of CF PLA (this polymer claims to have a 15% content of carbon fibers blended with PLA). Above a temperature of 340°C all the polymer is degraded and the residue that is not burned corresponds to carbon. According to the plot 83.87% of the sample's weight was burnt and 16.13% of the sample's weight remained.

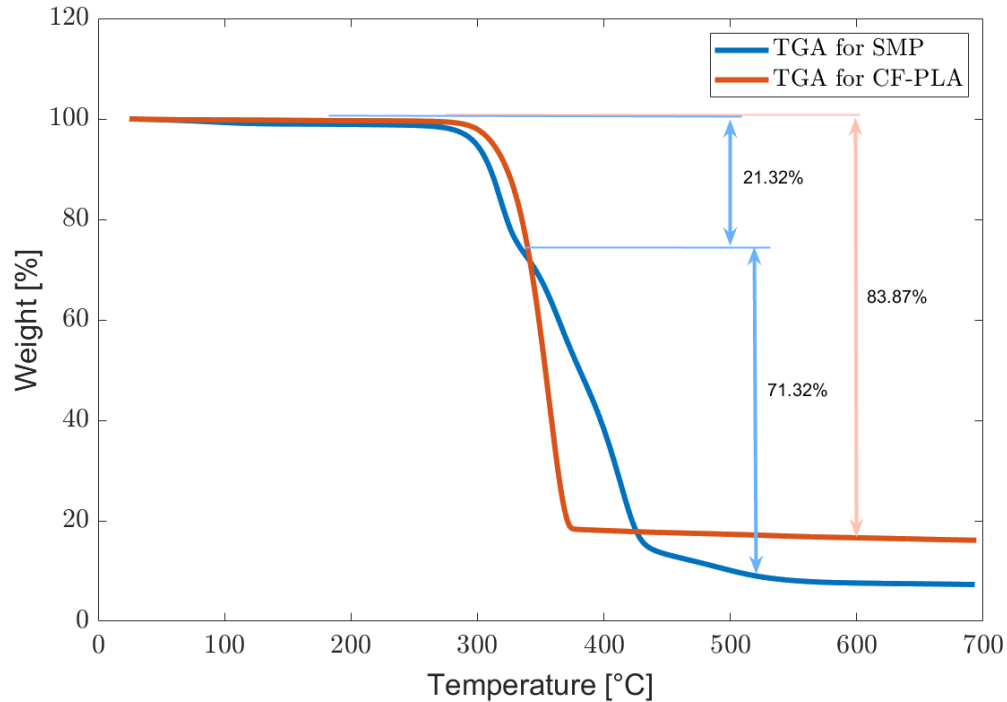


Figure 4.1. TGA of PLA with 15% content of carbon fibers and TGA of shape memory polymer MM4520 (SMP).

For SMP, a sample size of 8.696 mg was tested under similar conditions as CF PLA sample. Heating rate of 10C/min ramp, range from room temperature up to 700°C, and nitrogen as inert gas. For CF PLA in Figure 4.1 can be seen two instants of weight lost. The first lost is about 21.32% of the weight, starts at 100°C and ends around 350°C. This first weight lost is related with water lost (moisture trapped) due to the initial temperature of 100°C which corresponds to the boiling temperature of water. The polymer due to the time exposed to the environment has trapped moisture. Then a second weight lost of 71.32% is observed, which corresponds to polymer degradation. The residual weight corresponds to ash related to inorganic materials present in the material.

4.2.2. Differential scanning calorimetry (DSC)

In this thermal technique, the quantity of heat exchanged with the surroundings by a sample is measured in relationship with temperature or time. This heat flow can be released or absorbed, representing different phase changes of the material.

For CF PLA, a sample of 6.4 mg was tested with 5°C increments every minute from 0°C up to 210°C. The temperature was modulated ± 1.00 °C every 60 seconds. Three remarkable zones can be distinguished in Figure 4.2.a The first zone is located around 57°C and corresponds to the transition of a hard and glassy material to a rubbery or viscous, also known as glass transition temperature (T_g). In the second zone there is a peak at 96°C corresponds to an endothermic reaction due to melting of the polymer.

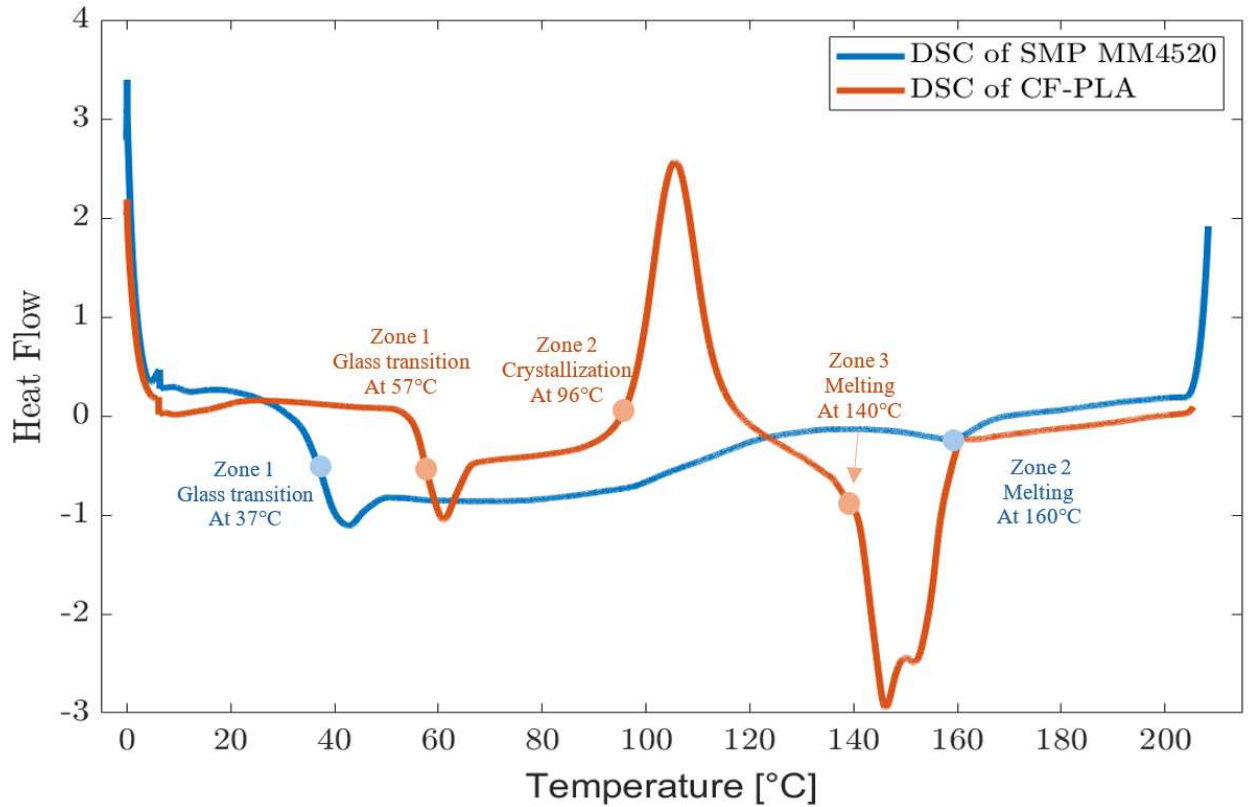


Figure 4.2. Modulated DSC of PLA plus 15% carbon fiber (CF PLA) and Shape memory polyurethane MM4520 (SMP).

A SMP sample of 4.6 mg was tested with a modulated DSC of ± 1.00 °C every 60 seconds, using a ramp of 5°C up to 210°C. In Figure 4.2b two important zones were found. The first zone related with the glass transition temperature is around 37°C. This shift of value of T_g could be due to plasticization of the polymer due to moisture trapped inside (this was corroborated with the TGA performed before). And the last zone is a valley due to an endothermic reaction. This is the melting zone of the polymer. SMP melts around 160°C.

4.3. Experimental approach

Two different paths were studied to obtain the composite polymer in order to choose the most feasible.

4.3.1. Laminate composite.

The first approach was the elaboration of a laminate composite material using the two toolheads of the 3D printer. The material extruded would change with every layer, creating a different lamina for each layer and the direction of the lamina would be controlled with the printing orientation.

The large-scale 3D printer available in the lab has two extruders, one of them works with pellets and the other with 2.85mm filament. The CF PLA is planned to be used in pellet form and the SMP in filament form. For this reason, it was necessary to use SMP with 2.85mm filament diameter.

The main equipment used for filament production were a single screw extruder model ATR Plasti-Corder from Brabender, a water bath, and a winding mechanism. The extruder melts and moves the pellets from the hopper through all the barrel and pushes them through a die with a specific geometry. Then the melted plastic is cooled in water. Finally, the winding mechanism pull and wind the filament at a constant speed to have the filament diameter desire. The extruder has four heating zones and the selected temperature profile for the SMP can be seen in Figure 4.3.

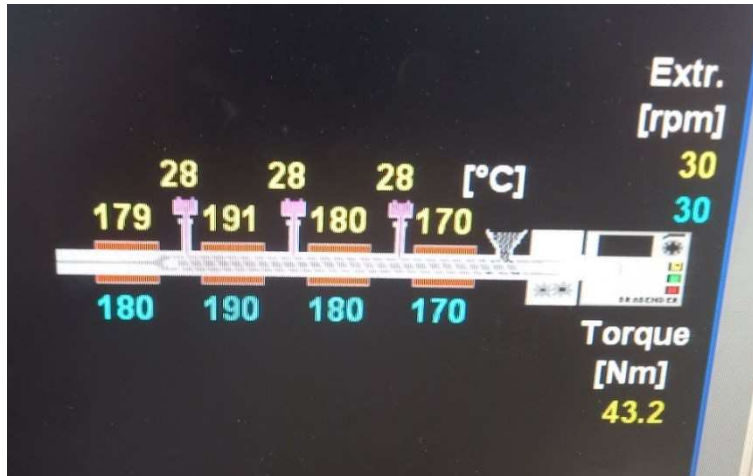


Figure 4.3. Extrusion temperature profile.

The filament was used in a large-scale 3D printer to get a laminate composite with a lay-up of SMP and CF PLA. Nevertheless, this approach was not feasible due to a poor layer adhesion between the SMP and the CF PLA. This poor interface bonding caused delamination of the materials (see Figure 4.4).



Figure 4.4. Delamination between layers in specimen, layers completely separated showing a clean surface (left), as printed sample (right)

4.3.2. Pellet extrusion

The next approach was the use of both materials as pellets. Depending on the ratio study the pellets should be weighted and mixed (Figure 4.5). Then, only the Pulsar Pellet Extruder was used to print

a homogenous material made of shape memory material and Carbon Fiber PLA. This approach was the one developed in this thesis and is detailed in depth in the next section.



Figure 4.5. Different percentages of carbon fiber and SMP.

4.4. Obtaining test specimens

4.4.1. Material preparation.

The first step to get a sample of the composite materials starts eliminating the moisture trapped inside the polymers. In previous stages, when SMP was extruded, it could be observed the presence of bubbles inside the material. This moisture leads to phenomenon known as plasticization that reduces the glass transition temperature (T_g) and negatively affects mechanical properties and melt viscosity of the material [70]. In order to remove moisture, pellets were dried out in a vacuum oven Lindberg/Blue M™ at a temperature of 80°C for 48 hours, and CF15 PLA pellets were dried in the same oven at 50°C for 6 hours. It is possible to compare the material after drying in Figure 4.6



(a)



(b)

Figure 4.6. Comparison of material with moisture trapped and dried material. (a) Presence of bubbles in extruded material. (b) Material after a drying stage in vacuum oven

Then, aiming for a homogenous blending between the materials and avoid nozzle clogging, it is chosen to study three different wt% of SMP and CP PLA. 100 wt. % SMP, 90 wt. %SMP plus 10 wt. %CF PLA, and 80 wt. %SMP plus 20 wt. %CF PLA. Higher contents of CF PLA in SMP were not possible to print due to continuous clogging of the nozzle and nonhomogeneous blending of polymers (Figure 4.7).

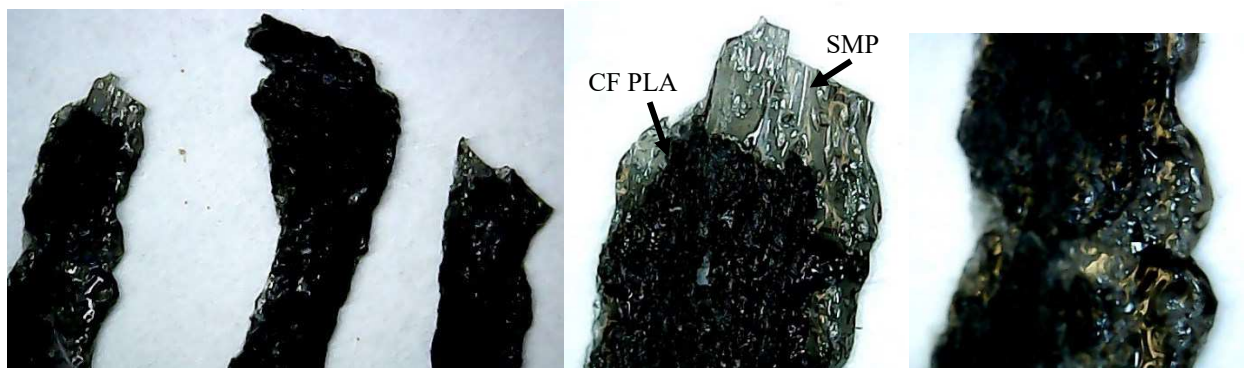


Figure 4.7. Phase separation between SMP and CF PLA. The proportion was 50% of each one.

Picture taken with a USB digital microscope.

4.4.2. Sample fabrication.

For the 3D printing stage as it was explained before, it starts with the CAD design of the desired geometry. Rectangular samples were designed using SolidWorks student edition. Sample's designed dimensions are 3.2[mm]x52[mm]x12.7[mm] (See Figure 4.8). The shape was chosen considering that samples were going to be tested in a three-point bending machine under bending according to the standard ASTM 790 [85].

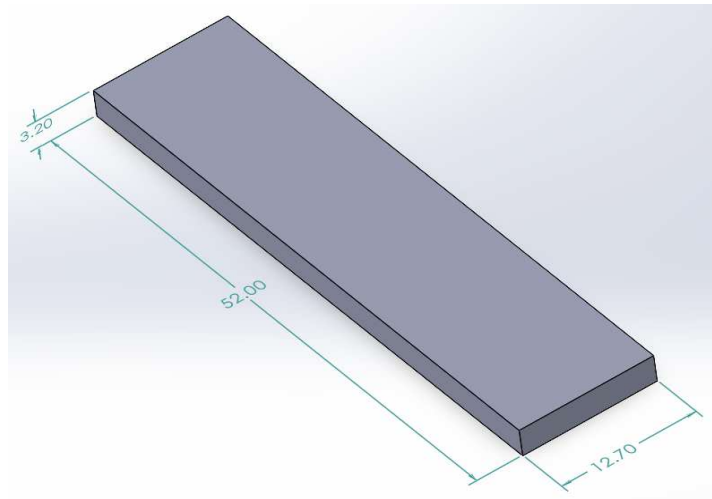


Figure 4.8. 3D specimen designed on SolidWorks.

On the second stage, the G-code is generated using the slicer Simplify3D. The printing parameters were chosen to ensure solid samples (100% infill) and avoid any voids. In addition, the temperature profile was selected based on DSC experiments performed in section 4.2.2. The same parameters were used for all samples and can be seen in Table 4.1. On the Figure 4.9 can be seen the 3D printed sample of 100% SMP.

Table 4.1. Printing parameters selected in Simplify3D.

| Parameter | Units |
|-----------------|----------|
| T | 40 [°C] |
| T1 | 180 [°C] |
| T2 | 185 [°C] |
| T3 | 190 [°C] |
| Layer height | 0.3[mm] |
| Print speed | 20[mm/s] |
| Fill density | 100[%] |
| Nozzle diameter | 1[mm] |

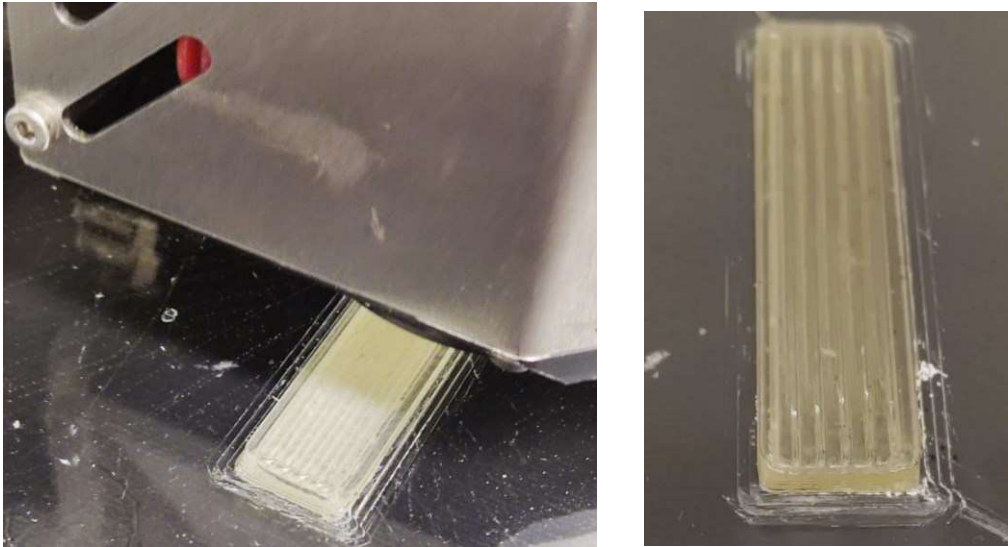


Figure 4.9. 100% Shape memory polymer 3D printed sample.

4.4.3. Annealing of samples.

Once the samples were obtained, some initial tests were performed. Samples were heated and deformed under three-point bending test configuration (Figure 4.10). Then, they were given time to cool down. For the recovery to take place, the samples were heated above its glass transition temperature. However, samples recovered their shape over a 100%. Instead of remaining like a flat sample, they bended upwards according with Figure 4.11. Reported by [86], this behavior may be due to internal stresses generated during 3D printed process.

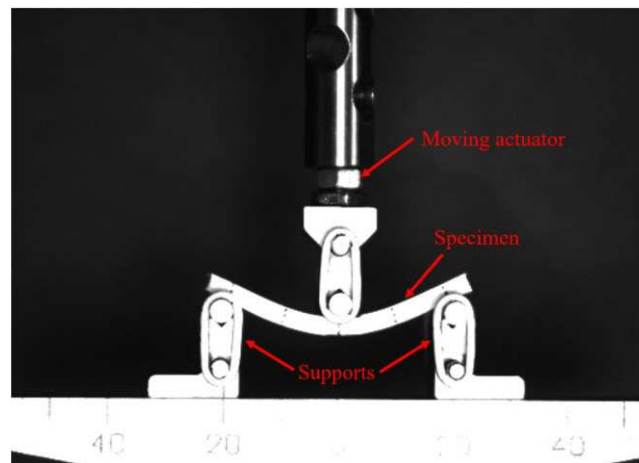


Figure 4.10. Pre-tests performed on SMP samples.

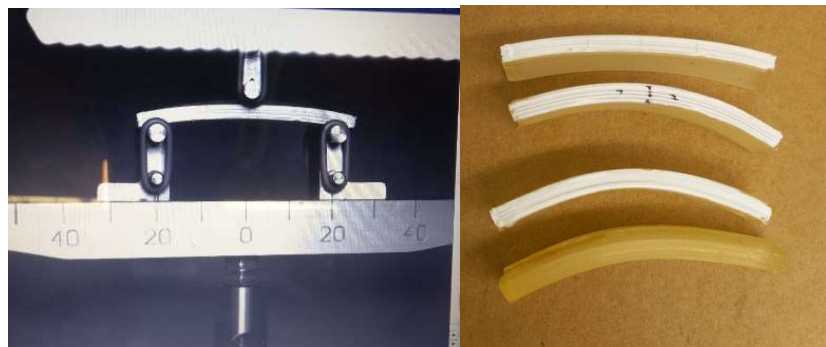


Figure 4.11. Recovery over 100% for SMP samples.

Therefore, to eliminate the internal stresses, the samples were annealed at 85°C for two hours in a vacuum oven Lindberg/Blue M™ (Vacuum was not used) that was heated to the desire temperature before. Then the samples are cooled to room temperature by switching off the oven. The annealing temperature was chosen according to a previous study that reported possible temperatures to have the highest recovery force of a SMP MM4520 sample [72]. To avoid any change in the geometry of the samples due to the exposure to relative high temperatures, a weight (book) was placed above the samples to keep their original shape during all the annealing process (Figure 4.12).

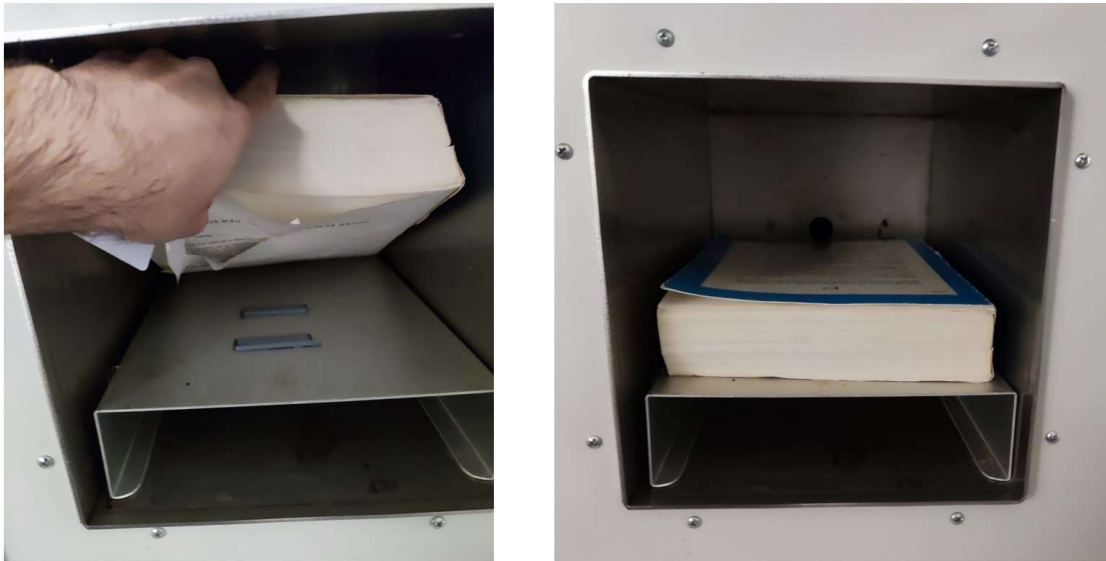


Figure 4.12. Weight placed on the top of samples before annealing.

The annealed samples showed a normal recovery (close to the initial shape) indicating that residual stresses were reduced or even eliminated (see Figure 4.13). Additionally, sample dimensions were measured and recorded after annealing. It was observed dimensional changes of annealed samples with respect design dimensions.

Finally, after annealing, the specimens were placed in vacuum bags with desiccant to avoid any absorption of humidity from the environment until they were tested.

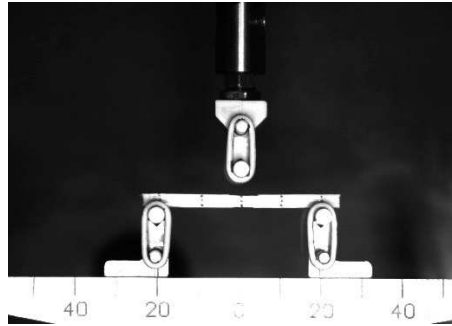


Figure 4.13. Recovery for annealed samples.

Until this point a diagram describing every step and time required for the sample obtention is detailed in Figure 4.14.

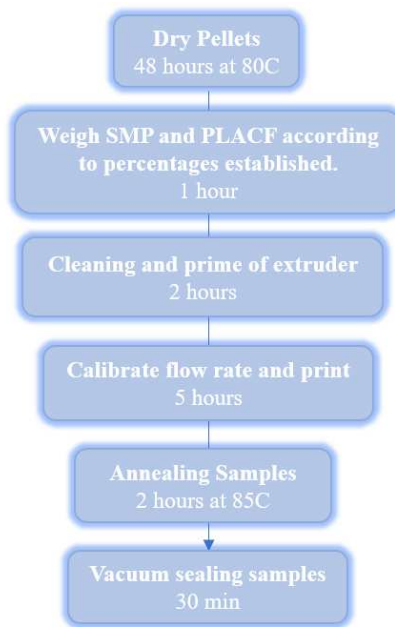


Figure 4.14. Sample preparation procedure.

4.5. Sample testing.

The tests performed in this thesis will help to compare the shape recovery properties of unreinforced SMP material with reinforced SMP. Tests can be divided in two groups: Shape Recovery Flexural Stress tests and Shape Recovery Ratio tests. Both tests were performed with

slight differences described in the following sections. The tests are based on a three-point bending test and an ElectroForce 3200 system manufactured by BOSE, equipped with a 450 N load cell (maximum load), is used. The equipment was used to heat up the samples in an isolated heating chamber that allows to control the temperature of samples during the experiment.

4.5.1. Shape Recovery Flexure Stress (SRFS)

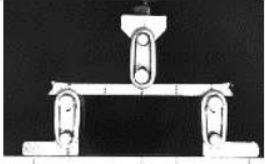
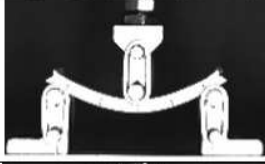
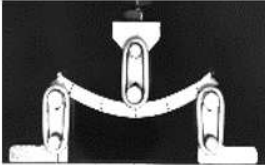
A detailed explanation of shape recovery flexural stress tests is described in Table 4.2. In the table can be seen how temperature and displacement of the actuator change with time to carry out the programming and recovery stages. In brief, this test begins with the samples being placed in the three-point bending machine and closing the chamber (isolating) to have precise temperature control of the environment in the testing chamber. The sample rests in simple supports at a distance of 40 mm between each other.

Samples are then heated to 50°C, this temperature is greater than the glass transition temperature of both materials (SMP MM4520 and CF PLA). The purpose of this is to bring the material to a rubbery state where it can be easily deformed, and the samples can be loaded under bending until a deflection of 6mm is reached by the neutral axis.

In order to keep the deformed shape (temporary shape) the sample is cooled down to 30°C (below T_g) and the actuator that was applying the load is removed. Ensuring that the sample is cold enough to keep the deformed shape, the actuator is placed barely touching the sample's surface and the chamber is heated up to 60°C.

The shape memory effect (SME) activates when temperatures above T_g are reached. In this case the T_g of the materials are around 45°C. So, the force exerted by the sample to recover its initial shape could be measured for the actuator (constrain recovery). All the force data is recorded at 10[Hz] rate.

Table 4.2. Shape recovery flexural stress test process

| Time [s] | Temp [C] | Displacement [mm] | Actions | Programming temperature | Programming displacement | Pictures |
|----------|----------|-------------------|--|-------------------------|--|---|
| 0 | 30 | 0 | Initial Conditions | 30 °C | Origin |  |
| 50 | 50 | 0 | Heating up sample | 0.4 °C/seg --> 50 °C | Dwell 50 seg | |
| 290 | 50 | 0 | Wait to stabilize | Dwell 240 seg | Dwell 240 seg | |
| 302 | 50 | -6 | Apply load to deform sample | Dwell 12 seg | 0.5 mm/seg --> -6mm |  |
| 362 | 50 | -6 | Keep load | Dwell 60 seg | Dwell 60 seg | |
| 365 | 30 | -6 | Cool down sample | 10 °C/seg --> 30 °C | Dwell 3 seg |  |
| 725 | 30 | -6 | Wait to stabilize | Dwell 360 seg | Dwell 360 seg | |
| 745 | 30 | 4 | Remove load | Dwell 14 seg | 0.5 mm/seg --> 1mm | |
| 805 | 30 | -5.9 | Manual positioning of gripper to measure force | Dwell 60 seg | Manual procedure using machine interface |  |
| 880 | 60 | -5.9 | Heating up sample | 0.8 °C/seg --> 60 °C | End programming (measurement) | |
| 1380 | 60 | -5.9 | Measuring recovery | 60 °C | End programming (measurement) | |

To verify that the tests were performed according to Table 4.2, data of the real behavior of the temperature and displacement for a shape memory sample (SMP) are plotted in Figure 4.15. Displacement reaches the desire position and hold it when it is required. Furthermore, the temperature increases and decreases smoothly with no large overshoots. So, it is possible to say that the experiment performs according to the specified programming.

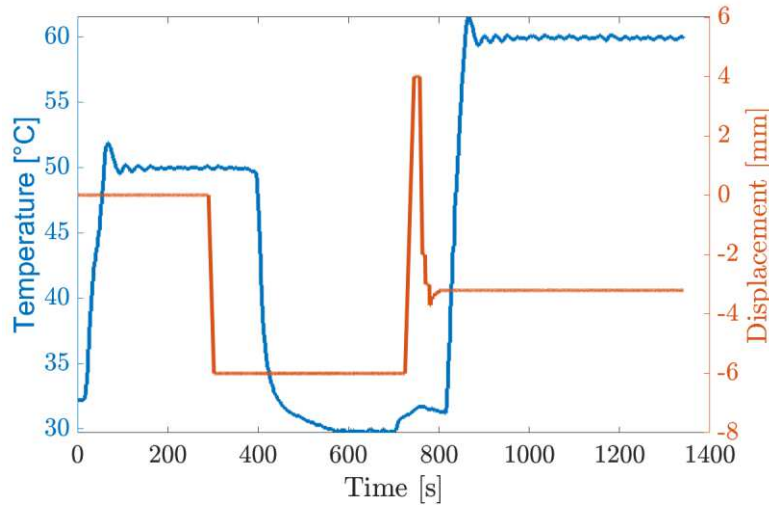


Figure 4.15. Real displacement and temperature running in shape recovery flexural tests.

In Figure 4.16a the evolution of the reaction force exerted by the specimen on the actuator is plotted versus displacement and in Figure 4.16b it is plotted versus temperature. According to Figure 4.16a force has close relation with the displacement (deformation of the sample). The higher displacement/deformation, the higher the reaction force is exerted by the sample in the programming stage. At 302 seconds the displacement and the force reach a peak (maximum value), follow by a relaxation of the sample shown by a decrease in force while the constrain is kept. The actuator is then removed (unloading) at 725 seconds, which leads to a jump to zero of the reaction force. Finally, when the actuator is placed again manually for measurement, it is possible to observe the evolution of the recovery force with time.

The information presented on Figure 4.16b helps to a better understanding of the observations of Figure 4.16a. After force reached its maximum values at the maximum displacement/deformation of the specimen, force values began to decrease only while it is exposed to a temperature above T_g . However, when the sample is cooled, it exerted a constant reaction force until the actuator moved backwards. In Figure 4.16b it is worth to be highlighted that values of force increase when the sample begins to be heated above T_g . In this context, this force is called shape recovery force and it is the focus of this thesis as it will be used to calculate the shape recovery flexural stress.

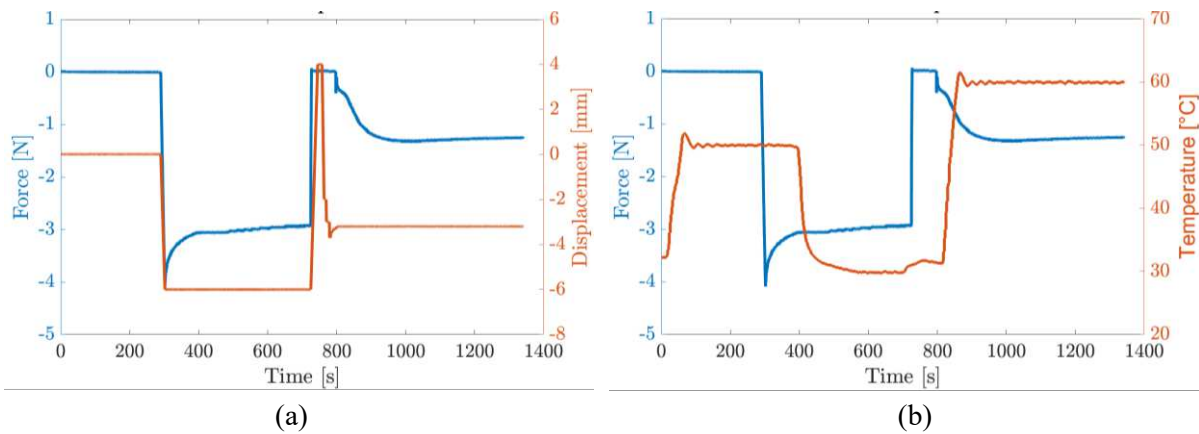
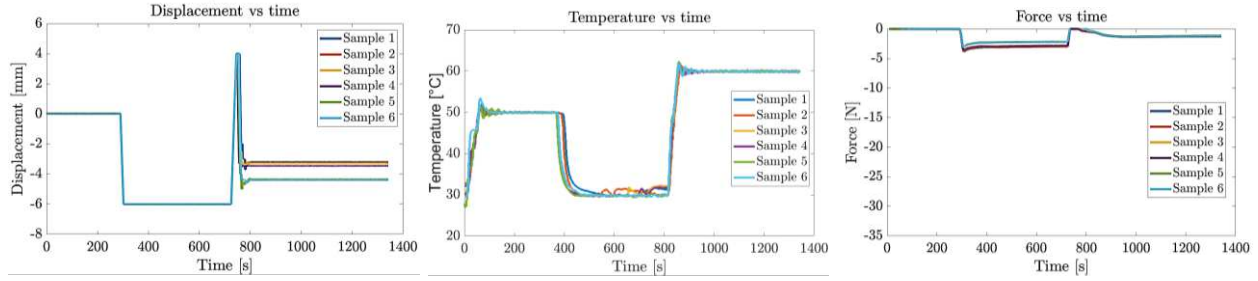
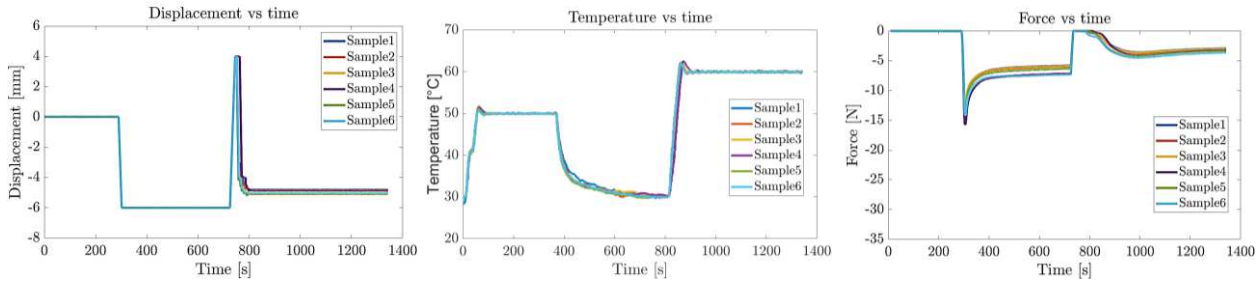


Figure 4.16. Force exerted by sample during shape recovery flexural stress tests. (a) Force vs displacement. (b) Force vs temperature

Finally, to check the repeatability of the experiment for all samples during testing process, plots of displacement, temperature and force are overlaid for each polymer. In each case, all the samples behaved similar, showing plots that followed the same trend with close values. For these reasons, the experiments can be considered repeatable and reliable, and the conclusions drawn from this thesis can be generalised (see Figure 4.17).



C10



C20

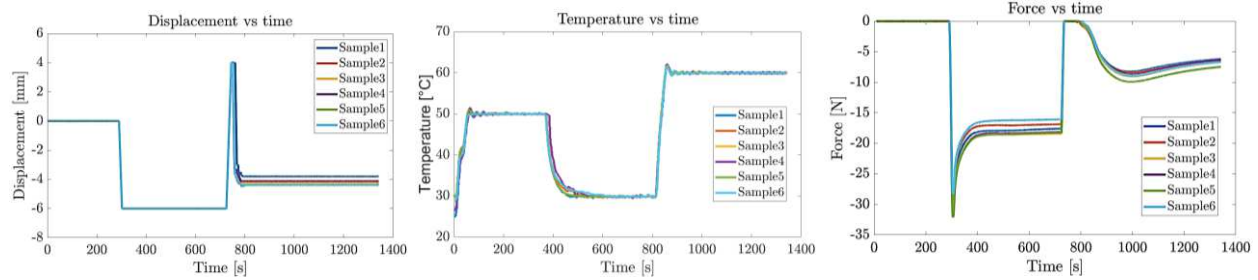


Figure 4.17. Repeatability of the experiments for SMP, SMP with 10% weight content of CF PLA (C10) and SMP with 20% weight content of CF PLA (C20)

The Shape Recovery Flexural Stress (SRFS) was calculated based on standard D790-Standard Test Methods for Flexural Properties of Unreinforced and Reinforced Plastics and Electrical Insulating Materials [87]. This stress corresponds to the maximum stress located in outer fiber and it is calculated according to the following equation.

$$\sigma_f = 3 PL/2bd^2 \quad \text{Equation 4.1}$$

Where:

σ = stress in the outer fibers at midpoint, MPa

P = load at a given point on the load-deflection curve, N

L = support span =40 [mm]

b = width of beam tested, mm

d = depth of beam tested, mm

4.5.2. Shape Recovery Ratio (SRR) and Shape Recovery Fixity (SRF)

Shape memory ratio (SRR) and shape recovery fixity (SRF) tests follow the same steps described before for shape memory flexural stress, with the exception that after the load is removed, it is not applied again. The specimen is subjected to a free recovery, this means that the sample can recover without restriction when it is heated. Hence, for image recognition and tracking of the shape recovery of sample, the lateral face was painted white and small black dots were drawn (Figure 4.18).



Figure 4.18. Preparation of SMP sample for SRR and SRF tests.

Photos were taken at a rate of 4[Hz] using a Basler ace acA3800-10gc camera during the experiment. The purpose of the pictures was to study the recovery of the sample with respect to the initial state (initial picture). From the photos taken, the displacement of the drawn speckles was tracked with ImageJ while the sample recovered the initial/permanent shape. On Figure 4.19 is possible to see the trajectories obtained for a sample.

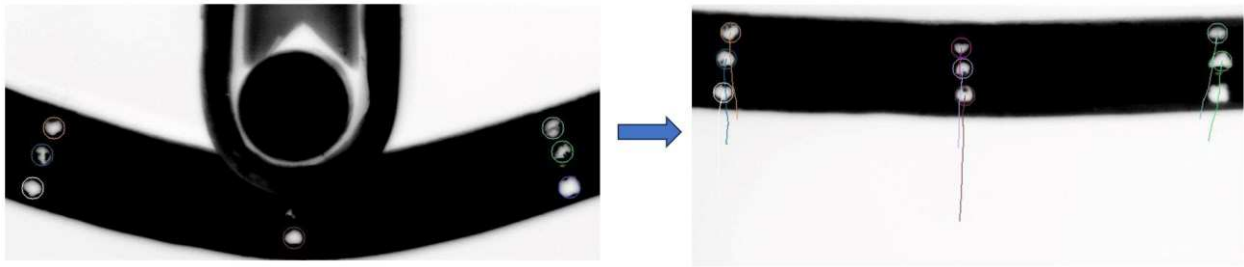


Figure 4.19. Trajectory tracked for shape recovery ratio analysis.

Shape Recovery Ratio (SRR) represents how much the sample can recover its initial shape when it is exposed to a temperature above T_g . SSR is calculated as the relationship in percentage of the initial position of a tracked point (midspan) in the sample before being deformed (programming stage) and the current position of the point for a specific time when the samples is recovering (recovery stage). The following equation was used to calculated SRR according to [13].

$$SRR = \frac{S_i - S_n}{S_i - S_0} \times 100\% \quad \text{Equation 4.2.}$$

Where:

S_i = initial position of point tracked (midspan) at the beginning of the recovery, mm

S_n = position of point tracked (midspan) with respect to time, mm

S_0 = initial position of point tracked (midspan) before programming, mm

Shape Recovery Fixity (SRF) corresponds to the relationship between the position of the tracked point (midspan) at the instant right after the programming and the beginning of recovery, and programmed position of point track. It represents how much of the programmed shape could be retained by the sample. The following equation was used to calculate the SRF.

$$SRF = \frac{S_2}{S_1} \times 100\% \quad \text{Equation 4.3.}$$

Where:

S_2 = position of tracked point (midspan) right programming and the beginning of recovery, mm.

S_1 = programmed position of point tracked (midspan), mm.

4.5.3. Data obtained for analysis.

Finally, a total of 18 samples were tested for SRFS, having 6 samples for each case of study. And 14 samples were tested for SRR, 5 samples for 100 wt. %SMP (SMP), 5 samples for 90 wt. %SMP and 10 wt. %CF PLA (C10) and 4 samples for 80 wt. %SMP and 20 wt. %CF PLA (C20). All the results are showed and discussed in the next section. Furthermore, the data obtained was loaded in MATLAB and processed using a moving average filter with a window size of 90 to filter noise in the measurements. Plots related to SRFS are discussed in the Chapter 5 (Results and Discussion).

5. RESULTS AND DISCUSSION

5.1. Annealing and its effects

In the initial stages of the shape recovery test process, it was observed that the specimens recovered more than 100%, as the specimens bent upwards, rather than recovering their initial flat configuration. (See Figure 4.11). This behavior can be attributed to internal stresses (or residual stresses) due to pre-strain during printing and nonuniform cooling or heating of layers [86]. In the layer that is being printed, pre-strain is caused when the melted material is deposited and dragged, having an initial stretching of the polymer. On the other hand, the nonuniform temperatures that produce thermal stresses are due to the temperature gradients between the nozzle, the heated bed, bottom layers, and the layers being deposited. As a result of the 3D printing process, internal stresses, that affect the recovery of the shape memory polymer, were generated.

For this reason, an annealing stage to reduce internal stresses was implemented. After the annealing process of 2 hours at 85°C, samples started to recover to their initial shape (flat shape), reaching values of shape recovery ratio close to 100%.

Although a proper recovery of the samples was achieved, the annealing stages caused a geometrical distortion in the samples. A shrinkage in the longitudinal axis and an expansion of the cross-sectional area of the specimens were observed. Changes in the 3D printed geometry of shape memory polymers has been reported by [86]. Hu et al., reported that depending on the printing orientation and temperature, the layers of the 3D printed part are pre-strained which affects the geometry of the part when it is heated [86].

Figure 4.8 presents the desired dimensions for the samples, but just like any other manufacturing process printed objects showed some deviations. Directly after being printed, the specimens had

an average height of 3.3 mm and an average width of 13.07 mm. Nevertheless, after annealing, the new dimensions of the samples are measured again and presented in Table 5.1. Longitudinal shrinkage does not influence the calculation of flexural stress; hence this was not considered in this thesis.

Table 5.1. Sample's cross-sectional area before testing for shape memory polyurethane (SMP), SMP with 10 wt. % of CF PLA (C10), and SMP with 20 wt. % of CF PLA (C20).

| Average height measured as printed =3.3mm Average width measured as printed =13.07mm | | | | | | |
|--|---------------|---------------|---------------|---------------|---------------|---------------|
| | SMP | | C10 | | C20 | |
| | Width [mm] | Heigh [mm] | Width [mm] | Heigh [mm] | Width [mm] | Heigh [mm] |
| SRR Samples | 3.9±0.08 | 13.53±0.08 | 3.76±0.15 | 13.49±0.19 | 4±0.28 | 13.98±0.4 |
| SRF Samples | 3.39±0.15 | 13.03±0.41 | 3.68±0.06 | 13.38±0.28 | 4.1±0.17 | 13.8±0.38 |
| Average difference with respect to initial average dimensions as printed | ±9.77 % | ±1.43% | ±12.61% | ±2.75% | ±22.74% | ±6.25% |

For 100% shape memory samples (SMP), SMP with 10 wt.% of CF PLA (C10), and SMP with 20 wt. % content of CF PLA (C20), the values of height, width and cross-sectional area average are compared in Figure 5.1a, Figure 5.1b, and Figure 5.1c respectively. It is noticed that height and width dimensions after annealing are greater than the as-printed average dimensions (expansion). The height expansion shows a greater variability among the composites in comparison with the width, having the biggest distortion on the composite C20 with an average value of 4.1mm and the

least on SMP with a value of 3.39mm (nominal average dimension as printed 3.3mm). These values are shown in the graph and orange lines represent the standard deviation of the height of the samples for each composite. In Figure 5.1a is possible to see that the height between samples does not have a big deviation.

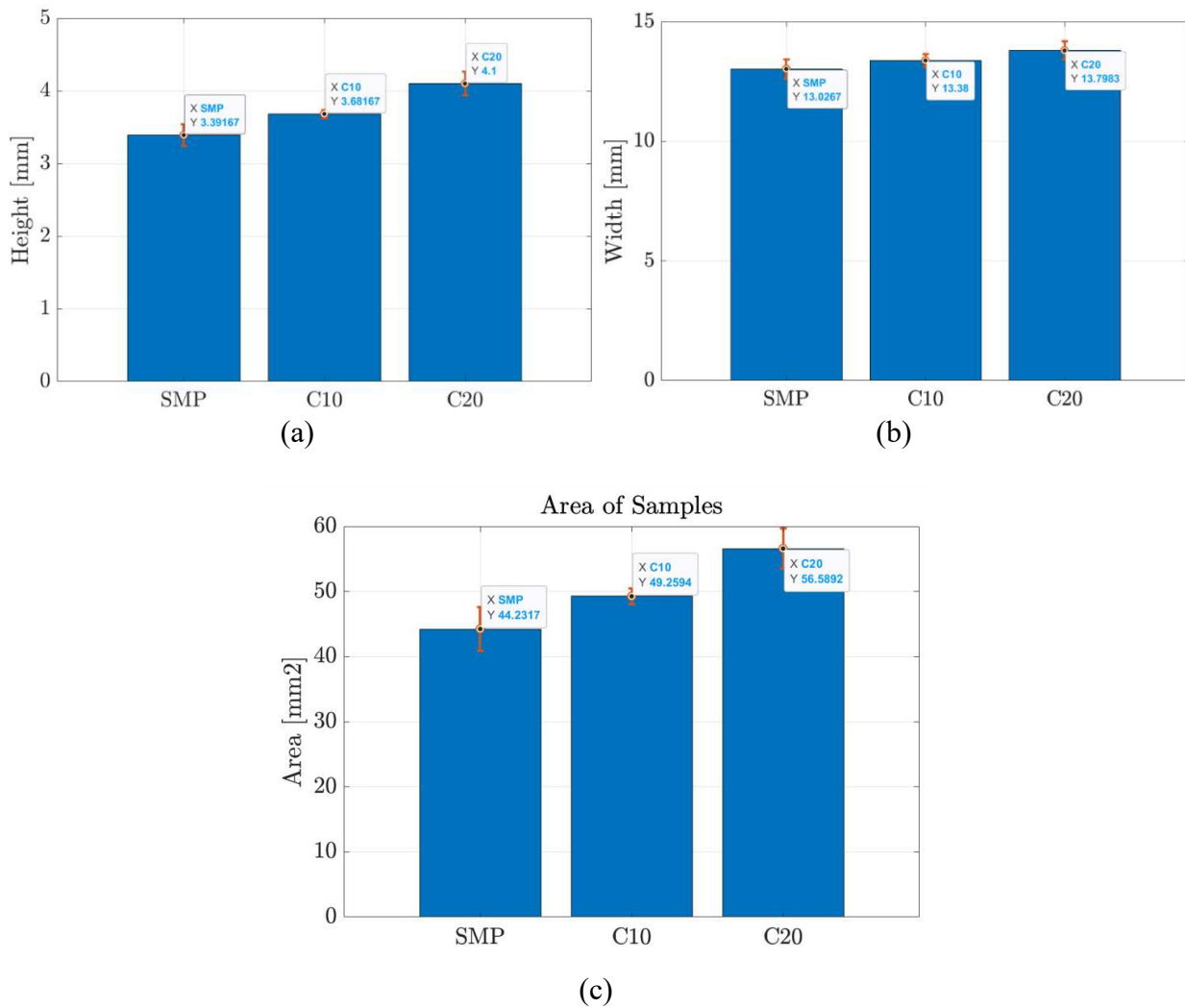


Figure 5.1. Height dimension comparison among composites with standard deviation. (a) Height of samples. (b) Width of samples. (c) Area of samples

Concerning Figure 5.1b, the width shows a small deviation among the polymers studied. And a small standard deviation means a small variability of the samples of the same polymer. Once again,

the composite C20 shows the biggest distortion in dimensions with respect to the initials. Considering that the pre-strain is constant across all samples, the higher carbon fiber content can explain the changes in dimensions/geometry of C20 composites. Carbon fibers have a low thermal conductivity which can produce larger temperature gradients in the samples and more internal stresses.

The change of dimensions plays an important role when the Shape Recovery Flexural Stress (SRFS) is calculated. The change in height and width involves a change in the cross-sectional area where the bending and recovery stress act. In Figure 5.1c can be seen that the annealing process has a big influence on that cross-sectional area. Having the biggest expansion on C20 samples (56.58mm^2) with respect to the initial average cross-sectional area of 43.13mm^2 . The closest composite's cross-sectional area with respect to the initial area is SMP with 44.23mm^2 . A bigger standard deviation of the sample's area is due to when width and height are multiplied to calculate the area, the deviation is multiplied too.

Even though the batch was subjected to the same conditions of temperature and annealing time, the results varied between samples. Not all the samples after annealing were tested. Some specimens were discarded because they shrunk too much in the longitudinal direction (and expanded the cross-sectional area) and weren't even able to be placed on the supports for the bending test. In Figure 5.2 can be seen with an "x" mark on the samples that were discarded from a batch after annealing. The reason why only some samples excessively shrunk is related to the additive manufacturing process. When pellets are mixed and melted inside the extruder it is impossible to ensure a perfect homogenous mixture across all the samples. In the same batch, samples may have slightly different carbon fiber contents that can produce more or less internal stresses, and with this more or less shrinkage (geometrical distortion).



Figure 5.2. Discarded sample comparison.

Related to large-scale 4D printing, it is suggested to conduct further studies on annealing and its effects on shape memory polymers as well as the influence of temperature gradients on internal stresses on polymers.

5.2. Shape Recovery Flexural Stress (SRFS)

The constrained shape recovery tests for shape recovery flexural stress were done on SMP samples (SMP), 90 wt. %SMP/10 wt. %CF PLA (C10), and 80 wt. %SMP/20 wt. %CF PLA(C20) as can be seen in Figure 5.3, Figure 5.4, and Figure 5.5 respectively. The graphs presented show only the recovery stage, which happened at 760 seconds since the beginning of the experiment.

On each figure, the plots for shape recovery force and shape recovery flexural stress (SRFS) are presented. SRFS is used to compare the performance of each composite because it takes into account the thickness of each sample.

In general, the samples show a fast increment in SRFS until they reach a maximum at approximately 975 seconds for pure SMP and SRFS reaches a peak at 990 seconds for the two cases of the composite (C10 and C20). Followed by a decrease and stabilization of SRFS for SMP, and an apparent continuing reduction of SRFS for the composites C10 and C20. The reason for the

composites' SRFS decrease may be due to the temperature used to activate the shape memory effect (SME) of the composite was 60°C, and as it was stated before, a constituent of the composite polymer is PLA, which has a glass transition temperature (T_g) of 60°C [88]. The temperature chosen activates the recovery of the sample which explains the initial fast increment on SRFS but as time goes on, the PLA content softens due to its exposure to its T_g, and the values of SRFS decrease.

According to Figure 5.3a, the six samples tested for pure SMP showed an identical behavior when exposed to T_g, having very close values for recovery force. But when the cross-sectional area is considered to calculate the shape recovery flexural stress (SRFS) the curves are shifted a little. However, they still follow the same trend.

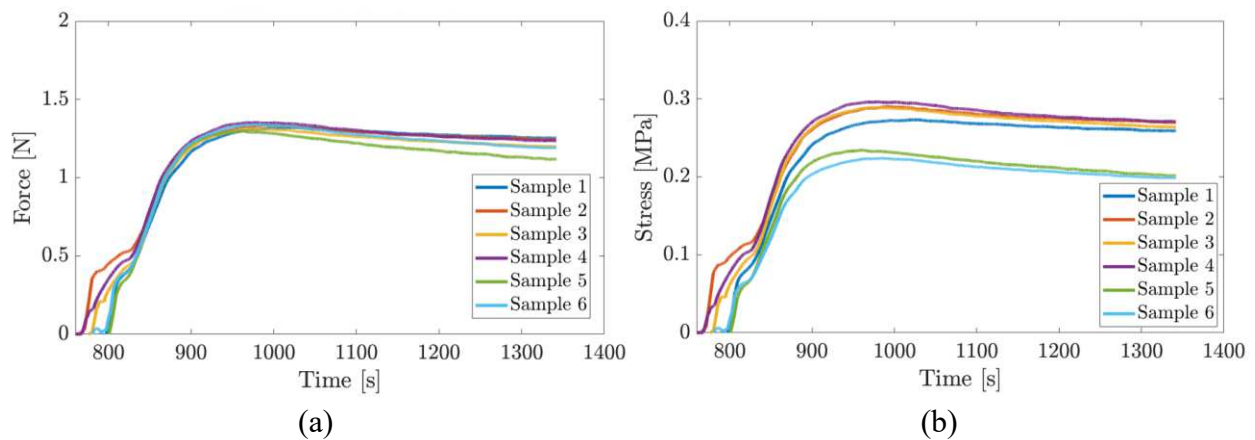


Figure 5.3. SMP constrained shape recovery test. (a) Shape Recovery Force. (b) Shape Recovery Flexural Stress

With respect to Figure 5.4, Figure 5.5 and Figure 5.5, shape recovery force plots and SRFS plots follow the same trend. Slightly differences in the graphs are due to the influence different cross-sectional area when SRFS was calculated.

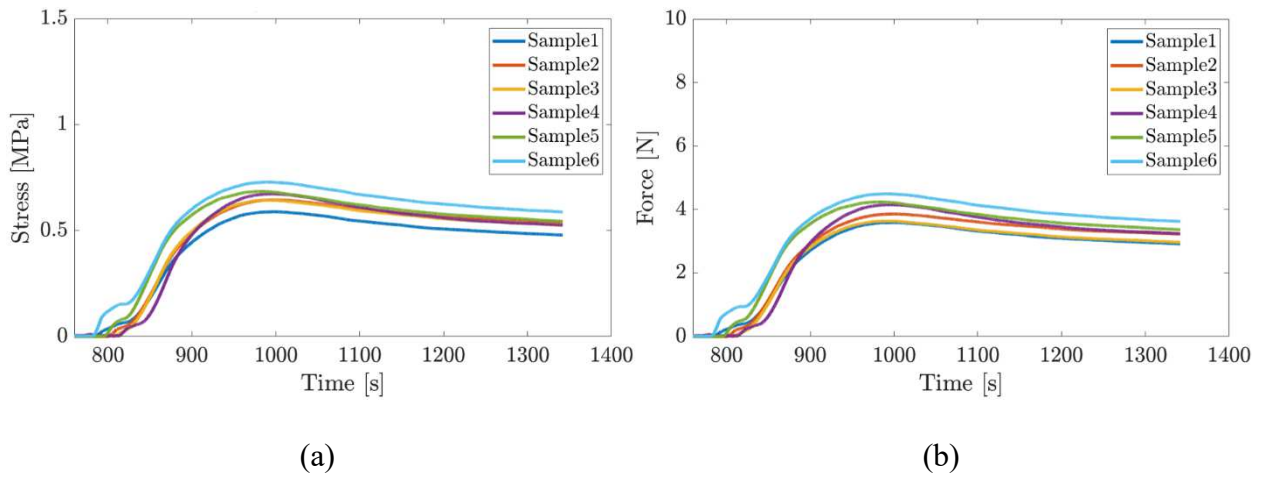


Figure 5.4. SMP and 10 wt. % CF PLA (C10) constrained shape recovery. (a) Shape Recovery Force. (b) Shape Recovery Flexural Stress.

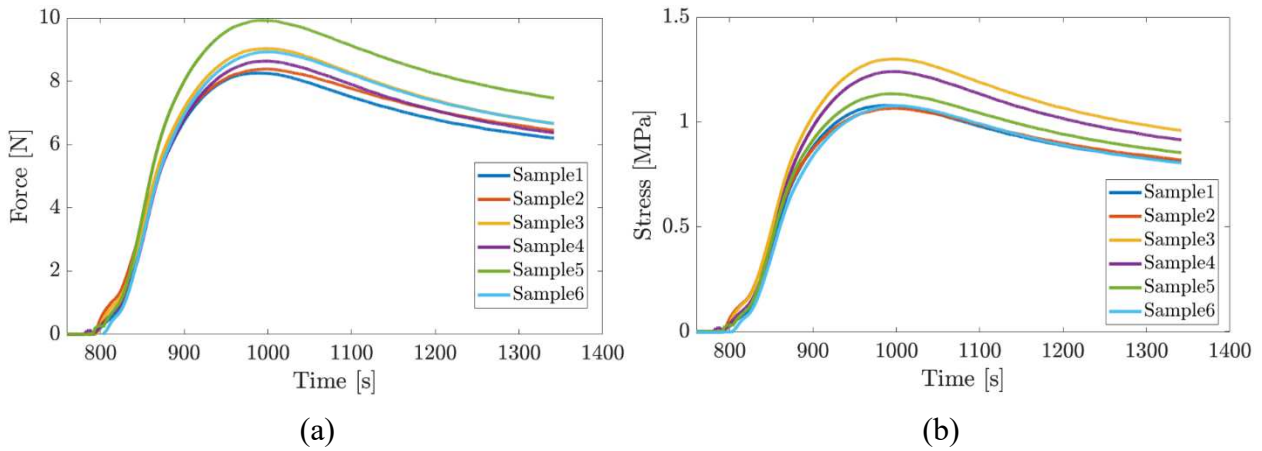


Figure 5.5. SMP and 20 wt. % CF PLA (C20) constrained shape recovery. (a) Shape Recovery Force. (b) Shape Recovery Flexural Stress.

For each case of study, all samples follow similar trends without any big outliers. For this reason, the median of all the data was calculated, and a representative curve is plotted. Figure 5.6a the curves of the pure shape memory polymer and its composites are plotted together. The averaged

curves show the same behavior as each individual sample. The composite curves have a fast increment of the SRFS values at the beginning of the recovery, followed by a decay that seems to stabilize with time. On the other hand, pure SMP shows an increment in SRFS, followed to a stabilization stage without decay. Figure 5.6b, the maximum average SRFS values for each material and in orange represent the standard deviation between samples. The highest deviation between samples corresponds to SMP with 20% CF PLA weight content.

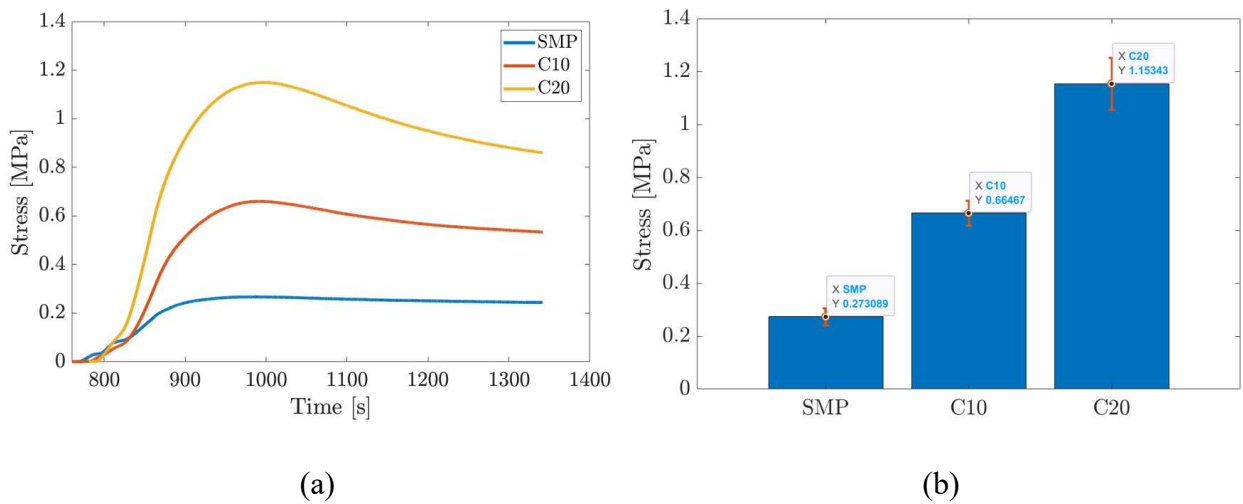


Figure 5.6. Shape recovery flexural stress for 100 wt. %SMP, 90 wt. %SMP and 10 wt. %CF15 PLA, 80 wt. %SMP and 20 wt. %CF15 PLA. (a) Shape Recovery Force vs time. (b) Maximum median SRFS with standard deviation.

From the plots, it is possible to say that the higher the weight content of CF PLA in the composite, the greater the values of SRFS. Having the biggest SRFS average of 1.15 MPa (standard deviation 0.0982) for SMP with 20wt. % CF PLA weight content (C20), the intermediate values of 0.66MPa (standard deviation 0.0466) for SMP with 10 wt. % CF PLA weight content (C10), and the lowest values of 0.27 MPa (standard deviation 0.0319) for pure SMP MM4520. These results are consistent with the ones found by Li et al., when unidirectional carbon fiber reinforced in an epoxy

based thermosetting SMP composite was studied, and the high values of SRFS are related to high values of carbon fiber content [28]. The carbon fiber content contributed stiffness to the composite, presenting greater resistance to deformation and facilitating recovery (increase in SRFS).

Because of the enhancement of SRFS of shape memory polyurethane MM4520 with the addition of CF PLA, it is recommended to reinforce shape memory polymers with carbon fibers in order to ensure a big enough recovery stress to overcome its own weight and have a proper recovery when a large-scale part is 3D printed.

5.3. Shape Recovery Displacement and Ratio

Data for the mid-span's displacement versus time for each sample is presented in Figure 5.7. All samples show an initial big displacement when they were exposed to $T_g+15^\circ\text{C}$, this is translated in a fast shape recovery. Curve reaches a stable state when there is almost no displacement, and the shape is about fully recovered. This behavior is aligned with the one described above for SRFS. At the initial moments of the recovery stage, the maximum values of SRFS are observed and these are the ones that drive the greatest displacements and fastest recovery of the initial (permanent) shape. From the composite specimens' plots, it can be noticed that even though all the samples are deformed at the same distance (6mm) in the programming stage, not all of them started the recovery from the same position. This means that the composite samples bounce back when the actuator is removed at a temperature below T_g , prior to heating. Some SMP samples and all C10 samples had a bounce back of approximately 1mm, this means that the recovery started with a sample deformation of 5mm instead of 6mm (See Figure 5.7a and Figure 5.7b). This is more pronounced for C20 samples that bounce back 2 mm and the value considered to calculate the shape recovery ratio (SRR) is 4mm deformation (Figure 5.7c). The bounced back could be due to

the added stiffness that carbon fibers provided in the composite, showing resistance to deformation. Moreover, the PLA contributes in some sense to the linear elastic behavior. This means that after the load (actuator) was removed the sample could have some elastic recuperation (this is only true if the specimen is not exposed for a long period of time to PLA glass transition temperature. Otherwise, PLA becomes rubber/soft).

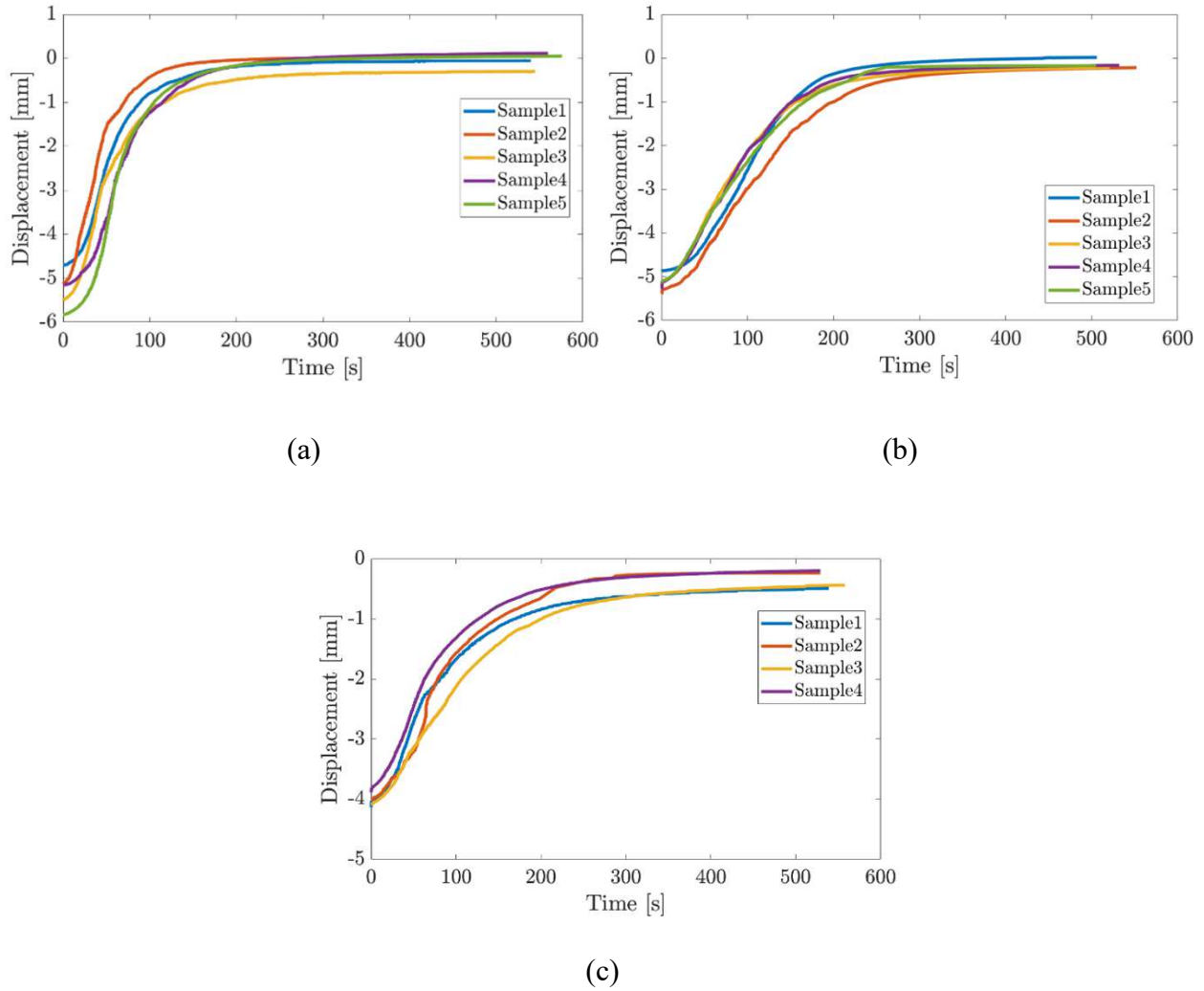


Figure 5.7. Shape recovery displacement. (a) Displacement for SMP samples. (b) Displacement for C10 samples. (c) Displacement for C20 samples

To be able to compare the recovery of the different kinds of composites, displacement graphs are normalized in terms of shape recovery ratio (SRR) (See Figure 5.8). In the Y axis is possible to see the percentage of the recovered shape with respect to the initial shape and on the X axis the time that the samples were exposed to $T_g+15^\circ\text{C}$.

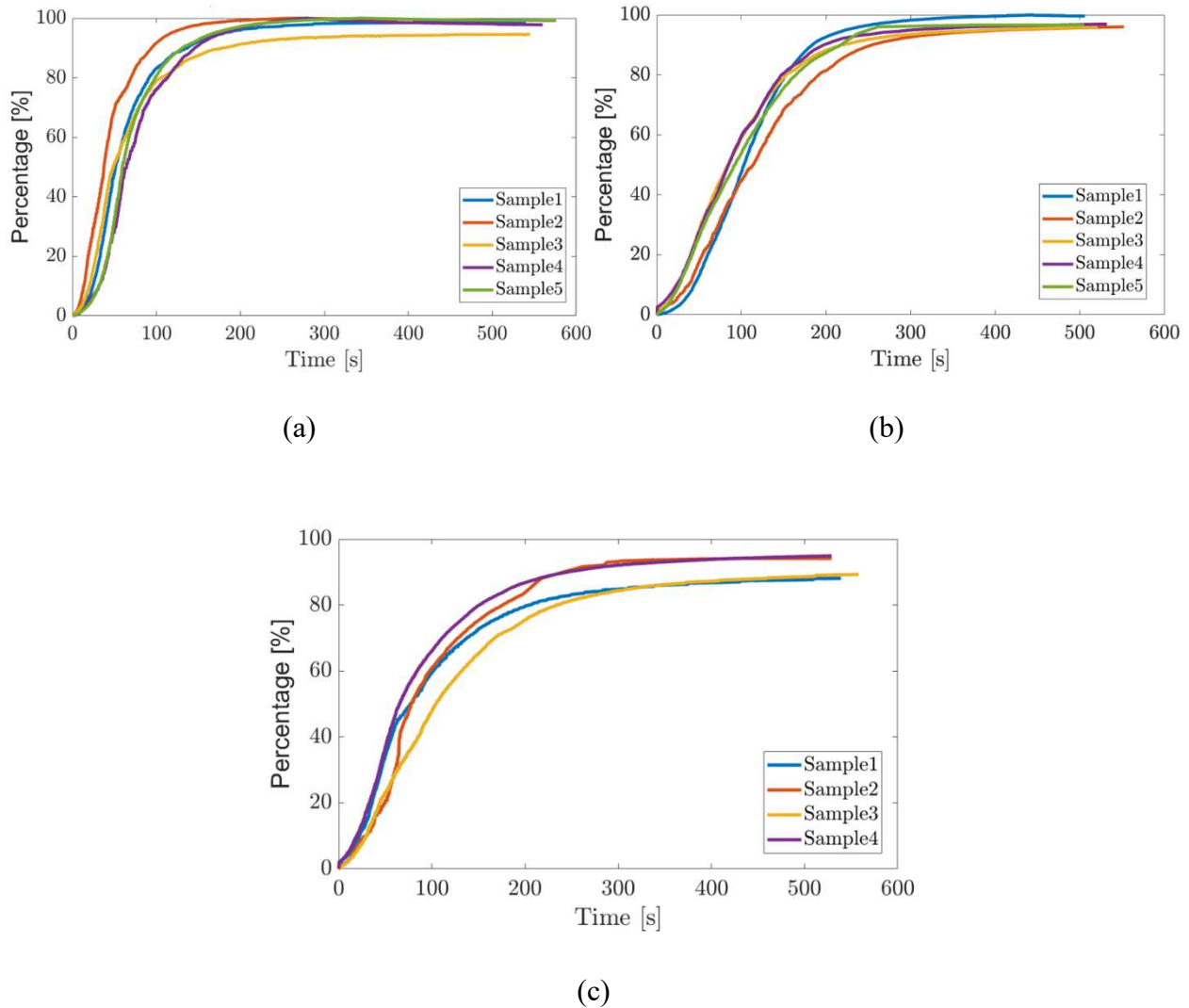


Figure 5.8. Shape recovery ratio. (a) SRR for SMP samples. (b) SRR for C10 samples. (c) SRR for C20 samples

In a previous study developed by Garces et al., about SMP MM4520, plots about Shape Recovery Ratio (SRR) with an activation temperature of 50°C were reported [70]. When those results are compared with in Figure 5.8a, it can be seen that the graphs follow the same and the values for SRR are similar (90% SRR for SMP).

To compare SRR among SMP, C10, and C20, the median of the data for each composite is plotted in Figure 5.9. Additionally, in Table 5.2 the values of the shape fixity ratio are presented.

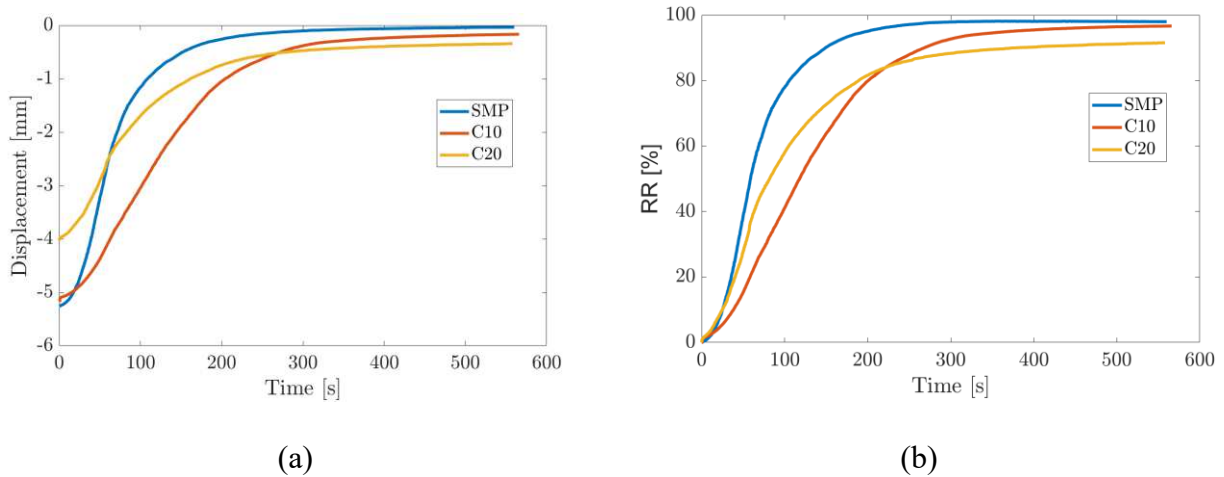


Figure 5.9. Median shape recovery displacement and ratio. (a) Median displacement. (b) Median SRR

Table 5.2. Shape fixity ratio for SMP, C10, C20

| Shape Fixity Ratio | | | |
|--------------------|-------|-------|-------|
| Samples | SMP | C10 | C20 |
| 1 | 81.46 | 85.93 | 71.50 |
| 2 | 85.71 | 87.79 | 68.04 |
| 3 | 89.05 | 87.56 | 69.90 |
| 4 | 92.46 | 89.81 | 66.67 |
| 5 | 92.75 | 87.80 | - |
| Average [%] | 88.29 | 87.78 | 69.03 |

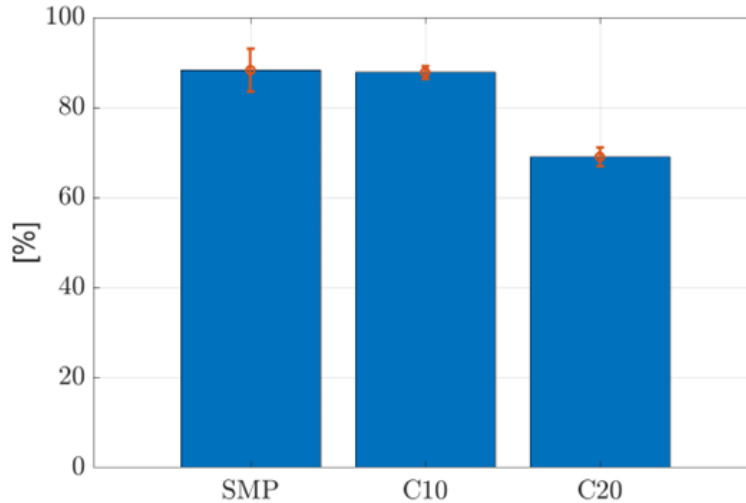


Figure 5.10. Shape Fixity Ratio for SMP, C10 and C20 with standard deviation.

In Figure 5.9 and Table 5.2 is observed that after removing the actuator that constrained the movement in the programming stage (deflection of 6mm), samples bounced back, being more notorious in the samples of SMP with 20wt. % of CF PLA. Considering the point 0mm as the initial coordinate of the mid-span along the Y axis, on average pure SMP samples started the recovery at -5.25mm of deflection, with a shape fixity ratio of 88.29% (bounce back) and recovered up to a distance of -0.03mm, SMP with 10 wt. % of CF PLA (C10) samples started the recovery at -5.16 mm with a shape fixity ratio (SRF) of 87.78% and recovered up to -0.17mm, and finally SMP with 20 wt. % of CF PLA (C20) samples started the recovery at -4.02mm with a shape fixity ratio (SRF) of 69.03% and recovered up to -0.34mm.

The reason for low recovery of the samples is the annealing stage. According to Raasch et al., shape memory polyurethane MM4520 3D printed samples decrease their T_g after annealing due to a decrease in crystallinity of the polymer and an increase of amorphous phase chain mobility [72]. A decrease in T_g could cause an early recovery of the samples, explaining the bounce back

at temperatures below T_g . Further studies of the molecular structure of the composites are recommended to verify changes in crystallinity.

Related to recovery velocity in Figure 5.9, it is observed that pure SMP samples have the fastest and greatest recovery, reaching 98% SRR after 600 seconds window that the experiment lasts. According to the slope of the curve, the next to recover is C20 but it only reaches 91.5% SRR and finally C10 with an SRR of 96.57%. About SRR, it is observed that an increment in the content of CF PLA in composite leads to a decrease in SRR. This outcome is similar to Li et al.,'s results, where SRRs of 94%, 93%, 95%, and 96% correspond to 37%, 30%, 23%, and 16% carbon fiber reinforcement mass fractions of an epoxy SMP respectively [28]. As stated before, the reduction of SRR is due to the addition of carbon fibers that contribute to increasing the stiffness of the composite as well as acting as an obstacle to the free movement of SMP [89].

6. CONCLUSIONS

6.1. Conclusions

Additive manufacturing brings multiple technologies with endless applications from automotive, robotic, manufacturing to aerospace industry. It has been seen that extrusion-based AM, also known as 3D printing, is one of the technologies that has undergone a great development and market expansion. Furthermore, the expectations for the near future are promising. To facilitate and encourage the adoption of 3D printing it will be necessary to scale up this technology. The next step is to jump from prototyping applications and desktop scale objects to larger products ready for real use applications. An important advantage of large-scale additive manufacturing (LSAM) is the reduction in printing times that also involve less energy consumption and decreases manufacturing costs.

However, when LSAM is used in conjunction with smart materials (LSAM 4D printing), two main drawbacks arise. The first is that the recovery stress is relatively low, and in the case of large 3D printed parts it causes that parts cannot recover properly under their own weight. The second drawback is related to the generation of internal stresses in large 3D-printed parts due to high temperature gradients between the top layers and bottom layers, which leads to problems like geometric distortion, warping, delamination, and cracks.

In the literature review the main focus of most studies related with SMP have been limited to characterize the polymer and its shape memory effect (SME). Limited research has been done regarding reinforcements in 4D printing. Having the opportunity to contribute valuable knowledge, the research done is developed to bring solutions to the problems faced by LSAM 4D printing.

The aims of this thesis are the commissioning of large-scale 3D printer to additive manufacture composites made of a thermoplastic polyurethane MM4520 (SMP) with different contents of a polymeric blend of PLA plus 15% (CF PLA) using direct pellet extrusion and analyze the effects of the constituents of the composite on shape memory properties.

The samples obtained proved that the modified 3D printer is able to get high quality 3D printed parts, this means parts with a consistent extrusion (neither under-extrusion nor over-extrusion), no gaps or voids, and no layer shifting. Besides, the mounting plates manufactured for the toolheads, allow to adjust the distance between the nozzle and the heated bed to the desire layer height in order to have a proper first 3D printed layer. Furthermore, the custom 3D printer was successfully able to not only direct pellet extrude but also can be used as filament printer (precise levelling between the printheads is recommended to avoid collisions between the printheads and the printed part before each print). This opens a door to research about manufacturing parts with materials that are only available in the market as pellets combined with common polymers that are sold as filaments.

To avoid heating cycles that could affect the properties of the SMP and CF PLA, the materials were bought in pellets form. The pellet extruder toolhead was used successfully to 4D printed samples of pure SMP MM4520 (SMP), SMP with 10 wt. % of CF PLA (C10), and SMP with 20 wt. % of CF PLA (C20).

It is observed that LSAM generates internal stresses on the 3D printed samples that affects their normal shape recovery. This was noticed when samples as printed were tested and the recovery shape reaches values over 100% (in the recovery the sample bent upwards instead of flat shape). For this reason, an annealing stage for 4D printed parts is recommended to mitigate internal stresses. In our case, annealing samples at 85°C for two hours showed a reduction of the internal

stresses, being able to have samples that recovered almost 100% of their original shape. Nevertheless, dimensional distortion of samples after annealing was observed. The distortion is attributed to the pre-strain in the material that is deposited during 3D printing. Although this is reported by Hu et al., it is recommended further studies to the particular case of LSAM and SMP due to the temperature gradients are much higher and their influence unknown.

Finally, to determine the influence of CF PLA in the shape memory effect, two kinds of experiments under bending conditions were performed successfully. The first is a constrain recovery test to study the shape recovery flexural stress (SRFS). The data reported indicate that the values of SRFS increase with increasing CF PLA weight content in the composite (C20's SRFS increased 400% more than SMP). C20 had the largest SRFS, followed by SMP C10 and pure SMP respectively. This finding proved that the use of a blend CF PLA with SMP could be a feasible solution to LSAM 4D printing low recovery response. The increment in SRFS allows 4D printing bigger parts that will be able to recover its initial shape. Even though the samples are tested under bending conditions, the results obtained provide insights to other loading scenarios.

The second experiment is a free recovery test to study the shape recovery ratio (SRR) and the shape recovery fixity (SRF). The addition of CF PLA reduces the SRF and SRR of the polymer. SMP have the greatest value of SRF followed by C10 and C20 (88.29%, 87.78% and 69.03% respectively).

Related to SRR, pure SMP samples almost fully recovered their permanent shape, having the highest value of SRR (98%), then C10 with an SRR of 96.57% and C20 with 91.5% SRR. This countereffect in SRR and SRF is undesired due to affect negatively final geometry of the recovered 4D printed part and the programmed shape respectively.

The addition of CF PLA to the studied shape memory polymer contributed stiffness to the composite and enhanced the shape recovery flexural stress. This directly addresses the problem of LSMA parts that can not overcome their own weight to recover the permanent shape. Nevertheless, SRR and SRF are influenced negatively by the addition of CF PLA. Some carbon fibers may hinder the free movement of the polymer when it wants to recover its permanent shape. It is concluded that the content of carbon fibers added is a trade off SRFS, SRR and SRF. The quantity of carbon fibres depends on the desire output for a specific application.

6.2. Future work

Related with the equipment modified, although no warping was reported in this thesis, it is recommended to install an enclosure to control the surrounding environment of the printed part and mitigate thermal gradients as future work. The feasibility of installation of heating elements to precise control the temperature of the air surrounding the 3D printer should be studied.

About the 3D printing process, this thesis was developed only around SMP MM4520, it is recommended to expand this study to other kind of SMPs suitable for 3D printing (printing parameters could need further tuning). Depending on the specific application and the SMPs used, research about the tradeoff of shape memory properties with the addition of CF PLA would be desired. Moreover, compatibility and delamination solutions should be investigated to make feasible the obtention of a laminate composite using the equipment available.

Regarding the testing procedure, the samples in this thesis were tested under bending conditions, it is recommended to investigate other scenarios under different loading conditions. Furthermore, mechanical characterization (Young's modulus, ultimate strength) of the composite is also needed to analyze the influence of CF PLA in mechanical properties. Different testing parameters, such

as, heating rates, loading rate and recovery temperature are parameters that have a high influence on the shape memory response and must be studied further.

Finally, a study of conceptual ideas and real size designs about large scale-structures using SMPs composites that could be printed in the modified big area 3D printer needs to be done to start with the manufacturing of large scale 4D printing parts in the laboratory.

REFERENCES

- [1] K.T. Maheswari, R. Srimathi, S. Jaanaa Rubavathy, al -, R. Shanmugam, M. ORamoni, J. Chandran, V. Mohanavel, L. Pugazhendhi, A Review on the significant classification of Additive Manufacturing, *J Phys Conf Ser* 2027 (2021) 12026. <https://doi.org/10.1088/1742-6596/2027/1/012026>.
- [2] P. Stavropoulos, P. Foteinopoulos, Modelling of additive manufacturing processes: a review and classification, (n.d.). <https://doi.org/10.1051/mfreview/2017014>.
- [3] S. El-Sayegh, L. Romdhane, S. Manjikian, A critical review of 3D printing in construction: benefits, challenges, and risks, *Archives of Civil and Mechanical Engineering* 20 (2020) 1–25. <https://doi.org/10.1007/S43452-020-00038-W/FIGURES/3>.
- [4] T.T. Wohlers, I. Campbell, O. Diegel, J. Kowen, 2018 Wohlers Report, Wohlers Associates (2018). <https://wohlersassociates.com/product/wohlers-report-2018/> (accessed November 25, 2023).
- [5] E.G. Bishop, S.J. Leigh, Using Large-Scale Additive Manufacturing as a Bridge Manufacturing Process in Response to Shortages in Personal Protective Equipment during the COVID-19 Outbreak, *Int J Bioprint* 6 (2020). <https://doi.org/10.18063/IJB.V6I4.281>.
- [6] K.M.M. Billah, J. Heineman, P. Mhatre, A. Roschli, B. Post, V. Kumar, S. Kim, G. Haye, J. Jackson, Z. Skelton, V. Kunc, A.A. Hassen, Large-scale additive manufacturing of self-heating molds, *Addit Manuf* 47 (2021) 102282. <https://doi.org/10.1016/J.ADDMA.2021.102282>.
- [7] F. Calignano, D. Manfredi, E.P. Ambrosio, S. Biamino, M. Lombardi, E. Atzeni, A. Salmi, P. Minetola, L. Iuliano, P. Fino, Overview on additive manufacturing technologies,

- Proceedings of the IEEE 105 (2017) 593–612.
<https://doi.org/10.1109/JPROC.2016.2625098>.
- [8] Y.P. Shaik, J. Schuster, A. Shaik, Y.P. Shaik, J. Schuster, A. Shaik, A Scientific Review on Various Pellet Extruders Used in 3D Printing FDM Processes, *Open Access Library Journal* 8 (2021) 1–19. <https://doi.org/10.4236/OALIB.1107698>.
- [9] A.A. Hassen, J. Lindahl, R. Springfield, B. Post, L. Love, C. Duty, U. Vaidya, R.B. Pipes, V. Kunc, The Durability of Large-Scale Additive Manufacturing Composite Molds, (2016). <https://www.researchgate.net/publication/324391116> (accessed November 28, 2023).
- [10] A. Bellini, L. Shor, S.I. Guceri, New developments in fused deposition modeling of ceramics, *Rapid Prototyp J* 11 (2005) 214–220. <https://doi.org/10.1108/13552540510612901/FULL/PDF>.
- [11] F. Pignatelli, G. Percoco, An application- and market-oriented review on large format additive manufacturing, focusing on polymer pellet-based 3D printing, *Progress in Additive Manufacturing* 7 (2022) 1363–1377. <https://doi.org/10.1007/S40964-022-00309-3/FIGURES/10>.
- [12] H. Meng, G. Li, A review of stimuli-responsive shape memory polymer composites, *Polymer (Guildf)* 54 (2013) 2199–2221. <https://doi.org/10.1016/J.POLYMER.2013.02.023>.
- [13] T. Cersoli, A. Cresanto, C. Herberger, E. Macdonald, P. Cortes, 3D Printed Shape Memory Polymers Produced via Direct Pellet Extrusion, *Micromachines* 2021, Vol. 12, Page 87 12 (2021) 87. <https://doi.org/10.3390/MI12010087>.
- [14] F. Soto, E. Karshalev, F. Zhang, B. Esteban Fernandez de Avila, A. Nourhani, J. Wang, Smart Materials for Microrobots, *Chem Rev* 122 (2022) 5365–5403.

https://doi.org/10.1021/ACS.CHEMREV.0C00999/ASSET/IMAGES/LARGE/CR0C00999_0016.JPEG.

- [15] M.I. Farid, W. Wu, L. Guiwei, Z. Yu, Research on imminent enlargements of smart materials and structures towards novel 4D printing (4DP: SMS-SSs), *The International Journal of Advanced Manufacturing Technology* 2023 126:7 126 (2023) 2803–2823. <https://doi.org/10.1007/S00170-023-11180-Z>.
- [16] S.Q. Ma, Y.P. Zhang, M. Wang, Y.H. Liang, L. Ren, L.Q. Ren, Recent progress in 4D printing of stimuli-responsive polymeric materials, *Sci China Technol Sci* 63 (2020) 532–544. <https://doi.org/10.1007/S11431-019-1443-1/METRICS>.
- [17] J.J. Wu, L.M. Huang, Q. Zhao, T. Xie, 4D Printing: History and Recent Progress, *Chinese Journal of Polymer Science (English Edition)* 36 (2018) 563–575. <https://doi.org/10.1007/S10118-018-2089-8/METRICS>.
- [18] J. Jiang, Y. Ma, Path Planning Strategies to Optimize Accuracy, Quality, Build Time and Material Use in Additive Manufacturing: A Review, *Micromachines (Basel)* 11 (2020). <https://doi.org/10.3390/MI11070633>.
- [19] E. Fernández, C. Ayas, M. Langelaar, P. Duysinx, Topology optimisation for large-scale additive manufacturing: generating designs tailored to the deposition nozzle size, *Virtual Phys Prototyp* 16 (2021) 196–220. <https://doi.org/10.1080/17452759.2021.1914893>.
- [20] H. Shen, L. Pan, J. Qian, Research on large-scale additive manufacturing based on multi-robot collaboration technology, *Addit Manuf* 30 (2019) 100906. <https://doi.org/10.1016/J.ADDMA.2019.100906>.

- [21] B.G. Compton, B.K. Post, C.E. Duty, L. Love, V. Kunc, Thermal analysis of additive manufacturing of large-scale thermoplastic polymer composites, *Addit Manuf* 17 (2017) 77–86. <https://doi.org/10.1016/J.ADDMA.2017.07.006>.
- [22] L.J. Love, Utility of Big Area Additive Manufacturing (BAAM) For The Rapid Manufacture of Customized Electric Vehicles, (2015). <https://doi.org/10.2172/1209199>.
- [23] M. Mehrpouya, H. Vahabi, S. Janbaz, A. Darafsheh, T.R. Mazur, S. Ramakrishna, 4D printing of shape memory polylactic acid (PLA), *Polymer (Guildf)* 230 (2021) 124080. <https://doi.org/10.1016/J.POLYMER.2021.124080>.
- [24] A. Mitchell, U. Lafont, M. Hołyńska, C. Semprimoschnig, Additive manufacturing — A review of 4D printing and future applications, *Addit Manuf* 24 (2018) 606–626. <https://doi.org/10.1016/J.ADDMA.2018.10.038>.
- [25] T.T. Nguyen, J. Kim, 4D-Printing — Fused Deposition Modeling Printing and PolyJet Printing with Shape Memory Polymers Composite, *Fibers and Polymers* 21 (2020) 2364–2372. <https://doi.org/10.1007/S12221-020-9882-Z/METRICS>.
- [26] L. Tzounis, M. Petousis, S. Grammatikos, N. Vidakis, 3D Printed Thermoelectric Polyurethane/Multiwalled Carbon Nanotube Nanocomposites: A Novel Approach towards the Fabrication of Flexible and Stretchable Organic Thermoelectrics, *Materials (Basel)* 13 (2020). <https://doi.org/10.3390/MA13122879>.
- [27] J.W. Cho, J.W. Kim, Y.C. Jung, N.S. Goo, Electroactive Shape-Memory Polyurethane Composites Incorporating Carbon Nanotubes, *Macromol Rapid Commun* 26 (2005) 412–416. <https://doi.org/10.1002/MARC.200400492>.
- [28] F. Li, F. Scarpa, X. Lan, L. Liu, Y. Liu, J. Leng, Bending shape recovery of unidirectional carbon fiber reinforced epoxy-based shape memory polymer composites, *Compos Part A*

- Appl Sci Manuf 116 (2019) 169–179.
<https://doi.org/10.1016/J.COMPOSITESA.2018.10.037>.
- [29] C.E. Duty, V. Kunc, B. Compton, B. Post, D. Erdman, R. Smith, R. Lind, P. Lloyd, L. Love, Structure and mechanical behavior of Big Area Additive Manufacturing (BAAM) materials, *Rapid Prototyp J* 23 (2017) 181–189. <https://doi.org/10.1108/RPJ-12-2015-0183/FULL/PDF>.
- [30] A. Cano-Vicent, M.M. Tambuwala, S.S. Hassan, D. Barh, A.A.A. Aljabali, M. Birkett, A. Arjunan, Á. Serrano-Aroca, Fused deposition modelling: Current status, methodology, applications and future prospects, *Addit Manuf* 47 (2021) 102378. <https://doi.org/10.1016/J.ADDMA.2021.102378>.
- [31] V. Mishra, S. Negi, S. Kar, FDM-based additive manufacturing of recycled thermoplastics and associated composites, *Journal of Material Cycles and Waste Management* 2023 25:2 25 (2023) 758–784. <https://doi.org/10.1007/S10163-022-01588-2>.
- [32] B. Kading, J. Straub, Utilizing in-situ resources and 3D printing structures for a manned Mars mission, *Acta Astronaut* 107 (2015) 317–326. <https://doi.org/10.1016/J.ACTAASTRO.2014.11.036>.
- [33] Covid 19 | Original Prusa 3D printers directly from Josef Prusa, (n.d.). https://www.prusa3d.com/page/covid-19_379/ (accessed November 13, 2023).
- [34] B.I. Oladapo, S.O. Ismail, T.D. Afolalu, D.B. Olawade, M. Zahedi, Review on 3D printing: Fight against COVID-19, *Mater Chem Phys* 258 (2021) 123943. <https://doi.org/10.1016/J.MATCHEMPHYS.2020.123943>.

- [35] J. Villacres, D. Nobes, C. Ayranci, Additive manufacturing of shape memory polymers: effects of print orientation and infill percentage on mechanical properties, *Rapid Prototyp J* 24 (2018) 744–751. <https://doi.org/10.1108/RPJ-03-2017-0043/FULL/PDF>.
- [36] M.R. Khosravani, F. Berto, M.R. Ayatollahi, T. Reinicke, Characterization of 3D-printed PLA parts with different raster orientations and printing speeds, *Sci Rep* 12 (2022). <https://doi.org/10.1038/s41598-022-05005-4>.
- [37] S.H.R. Sanei, D. Popescu, 3D-Printed Carbon Fiber Reinforced Polymer Composites: A Systematic Review, *Journal of Composites Science* 2020, Vol. 4, Page 98 4 (2020) 98. <https://doi.org/10.3390/JCS4030098>.
- [38] R.B. Kristiawan, F. Imaduddin, D. Ariawan, Ubaidillah, Z. Arifin, A review on the fused deposition modeling (FDM) 3D printing: Filament processing, materials, and printing parameters, *Open Engineering* 11 (2021) 639–649. https://doi.org/10.1515/ENG-2021-0063/ASSET/GRAPHIC/J_ENG-2021-0063_FIG_003.JPG.
- [39] L. Ren, Z. Wang, L. Ren, C. Xu, B. Li, Y. Shi, Q. Liu, Understanding the role of process parameters in 4D printing: A review, *Compos B Eng* 265 (2023) 110938. <https://doi.org/10.1016/J.COMPOSITESB.2023.110938>.
- [40] T. Rayna, L. Striukova, From rapid prototyping to home fabrication: How 3D printing is changing business model innovation, *Technol Forecast Soc Change* 102 (2016) 214–224. <https://doi.org/10.1016/J.TECHFORE.2015.07.023>.
- [41] J. Shah, B. Snider, T. Clarke, S. Kozutsky, M. Lacki, A. Hosseini, Large-scale 3D printers for additive manufacturing: design considerations and challenges, *International Journal of Advanced Manufacturing Technology* 104 (2019) 3679–3693. <https://doi.org/10.1007/S00170-019-04074-6/FIGURES/16>.

- [42] P. Minetola, M. Galati, A challenge for enhancing the dimensional accuracy of a low-cost 3D printer by means of self-replicated parts, *Addit Manuf* 22 (2018) 256–264. <https://doi.org/10.1016/J.ADDMA.2018.05.028>.
- [43] Local Motors shows Strati, the world's first 3D-printed car | Fortune, (n.d.). <https://fortune.com/2015/01/13/local-motors-shows-strati-the-worlds-first-3d-printed-car/> (accessed November 26, 2023).
- [44] C.E. Duty, V. Kunc, B. Compton, B. Post, D. Erdman, R. Smith, R. Lind, P. Lloyd, L. Love, Structure and mechanical behavior of Big Area Additive Manufacturing (BAAM) materials, *Rapid Prototyp J* 23 (2017) 181–189. <https://doi.org/10.1108/RPJ-12-2015-0183/FULL/PDF>.
- [45] Largest 3D printers in 2023 for XXL prints, (n.d.). https://www.aniwaa.com/buyers-guide/3d-printers/largest-3d-printers/#The_15_largest_3D_printers_in_2018 (accessed December 4, 2023).
- [46] Airbus had 1,000 parts 3D printed to meet deadline - BBC News, (n.d.). <https://www.bbc.com/news/technology-32597809> (accessed November 26, 2023).
- [47] D. Alberti, Towards the Design and Manufacturing of Products Using Large-Scale FFF Printers, (2020). <https://doi.org/10.7939/R3-7FPF-4A57>.
- [48] A. Pagés-Llobet, F.X. Espinach, F. Julián, H. Oliver-Ortega, J.A. Méndez, Effect of Extruder Type in the Interface of PLA Layers in FDM Printers: Filament Extruder Versus Direct Pellet Extruder, *Polymers* 2023, Vol. 15, Page 2019 15 (2023) 2019. <https://doi.org/10.3390/POLYM15092019>.
- [49] M.A.H. Khondoker, D. Sameoto, Direct coupling of fixed screw extruders using flexible heated hoses for FDM printing of extremely soft thermoplastic elastomers, *Progress in*

- Additive Manufacturing 4 (2019) 197–209. <https://doi.org/10.1007/S40964-019-00088-4/FIGURES/6>.
- [50] P. Oblak, J. Gonzalez-Gutierrez, B. Zupančič, A. Aulova, I. Emri, Processability and mechanical properties of extensively recycled high density polyethylene, *Polym Degrad Stab* 114 (2015) 133–145. <https://doi.org/10.1016/J.POLYMDEGRADSTAB.2015.01.012>.
- [51] K. Hamad, M. Kaseem, F. Deri, Effect of recycling on rheological and mechanical properties of poly(lactic acid)/polystyrene polymer blend, *J Mater Sci* 46 (2011) 3013–3019. <https://doi.org/10.1007/S10853-010-5179-8/FIGURES/12>.
- [52] F. Vilaplana, S. Karlsson, Quality Concepts for the Improved Use of Recycled Polymeric Materials: A Review, *Macromol Mater Eng* 293 (2008) 274–297. <https://doi.org/10.1002/MAME.200700393>.
- [53] I. Pillin, N. Montrelay, A. Bourmaud, Y. Grohens, Effect of thermo-mechanical cycles on the physico-chemical properties of poly(lactic acid), *Polym Degrad Stab* 93 (2008) 321–328. <https://doi.org/10.1016/J.POLYMDEGRADSTAB.2007.12.005>.
- [54] F.A. Cruz Sanchez, H. Boudaoud, S. Hoppe, M. Camargo, Polymer recycling in an open-source additive manufacturing context: Mechanical issues, *Addit Manuf* 17 (2017) 87–105. <https://doi.org/10.1016/J.ADDMA.2017.05.013>.
- [55] C. Cardona, A.H. Curdes, A.J. Isaacs, Effects of Filament Diameter Tolerances in Fused Filament Fabrication, *IU Journal of Undergraduate Research* 2 (2016) 44–47. <https://doi.org/10.14434/IUJUR.V2I1.20917>.
- [56] L. Fontana, A. Giubilini, R. Arrigo, G. Malucelli, P. Minetola, Characterization of 3D Printed Polylactic Acid by Fused Granular Fabrication through Printing Accuracy, Porosity,

- Thermal and Mechanical Analyses, *Polymers* 2022, Vol. 14, Page 3530 14 (2022) 3530.
<https://doi.org/10.3390/POLYM14173530>.
- [57] M.A. Kreiger, M.L. Mulder, A.G. Glover, J.M. Pearce, Life cycle analysis of distributed recycling of post-consumer high density polyethylene for 3-D printing filament, *J Clean Prod* 70 (2014) 90–96. <https://doi.org/10.1016/J.JCLEPRO.2014.02.009>.
- [58] D.J. Byard, A.L. Woern, R.B. Oakley, M.J. Fiedler, S.L. Snabes, J.M. Pearce, Green fab lab applications of large-area waste polymer-based additive manufacturing, *Addit Manuf* 27 (2019) 515–525. <https://doi.org/10.1016/J.ADDMA.2019.03.006>.
- [59] M.Y. Khalid, Z.U. Arif, R. Noroozi, A. Zolfagharian, M. Bodaghi, 4D printing of shape memory polymer composites: A review on fabrication techniques, applications, and future perspectives, *J Manuf Process* 81 (2022) 759–797. <https://doi.org/10.1016/J.JMAPRO.2022.07.035>.
- [60] M. Bengisu, M. Ferrara, *Materials that Move*, (2018). <https://doi.org/10.1007/978-3-319-76889-2>.
- [61] S. Tibbits, 4D Printing: Multi-Material Shape Change, *Architectural Design* 84 (2014) 116–121. <https://doi.org/10.1002/AD.1710>.
- [62] I.T. Garces, C. Ayranci, A view into additive manufactured electro-active reinforced smart composite structures, *Manuf Lett* 16 (2018) 1–5. <https://doi.org/10.1016/J.MFGLET.2018.02.008>.
- [63] S.K. Leist, J. Zhou, Current status of 4D printing technology and the potential of light-reactive smart materials as 4D printable materials, *Virtual Phys Prototyp* 11 (2016) 249–262. <https://doi.org/10.1080/17452759.2016.1198630>.

- [64] M. Zarek, M. Layani, I. Cooperstein, E. Sachyani, D. Cohn, S. Magdassi, 3D Printing of Shape Memory Polymers for Flexible Electronic Devices, *Advanced Materials* 28 (2016) 4449–4454. <https://doi.org/10.1002/ADMA.201503132>.
- [65] T. Kim, Y.G. Lee, Shape transformable bifurcated stents, *Scientific Reports* 2018 8:1 8 (2018) 1–9. <https://doi.org/10.1038/s41598-018-32129-3>.
- [66] Y. Yang, Y. Chen, Novel design and 3D printing of variable stiffness robotic fingers based on shape memory polymer, *Proceedings of the IEEE RAS and EMBS International Conference on Biomedical Robotics and Biomechatronics 2016-July* (2016) 195–200. <https://doi.org/10.1109/BIOROB.2016.7523621>.
- [67] C.H. Son, S. Jeong, S. Lee, P.M. Ferreira, S. Kim, Tunable Adhesion of Shape Memory Polymer Dry Adhesive Soft Robotic Gripper via Stiffness Control †, *Robotics* 12 (2023) 59. <https://doi.org/10.3390/ROBOTICS12020059/S1>.
- [68] W.M. Huang, C.L. Song, Y.Q. Fu, C.C. Wang, Y. Zhao, H. Purnawali, H.B. Lu, C. Tang, Z. Ding, J.L. Zhang, Shaping tissue with shape memory materials, *Adv Drug Deliv Rev* 65 (2013) 515–535. <https://doi.org/10.1016/J.ADDR.2012.06.004>.
- [69] Shape Memory Polymer | SMP Technologies Inc. | DiAPLEX, (n.d.). <http://www2.smp techno.com/en/smp/> (accessed November 14, 2023).
- [70] I.T. Garces, S. Aslanzadeh, Y. Boluk, C. Ayrançi, Effect of Moisture on Shape Memory Polyurethane Polymers for Extrusion-Based Additive Manufacturing, *Materials* 2019, Vol. 12, Page 244 12 (2019) 244. <https://doi.org/10.3390/MA12020244>.
- [71] A.A. Ameen, A.M. Takhakh, A. Abdal-hay, An overview of the latest research on the impact of 3D printing parameters on shape memory polymers, *Eur Polym J* 194 (2023) 112145. <https://doi.org/10.1016/J.EURPOLYMJ.2023.112145>.

- [72] J. Raasch, M. Ivey, D. Aldrich, D.S. Nobes, C. Ayranci, Characterization of polyurethane shape memory polymer processed by material extrusion additive manufacturing, *Addit Manuf* 8 (2015) 132–141. <https://doi.org/10.1016/J.ADDMA.2015.09.004>.
- [73] J. Villacres, D. Nobes, C. Ayranci, Additive manufacturing of shape memory polymers: effects of print orientation and infill percentage on shape memory recovery properties, *Rapid Prototyp J* 26 (2020) 1593–1602. <https://doi.org/10.1108/RPJ-09-2019-0239/FULL/PDF>.
- [74] D. Zonoobi, Mechanical Properties of Extrusion-Based Additive Manufacturing of Shape Memory Polymers, Master Thesis, University of Alberta, 2019. <https://doi.org/10.7939/R3-EQ6A-QE05>.
- [75] I.A. Rousseau, Challenges of shape memory polymers: A review of the progress toward overcoming SMP's limitations, *Polym Eng Sci* 48 (2008) 2075–2089. <https://doi.org/10.1002/PEN.21213>.
- [76] L. Zhang, Z. Lin, Q. Zhou, S. Ma, Y. Liang, Z. Zhang, PEEK modified PLA shape memory blends: towards enhanced mechanical and deformation properties, *Front Mater Sci* 14 (2020) 177–187. <https://doi.org/10.1007/S11706-020-0502-Z/METRICS>.
- [77] Y. Ding, H. Ma, X. Liu, S. Qin, J. Liu, G. Qu, Y. Bai, L. Zhao, Improvement of the mechanical and shape memory properties in polylactide/polyethylene glycol blends by reactive graphene oxide, *Int J Biol Macromol* 253 (2023) 127346. <https://doi.org/10.1016/J.IJBIOMAC.2023.127346>.
- [78] Y. Wang, J. Zhang, M. Li, M. Lei, Y. Wang, Q. Wei, 3D printing thermo-responsive shape memory polymer composite based on PCL/TPU blends, *Journal of Polymer Research* 29 (2022) 1–14. <https://doi.org/10.1007/S10965-022-03095-2/FIGURES/10>.

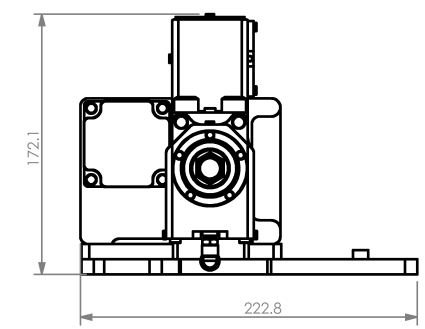
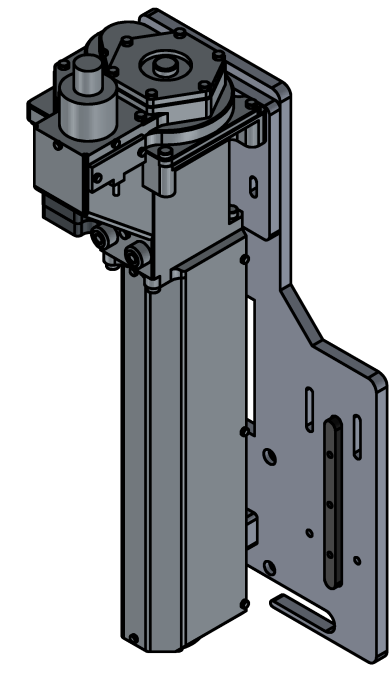
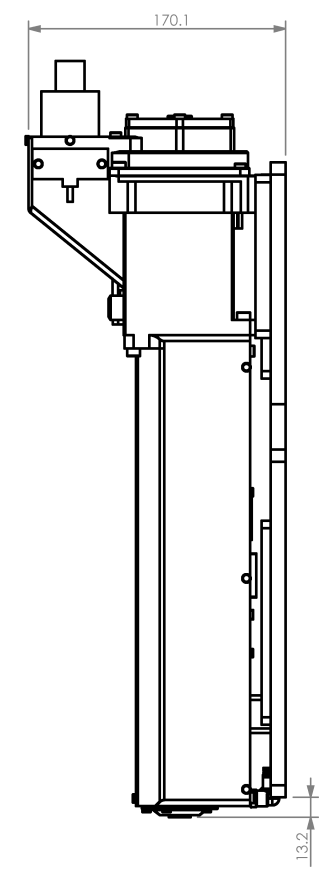
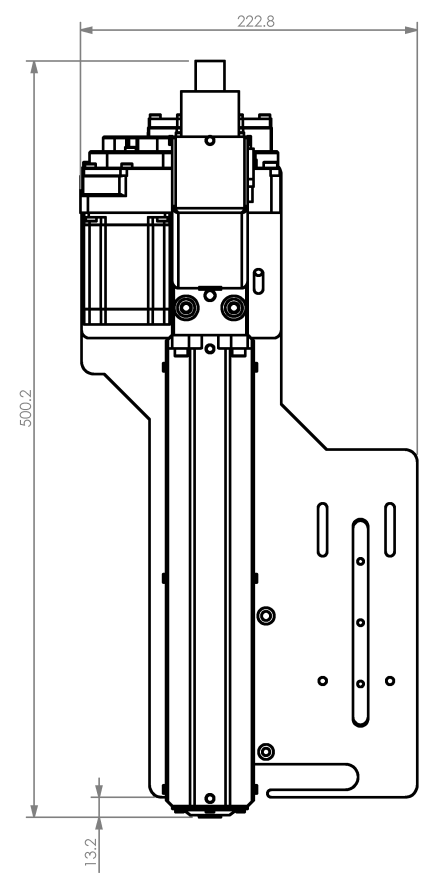
- [79] S. Jafari Horastani, M. Karevan, M. Ghane, Structural, thermal, and viscoelastic response of nanoclay reinforced polylactic acid/thermoplastic polyurethane shape-memory nanocomposites of low transition temperature, *Polym Adv Technol* 33 (2022) 2720–2735. <https://doi.org/10.1002/PAT.5727>.
- [80] M. Lei, Z. Chen, H. Lu, K. Yu, Recent progress in shape memory polymer composites: Methods, properties, applications and prospects, *Nanotechnol Rev* 8 (2019) 327–351. https://doi.org/10.1515/NTREV-2019-0031/ASSET/GRAPHIC/J_NTREV-2019-0031_FIG_005.JPG.
- [81] Welcome to 3D Platform, (n.d.). <https://www.3dplatform.com/> (accessed December 13, 2023).
- [82] High Performance 3D Printer Extruders, Hotends & Parts - DYZE DESIGN, (n.d.). <https://dyzedesign.com/> (accessed December 13, 2023).
- [83] Duet 2 WiFi and Ethernet Hardware Overview | Duet3D Documentation, (n.d.). https://docs.duet3d.com/Duet3D_hardware/Duet_2_family/Duet_2_WiFi_Ethernet_Hardware_Overview (accessed December 19, 2023).
- [84] CF15 PLA Pellets | Make your own awesome filament!, (n.d.). <https://www.3dxtech.com/product/cf15-pla-pellets/> (accessed December 25, 2023).
- [85] ASTM standard D790, Standard Test Methods for Flexural Properties of Unreinforced and Reinforced Plastics and Electrical Insulating Materials, ASTM International (2017).
- [86] G. Hu, M. Bodaghi, Direct Fused Deposition Modeling 4D Printing and Programming of Thermoresponsive Shape Memory Polymers with Autonomous 2D-to-3D Shape Transformations, *Adv Eng Mater* (2023). <https://doi.org/10.1002/adem.202300334>.

- [87] ASTM standard D790, Standard Test Methods for Flexural Properties of Unreinforced and Reinforced Plastics and Electrical Insulating Materials, ASTM International (2017).
- [88] J. Suder, Z. Bobovsky, M. Safar, J. Mlotek, M. Vocetka, Z. Zeman, Experimental analysis of temperature resistance of 3d printed PLA components, *MM Science Journal* 2021 (2021) 4322–4327. https://doi.org/10.17973/MMSJ.2021_03_2021004.
- [89] M. Ramesh, L. Rajeshkumar, D. Balaji, Influence of Process Parameters on the Properties of Additively Manufactured Fiber-Reinforced Polymer Composite Materials: A Review, *J Mater Eng Perform* 30 (2021) 4792–4807. <https://doi.org/10.1007/s11665-021-05832-y>.

Appendix 1

8 7 6 5 4 3 2 1

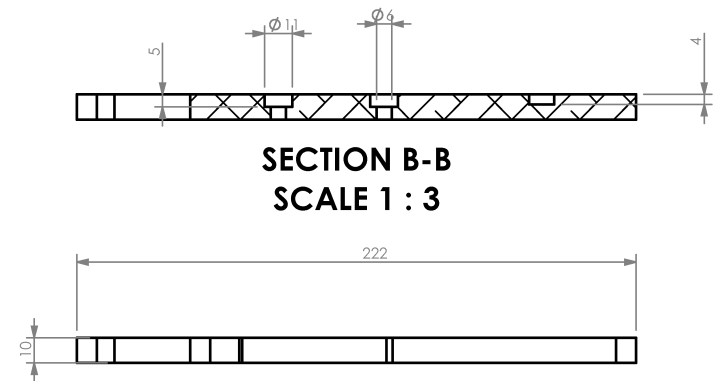
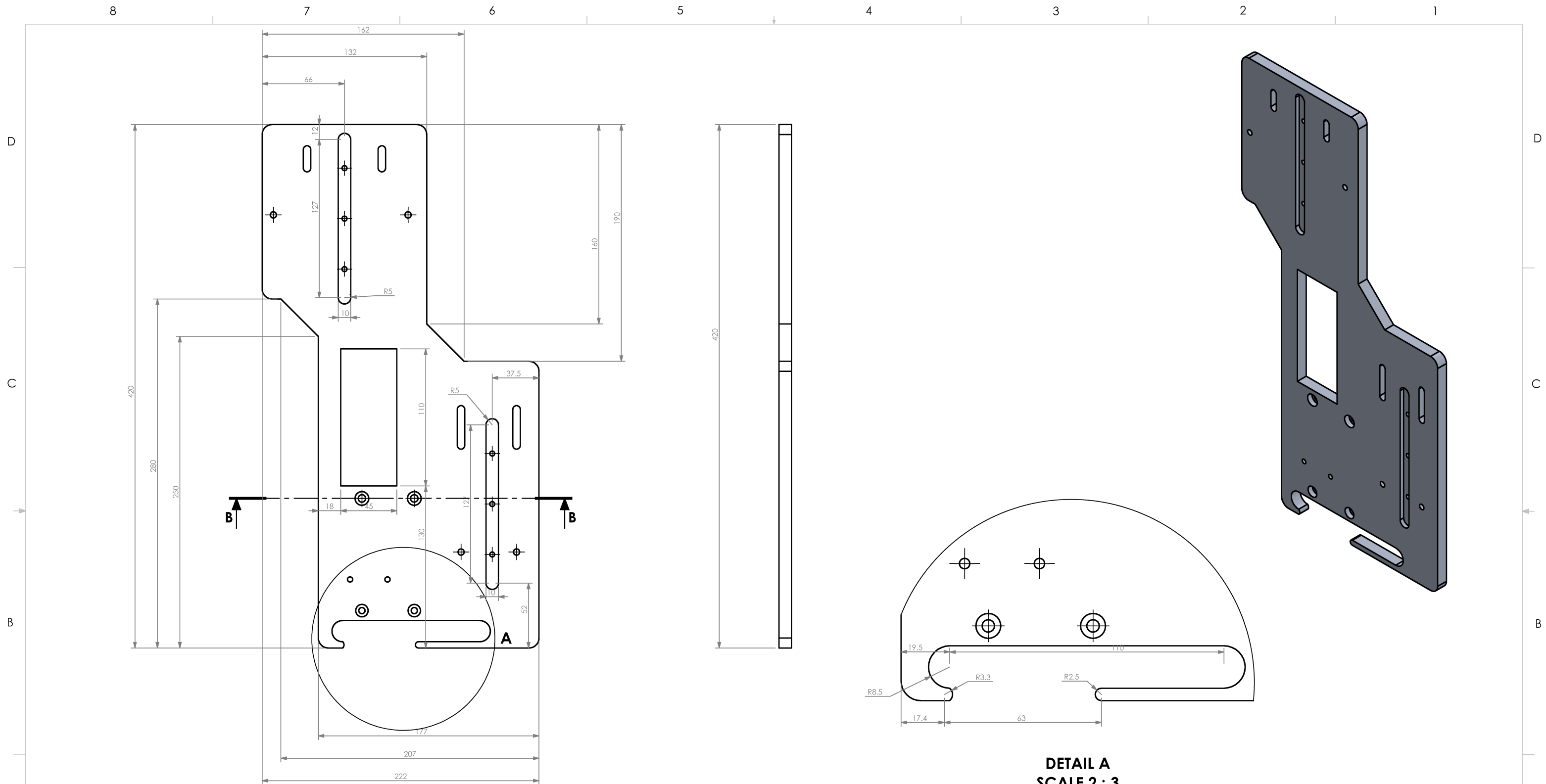
D
C
B
A



Note:
 The height of the nozzle with respect the heated bed can be adjusted.
 The plates "Plate-printer" and "Plate-extruder" can slide into each other.
 The dimensions shown here are only for reference, could change depending on the desire layer height.

| | | | | |
|---|--|---|-----------------------------------|---|
| Department: Mechanical Engineering Comments:  | UNLESS OTHERWISE SPECIFIED: DIMENSIONS ARE IN MM TOLERANCES: ANGULAR: $\pm 0.5^\circ$ LINEAR X = ± 0.5 X.X = ± 0.1 X.XX = ± 0.025 SURFACE FINISH μm 0.6 ✓ DO NOT SCALE DRAWING | DRAWN BY: Marco Paez | |  The Department of Mechanical Engineering UNIVERSITY OF ALBERTA |
| | | Checked Marco Paez Approved Marco Paez Comments None Date 2/2/2024 | TITLE: <h1>Plate extruder</h1> | |
| MATERIAL: Aluminum 6061 Appendix 01 | | SIZE B | Drawing Number MP 001 | REV |
| | | SCALE: 1:5 | Mass: | Page 96 |

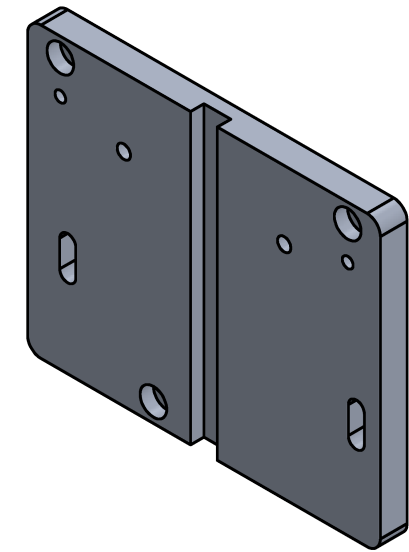
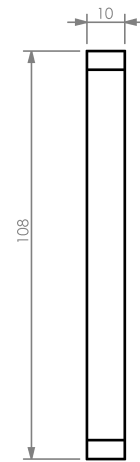
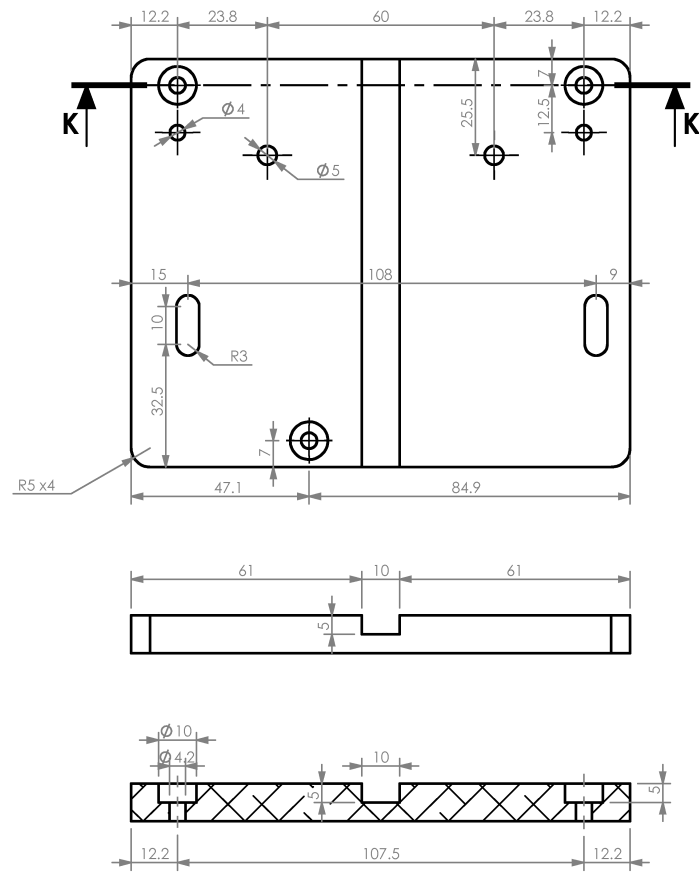
8 7 6 5 4 3 2 1



SECTION B-B
SCALE 1 : 3

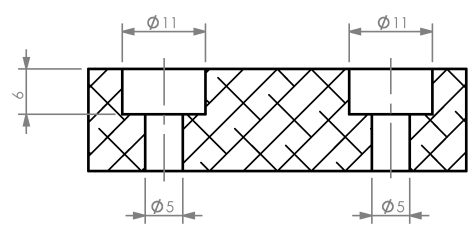
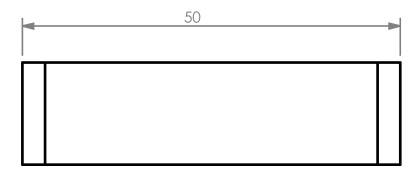
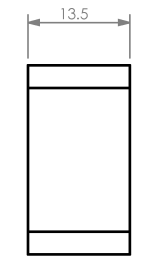
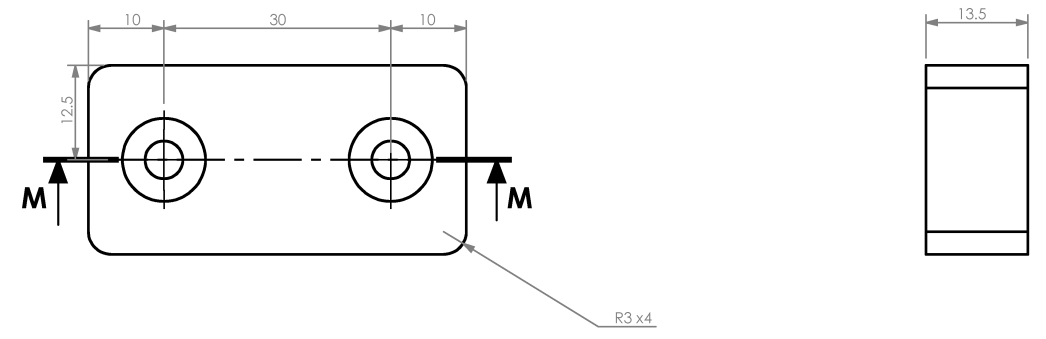
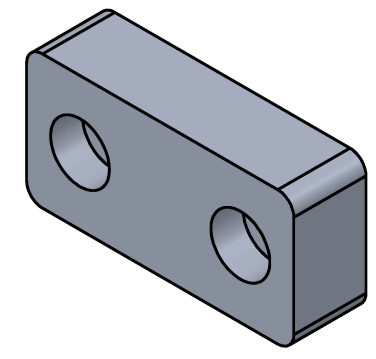
DETAIL A
SCALE 2 : 3

| | | | | | | |
|---|--|---|---|---|-------------------------|--|
| Department: Mechanical Engineering Comments:  | UNLESS OTHERWISE SPECIFIED: DIMENSIONS ARE IN MM TOLERANCES: ANGULAR: $\pm 0.5^\circ$ LINEAR X = ± 0.5 X.X = ± 0.1 X.XX = ± 0.025 SURFACE FINISH μm 0.6 ✓ DO NOT SCALE DRAWING | DRAWN BY: Marco Paez | |  The Department of Mechanical Engineering UNIVERSITY OF ALBERTA | | |
| | | Checked: Marco Paez Approved: Marco Paez Comments: None Date: 2/2/2024 | TITLE: <h1>Plate-printer</h1> | | SIZE B | Drawing Number MP 002 |
| MATERIAL: Aluminum 6061 Appendix 01 | | SCALE: 1:3 | | Mass: | | Page 97 |



**SECTION K-K
SCALE 1 : 2**

| | | | | |
|---|--|---|--|--|
| Department: Mechanical Engineering Comments:  | UNLESS OTHERWISE SPECIFIED: DIMENSIONS ARE IN MM TOLERANCES: ANGULAR: $\pm 0.5^\circ$ LINEAR X = ± 0.5 X.X = ± 0.1 X.XX = ± 0.025 SURFACE FINISH μm 0.6 ✓ DO NOT SCALE DRAWING | DRAWN BY: Marco Paez | |  The Department of Mechanical Engineering UNIVERSITY OF ALBERTA TITLE: Plate-extruder |
| | | Checked Marco Paez Approved Marco Paez Comments None Date 2/2/2024 | SIZE B Drawing Number MP 004 REV | |
| MATERIAL: Aluminum 6061 Appendix 01 | | SCALE: 1:2 Mass: | | Page 99 |



**SECTION M-M
SCALE 1 : 1**

| | | | | |
|---|--|---|--|--|
| Department: Mechanical Engineering Comments:  | UNLESS OTHERWISE SPECIFIED: DIMENSIONS ARE IN MM TOLERANCES: ANGULAR: $\pm 0.5^\circ$ LINEAR X = ± 0.5 X.X = ± 0.1 X.XX = ± 0.025 SURFACE FINISH μm 0.6 ✓ DO NOT SCALE DRAWING | DRAWN BY: Marco Paez | |  The Department of Mechanical Engineering UNIVERSITY OF ALBERTA TITLE: <h2 style="text-align: center;">Support extruder</h2> |
| | | Checked Marco Paez Approved Marco Paez Comments None Date 2/2/2024 | SIZE B Drawing Number MP 005 REV | |
| MATERIAL: Aluminum 6061 Appendix 01 | | SCALE: 1:1 Mass: | Page 100 | |

Appendix 2

```
; Configuration file for Duet WiFi (firmware version 3.3)
; executed by the firmware on start-up
;
; generated by RepRapFirmware Configuration Tool v3.3.13 on Sat Oct 08
2022 18:01:37 GMT-0600 (Mountain Daylight Time)

; General preferences
M111 S0 ; Debugging off
M575 P1 S1 B57600 ; enable support for
PanelDue
G90 ; send absolute
coordinates
M82 ; but relative extruder
moves
M550 P"Marco Paez" ; set printer name
M302 S140 P0

; Network
M552 P0.0.0.0 S1 ; enable network and
acquire dynamic address via DHCP
M586 P0 S1 ; enable HTTP
M586 P1 S0 ; disable FTP
M586 P2 S0 ; disable Telnet

; Drives
M569 P0 R-1 ; Drive 0 disabled
M569 P1 R-1 ; Drive 1 disabled
M569 P2 R-1 ; Drive 2 disabled
M569 P3 S1 ; physical drive 3 goes
forwards
M569 P4 S1 ; physical drive 4 goes
forwards
M569 P5 S1 ; 2 microsecond
minimum step pulse width for x-axis
M569 P6 S1 ; 2 microsecond
minimum step pulse width for y-axis
M569 P7 S1 ; 2 microsecond
minimum step pulse width for z-axis
M584 X5 Y6 Z7 E9:4 ; set drive mapping
M350 X16 Y16 Z16 E16:16 I1 ; configure
microstepping with interpolation
M92 X120.00 Y120.00 Z2000.00 E224.6:450.00 ; set steps per mm
M566 X100.00 Y100.00 Z12.00 E300.00:300.00 ; set maximum
instantaneous speed changes (mm/min)
M203 X6000.00 Y6000.00 Z120.00 E9000.00:1200.00 ; set maximum speeds
(mm/min)
M201 X200.00 Y200.00 Z200.00 E250.00:250.00 ; set accelerations
(mm/s^2)
M906 X0 Y0 Z0 E2700:1950 I30 ; set motor currents (mA) and
motor idle factor in per cent
```

```

M569 P9 S1 R1 T3:3:5:0
M569 P5 T2.2
M569 P6 T2.2
M569 P7 T2.2
M569 P4 T2.2
M569 P3 T2.2
M84 S30 ; Set idle timeout

; Axis Limits
M208 X0 Y0 Z0 S1 ; set axis minima
M208 X900 Y1000 Z710 S0 ; set axis maxima

; Endstops
M574 X1 S1 P"!xstop" ; configure switch-type
(e.g. microswitch) endstop for low end on X via pin xstop
M574 Y1 S1 P"!ystop" ; configure switch-type
(e.g. microswitch) endstop for low end on Y via pin ystop
M574 Z1 S1 P"!zstop" ; configure switch-type
(e.g. microswitch) endstop for low end on Z via pin zstop

;M574 E0 S0 ; MARCO Define E0 endstop active low
for filament sensor

; Z-Probe
;M558 P5 C"^zprobe.in" H5 F0 T6000 ; set Z probe type to
switch and the dive height + speeds
;G31 P500 X0 Y0 Z0 ; set Z probe trigger
value, offset and trigger height
;M557 X15:215 Y15:195 S20 ; define mesh grid

; Heaters
M308 S0 P"bedtemp" Y"thermistor" T47500 B3988 C0 R4700 ; configure
sensor 0 as thermistor on pin bedtemp
M950 H0 C"bedheat" T0 ; create bed heater
output on bedheat and map it to sensor 0
M307 H0 B0 S1.00 ; disable bang-bang mode
for the bed heater and set PWM limit
M140 H0 ; map heated bed to
heater 0
M143 H0 S150

M308 S1 P"spi.cs3" Y"rtd-max31865" ; configure sensor 1 as
thermocouple via CS pin spi.cs1
M950 H1 C"e0heat" T1 ; create nozzle heater
output on e0heat and map it to sensor 1
M307 H1 B0 S1.00 ; disable bang-bang mode
for heater and set PWM limit
M143 H1 S480

M308 S2 P"spi.cs2" Y"rtd-max31865"
M950 H2 C"elheat" T2

```

```

M307 H2 B0 S1.00 ; disable bang-bang mode
for heater and set PWM limit
M143 H2 S480

M308 S3 P"spi.cs1" Y"rtd-max31865"
M950 H3 C"!exp.heater6" T3
M307 H3 B0 S1.00 ; disable bang-bang mode
for heater and set PWM limit
M143 H3 S480

M308 S4 P"eltemp" Y"thermistor" T110000 B4550 C0 R4700
M950 H4 C"!exp.heater7" T4
M307 H4 B0 S1.00 ; disable bang-bang mode
for heater and set PWM limit
M143 H4 S300

;M301 H0 S1.00 P10 I0.1 D200 T0.4 W180 B30 ; Use PID on bed
heater(may require further tuning)
;M301 H1 P15 I0.5 D100 T0.4 S1 W180 B30 ; Use PID on
extruder 1 HFE300
;M301 H2 P15 I0.5 D100 T0.4 S1 W180 B30 ; Use PID on
extruder 2 HFE300
;M301 H3 P15 I0.5 D100 T0.4 S1 W180 B30
;M301 H4 P15 I0.5 D100 T0.4 S1 W180 B30
M307 H0 R0.191 K0.223:0.000 D19.80 E1.35 S1.00 B0
;A partir de aqui mio
M307 H1 R2.48 K0.096:0.000 D40.55 E1.35 S0.2 B0
M307 H2 R2.482 K0.100:0.000 D40.19 E1.35 S0.2 B0
M307 H3 R2.573 K0.105:0.000 D36.92 E1.35 S0.2 B0

M301 H4 P15 I0.5 D100 T0.4 S1 W180 B30

;M307 H2 A940 C810 D22 S0.3 B0
;M307 H3 A795 C920 D10 S0.3 B0

; Fans
;M950 F0 C"fan0" Q500 ; create fan 0 on pin
fan0 and set its frequency
;M106 P0 S0 H-1 ; set fan 0 value.
Thermostatic control is turned off
;M950 F1 C"fan1" Q500 ; create fan 1 on pin
fan1 and set its frequency
;M106 P1 S1 H1:2 T45 ; set fan 1 value.
Thermostatic control is turned on

; Tools
M563 P0 D0 H1:2:3 S"Pulsar"

M563 P1 D1 H4 F0 ; define tool 0
G10 P0 X0 Y0 Z0 ; set tool 0 axis
offsets

```

```
G10 P0 R0 S0  
active and standby temperatures to 0C  
G10 P1 R0 S0
```

```
; set initial tool 0
```

```
; Custom settings are not defined
```

Appendix 3

FFF Settings ? X

Process Name:

Select Profile:

General Settings

Infill Percentage: 2% Include Raft Generate Support

Extruder | Layer | Additions | Infill | Support | Temperature | Cooling | G-Code | Scripts | Speeds | Other | Advanced

Extruder List
(click item to edit settings)

- Extruder 1
- Extruder 2

Extruder 1 Toolhead

Overview

Extruder Toolhead Index:

Nozzle Diameter: mm

Extrusion Multiplier:

Extrusion Width: Auto Manual mm

Ooze Control

| | | | |
|---------------------------------------|--------------------------|-----------------------------------|------|
| <input type="checkbox"/> Retraction | Retraction Distance | <input type="text" value="1.50"/> | mm |
| | Extra Restart Distance | <input type="text" value="0.00"/> | mm |
| | Retraction Vertical Lift | <input type="text" value="0.00"/> | mm |
| | Retraction Speed | <input type="text" value="35.0"/> | mm/s |
| <input type="checkbox"/> Coast at End | Coasting Distance | <input type="text" value="0.20"/> | mm |
| <input type="checkbox"/> Wipe Nozzle | Wipe Distance | <input type="text" value="5.00"/> | mm |

Process Name:

Select Profile:

General Settings

Infill Percentage: 2% Include Raft Generate Support

- Extruder
- Layer
- Additions
- Infill
- Support
- Temperature
- Cooling
- G-Code
- Scripts
- Speeds
- Other
- Advanced

Layer Settings

Primary Extruder

Primary Layer Height mm

Top Solid Layers

Bottom Solid Layers

Outline/Perimeter Shells

Outline Direction: Inside-Out Outside-In

Print islands sequentially without optimization

Single outline corkscrew printing mode (vase mode)

First Layer Settings

First Layer Height %

First Layer Width %

First Layer Speed %

Start Points

Use random start points for all perimeters

Optimize start points for fastest printing speed

Choose start point closest to specific location

X: Y: mm

FFF Settings ? X

Process Name:

Select Profile:

General Settings

Infill Percentage: 2% Include Raft Generate Support

Extruder Layer Additions Infill Support Temperature Cooling G-Code Scripts Speeds Other **Advanced**

Use Skirt/Brim

Skirt Extruder:

Skirt Layers:

Skirt Offset from Part: mm

Skirt Outlines:

Use Prime Pillar

Prime Pillar Extruder:

Pillar Width: mm

Pillar Location:

Speed Multiplier: %

Use Raft

Raft Extruder:

Raft Top Layers:

Raft Base Layers:

Raft Offset from Part: mm

Separation Distance: mm

Raft Top Infill: %

Above Raft Speed: %

Use Ooze Shield

Ooze Shield Extruder:

Offset from Part: mm

Ooze Shield Outlines:

Sidewall Shape:

Sidewall Angle Change: deg

Speed Multiplier: %

Process Name:

Select Profile:

General Settings

Infill Percentage: 100% Include Raft Generate Support

- Extruder
- Layer
- Additions
- Infill
- Support
- Temperature
- Cooling
- G-Code
- Scripts
- Speeds
- Other
- Advanced

General

Infill Extruder:

Internal Fill Pattern:

External Fill Pattern:

Interior Fill Percentage: %

Outline Overlap: %

Infill Extrusion Width: %

Minimum Infill Length: mm

Combine Infill Every: layers

Include solid diaphragm every layers

Internal Infill Angle Offsets

deg

Print every infill angle on each layer

External Infill Angle Offsets

deg

FFF Settings

Process Name:

Select Profile:

General Settings

Infill Percentage: 100% Include Raft Generate Support

Extruder Layer Additions Infill Support Temperature Cooling G-Code **Scripts** Speeds Other Advanced

Starting Script Layer Change Script Retraction Script Tool Change Script Ending Script

```
G10 P0 S170:180:195
M302 P0
G28 ; home all axes
```

Post Processing

Export file format

Add celebration at end of build (for .x3g files only)

Additional terminal commands for post processing

Process Name:

Select Profile:

General Settings

Infill Percentage: 100% Include Raft Generate Support

- Extruder
- Layer
- Additions
- Infill
- Support
- Temperature
- Cooling
- G-Code
- Scripts
- Speeds
- Other
- Advanced

Speeds

| | | |
|------------------------------|-----------------------------------|------|
| Default Printing Speed | <input type="text" value="40.0"/> | mm/s |
| Outline Underspeed | <input type="text" value="50"/> | % |
| Solid Infill Underspeed | <input type="text" value="80"/> | % |
| Support Structure Underspeed | <input type="text" value="80"/> | % |
| X/Y Axis Movement Speed | <input type="text" value="50.0"/> | mm/s |
| Z Axis Movement Speed | <input type="text" value="16.7"/> | mm/s |

Speed Overrides

Adjust printing speed for layers below sec
 Allow speed reductions down to %